# Offshore Wind Farm using Grid Forming Control & Energy Storage System for Frequency Stability

Aravind Devaraj, Konstantinos Papadopoulos
Electrical Power Systems and High Voltage Engineering, EPSH4-1034, 2023-06

Master Thesis

**Department of Energy Technology**
Aalborg University
https://www.energy.aau.dk/

**AALBORG UNIVERSITY**
STUDENT REPORT

**Title:**
Offshore Wind Farm using Grid Forming Control & Energy Storage System for Frequency Stability

**Theme:**
Electrical Power Systems and High Voltage

**Project Period:**
Spring Semester 2023

**Project Group:**
EPSH4-Group 1034

**Participant(s):**
Aravind Devaraj
Konstantinos Papadopoulos

**Supervisor(s):**
Jayakrishnan Radhakrishna Pillai
Sanjay Chaudhary

**Copies:** 1

**Page Numbers:** 77

**Date of Completion:**
June 2, 2023

**Abstract:**

The proliferation of inverter based resources (IBR), has changed power systems drastically. Synchronous generator (SG) units are getting decommissioned as part of clean energy policies. One major problem that arises from a high penetration level of electronic-based wind generation is the reduction of overall system inertia. At the same time, most of the IBR do not have controllable source of energy and hence they cannot provide upwards frequency regulation support unless they keep some margin. Which has a disadvantage that it won't allow for complete utilization of the renewable generation resulting in economic challenges. The thesis investigates the implementation of grid-forming (GFM) control towards frequency stability and inertial response (IR) and how the addition of energy storage system (ESS) can enhance the system response. DIgSILENT PowerFactory is used to model the power system and RMS studies were performed. The thesis uses a generic ESS and does not point to a specific type. Based on the largest contingency and the rate of change of frequency (RoCoF) limit, ESS sizing was calculated to provide IR. Various parameters that affect the ESS sizing are addressed and the impact of these parameters on frequency dynamics are assessed. Though the simulations clearly reveal the upper hand of ESS in terms of frequency stability, the trade-offs that need to be considered while sizing the ESS are also addressed in the thesis. Besides IR, the ESS sizing to provide primary frequency response (PFR) was also calculated and the frequency metrics improvement was noted. The thesis concludes with the benefit of operating a wind power plant and ESS in GFM mode. The results and analysis of the thesis could be used to make an improved GFM control, in coordination with the ESS to address the power system stability.

# Preface

This report is written by EPSH4-1034 on the 4th semester of the master's degree, with specialization in Electrical Power Systems and High Voltage Engineering at Aalborg University. The project was made under the supervision of Jayakrishnan Radhakrishna Pillai and Sanjay Chaudhary from Aalborg University.

Special thanks to our contact person Thyge Knueppel from Siemens Gamesa Renewable Energy and the Grid Compliance team, for assisting us with comments and guidance throughout the project period.

Aalborg University, June 2, 2023

Aravind Devaraj
<adevar21@student.aau.dk>

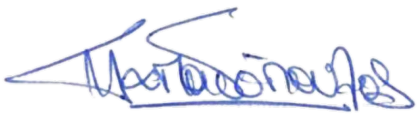

Konstantinos Papadopoulos
<kpapad21@student.aau.dk>

# Contents

# List of Figures

# List of Tables

# List of Abbreviations

| | |
|---|---|
| aFRR | Automatic Frequency Restoration Reserve |
| AVR | Automatic Voltage Regulation |
| BESS | Battery Energy Storage System |
| DFIG | Double Fed Induction Generator |
| ESS | Energy Storage System |
| FCR | Frequency Containment Reserve |
| FFR | Fast Frequency Response |
| GFL | Grid Following |
| GFM | Grid Forming |
| GSC | Grid Side Converter |
| IBPS | Inverter Based Power Sources |
| IR | Inertial Response |
| mFRR | Manual Frequency Restoration Reserve |
| MPPT | Maximum Power Point Tracking |
| MSC | Machine Side Converter |
| OEM | Original Equipment Manufacturer |
| PCC | Point of Common Coupling |
| PFR | Primary Frequency Response |
| PLL | Phase Locked Loop |
| PV | PhotoVoltaics |
| RES | Renewable Energy Sources |
| RMS | Root Mean Square |
| RoCoF | Rate of Change of Frequency |
| RPM | Revolutions per Minute |
| SFR | Secondary Frequency Response |
| SG | Synchronous Generators |

| | |
|---|---|
| SoC | State of Charge |
| TFR | Tertiary Frequency Response |
| TSO | Transmission System Operator |
| VSM | Virtual Synchronous Machine |
| WPP | Wind Power Plant |
| WT | Wind Turbine |
| WTG | Wind Turbine Generator |

# Chapter 1

# Introduction

## 1.1 Background Analysis

The unprecedented growth of the industrial world has led to highly increased electricity demand, while the European decarbonization agendas must cope with the imminent environmental crisis. Therefore, the operation of the electric power system is critical to ensure facilitating everyday activities, whereas its configuration changes drastically. The commitment of reducing CO2 emissions, in a power system is reflected in the increased integration of non-synchronous, renewable energy sources (RES). Today the European electrical power system contains 39% of RES, with expectations for further additions in the future [1]. The global cumulative RES capacity at the end of 2020 reached 2799 GW while solar and wind capacity share equally 50% of the total [2].

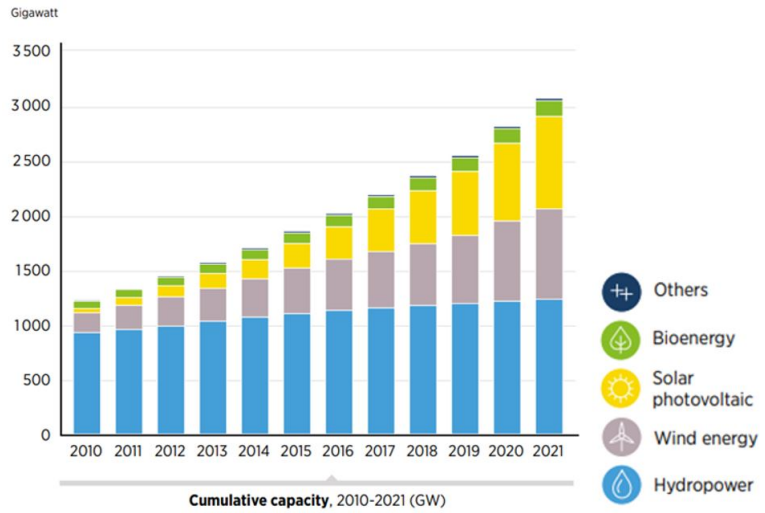


**Figure 1.1:** Global RES installed capacity between 2010-2021, according to International Renewable Energy Agency (IRENA) (Figure source: [3])

Wind power, both offshore and onshore is expected to be 20150 GW up to 2030, in global capacity. Currently Europe is the largest offshore wind market, having 75% of the total global offshore wind installations [4]. Denmark specifically, is expected to have more than 15 GW wind power, onshore and offshore combined by 2030 [5].

Nevertheless, these RES are typically inverter-based power sources (IBPS) implying that their integration significantly increases the complexity of the power system and affects power system stability.

The reason being the increased decommissioning of fossil-fuel based generation, which so far relied on synchronous generators (SG) and their properties to keep the power system stable [6]. Although inverter-based generation offers the advantage of harvesting RES, frequency stability might be compromised, since mechanical inertial response and damping tend to become remarkably less, due to SG replacement. In addition, the interface of RES, through inverter topologies, decouples them from the grid thus affecting the power system stability.

Due to inertia reduction, a sudden active power imbalance in generation or load would lead to a major frequency deviation. Furthermore, a system would exhibit an increased rate of change of frequency (RoCoF), and a low frequency nadir in a very short time. As such, protective relays which monitor RoCoF might be triggered, potentially leading to an under-frequency load shedding, and in the worst case to cascaded outages [7]. It should also be mentioned that the intermittent nature of RES makes matters worse, due to their dependance on weather conditions e.g., WT and Photovoltaics (PV). Thus, the power mismatch challenge between generation and demand becomes more relevant because of the intermittent nature of RES, while it is generally agreed that more than 20% of RES penetration may destabilize the grid. Levels of inertia are expected to drop further, as increasingly non-synchronous IBPS substitute SG.

Therefore, the frequency response of a power system is of utmost importance, especially after the aforementioned constraints. In accordance, the European Network Transmission System Operator of Electricity (ENTSO-E), proposes a sequence of controlled actions to arrest and stabilize the system frequency from continuous declination [8], by handling active power regulation. The response is comprised of four stages as illustrated in Figure 1.2 [9]. The inertial response, typically within ten seconds after the disturbance, is associated with the kinetic energy and inertia levels of the system. The primary frequency response (PFR) aims to reduce the frequency deviation within thirty seconds, while the secondary frequency response (SFR) restores the frequency back to its nominal value. Finally, the tertiary frequency response (TFR) involves the reserves deployment to get the resources ready for handling present or future disturbances.

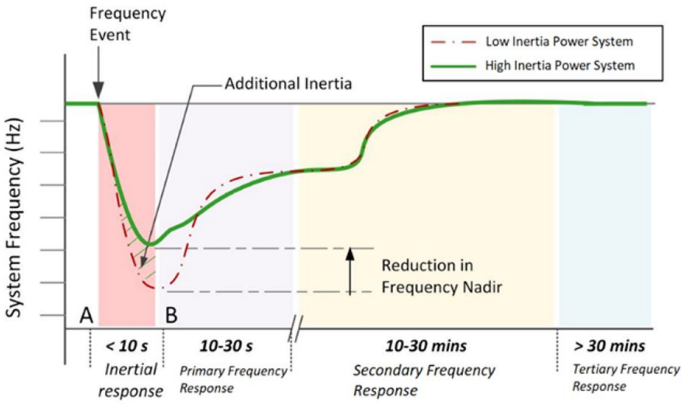


**Figure 1.2:** Multiple time frame frequency response stages accompanied by a control action, as proposed by ENTSO-E, in a high and low inertia system. (Figure source: [9])

As the inertia of a power system drastically drops by the proliferation of RES, measures should be taken to mitigate frequency decay due to an event, by decreasing both RoCoF and frequency nadir. In this way, adequate time would be provided for PFR to be activated. A fast active power injection or reduction in load would address the problem. As a result, a new control action is introduced as fast frequency response (FFR) [10].

The share of IBPS is projected to rise rapidly in the future. Thus, indicating that RES produces power at a cheaper cost when compared to SGs, thus a steady reduction in the use of SGs are forecasted. However, from a power system stability point of view, SGs are needed to maintain power

system stability [11].

In the case with 100% operation of IBPS, the converter is expected to have the characteristics such as system voltage creation, fast dynamics supporting during black start, prevention of adverse interaction between control systems, acting as a sink to system voltage unbalances counter harmonics and inter-harmonics [12].

Various TSOs (Transmission System Operator) are involved into studies to evaluate different potential solutions to bring stability to the grid, considering the high penetration of RES. National Grid (Electricity operator in Britain), is an example of TSO who is performing studies to assess all potential solutions [11].

Studies from National grid reveal that Virtual Synchronous machine (VSM) is a holistic approach. VSM is another form of control concept that can be implemented on converter-based plants such that WTs and PVs which are traditionally grid following will behave like grid forming (GFM) [12]. VSM is a control scheme applied to the converter to emulate the behavior of SGs by using the models of SGs within the control scheme. This control scheme had been initially used in PVs and combined heat and power (CHP) in microgrids and is subsequently discussed for other applications like variable WTs [13].

Most of the RES do not have a controllable source of energy, and hence they cannot provide upwards frequency regulation support, unless they keep some margin. However, an important disadvantage of such a method is that it won't allow for complete utilization of the RES. Economic implications could also be considered. The frequency support characteristics of GFM WT control, during a large frequency deviation would cause a drop in WT speed. Considering a case with exceptionally low wind speed, an event could cause tripping of the WT [14].

The combination of RES with an energy storage system (ESS) can provide the most robust approach for implementing GFM capability as the size of can be decided based on the necessary grid support functions ESS can provide and the support does not intervene with optimum generation conditions [14]. Based on the availability of sufficient energy buffer, GFM controls e.g., VSM can be implemented in different IBPS. These can be integrated with ESS and supply droop frequency control and inertia response [15]. The main purpose of an ESS is to provide dynamic energy exchange during events which result in deviations in the system frequency. An example of an event that will result in a large frequency deviation would be unscheduled trips, loss of large power station or HVDC interconnector. In order for IBPS to provide this dynamic power and to avoid the post event loss of power production that would occur if the energy is extracted from the machine rotor, an ESS is required.

VSM control has been implemented by Siemens Gamesa at Dersalloch in 2019, where 23 turbines making up to 63 MW were operating in GFM mode and thus, exploring inertia contributions. To this date, this is the first and largest power electronic converter connected wind farm [16]. An extended trial was performed a year later to assess and evaluate whether the same farm could sustain in islanded condition, and support restoration of system and black start services [17]. Studies also show that turbine's capability to respond to events, especially during declining wind speed or low power operation could be significantly improved using ESS [17].

## 1.2 Problem Formulation

Based on the background analysis, investigating the ability of a wind farm operating in GFM control to enhance frequency stability is important, as well as how the addition of ESS will enable the WT to have GFM capabilities.

It is obvious that the proliferation of non-synchronous IBPS has given rise to control concepts, where the emulation of certain SG-based system characteristics is attainable. While the addition of ESS might help overcome some limitations, their cost is not to be taken lightly. In combination with the area they might occupy e.g., battery energy storage system (BESS), which might be comprised of bulky units. Their availability on the market, plus their differences regarding response times, energy accumulation capacity and capability, cycles of life etc., should not be neglected. Proper sizing of the selected ESS is essential.

Thus, a solid control structure of VSM and ESS combined, with proper parametrization could not only contribute to system stability but avoid potential excess costs. However, an investment in ESS could also support the islanded mode operation of a microgrid and augment the GFM mode. Is it possible though that proper parametrization could resolve a disturbance without ESS? What could be the system disturbance level, the system can withstand with and without ESS. Is the response compliant or exhibit improved behavior according to grid code requirements; will be this thesis' scope.

**Thesis Objective**

The thesis' main objective is to model and implement a VSM with an integrated ESS and evaluate its impact on frequency stability when subjected to a system disturbance. The sizing of ESS is done such a manner, that can accommodate services like inertial response (IR) and PFR.

The following tasks will be conducted to meet the objective:

- Understand the fundamental characteristics of a SG, and the respective mathematical equations.
- Implement the appropriate VSM control to replicate the behavior of an SG.
- Analysis of ESS based on literature review.
- ESS sizing for IR and PFR.
- Integration of the ESS along with the VSM, in the dynamic model of the wind farm using DIgSILENT PowerFactory.
- How will the combined architecture (VSM and ESS) contribute to improving the RoCoF, frequency nadir, rebound frequency and steady-state frequency, with proper active power response, by complying with grid code requirements?

## 1.3 Methodology

**State of the art:** The first phase of the project begins with a state-of-the-art analysis, wherein the theory of SGs is understood in detail. This knowledge is essential to implement VSM control in WT which is based on emulation of swing equation. State of the art literature on ESS will be done to analyze, classify and assess the parameters that could affect the sizing of ESS.

**Dynamic model:** All studies will be performed using RMS simulation in the simulation tool DIgSILENT PowerFactory which will be used to develop a dynamic model that shall represent an aggregated wind farm integrated with ESS and operating in grid-forming mode.

**Evaluations:** Once the dynamic model with GFM control integrated with ESS is developed, the frequency response from the aggregated wind farm subjected to various system disturbances will be evaluated. Events with lower RoCoF and lower frequency drop will be analyzed at earlier phases and the next phase will include severe events with higher RoCoF and large frequency drop. The frequency response of WT with GFM and ESS will be evaluated for these events to assess and conclude the impact of integrating ESS into the WT.

## 1.4 Limitations

Some limitations are made for the project. These limitations are listed below:

- The WT model won't represent a single unit, but an aggregated wind farm where the dynamic model will be analyzed.
- Dynamics of wind power curve, blade angle control are not considered. The WT will be treated as a constant power source.
- Detailed model of the ESS is not provided.
- The ESS is assumed to operate in VSM mode, hence the ESS is represented as a VSM.
- Frequency services like SFR and TFR are out of scope of work.
- Regulation of state of charge (SOC) of ESS, will not be considered.
- Other aspects of power system's stability such as: voltage and rotor angle stability are not studied.
- The dynamic GFM control model is developed in DIgSILENT PowerFactory, RMS domain. EMT simulations analyzing harmonic contribution and transient behavior, are not performed.
- PFR simulations for 15 minutes have not been performed.
- The DSL model templates are from DIgSILENT PowerFactory.

## 1.5 Outline of the Thesis

The outline of the thesis consists of five chapters. Each chapter is organized as follows:

**Chapter 1- Introduction:** In this chapter a brief introduction on the background of the problem is given, with the aspects concerned in this thesis. The structure of the thesis is presented as well.

**Chapter 2- Technical Background:** In this chapter, the relevant literature review is presented, regarding the VSM control and different implementations in order to emulate a SG. Different GFM control schemes are analyzed. Literature review on essential parameters of ESS and different types is done.

**Chapter 3- VSM Control Evaluation & ESS Sizing Methodology:** In this chapter, the dynamic model of the selected GFM control, using DIgSILENT PowerFactory template representing an aggregated wind farm evaluated. The sizing methodology of ESS based on grid code requirements, for ancillary services provision is formulated.

**Chapter 4- Case Study for Contingency Event:** In this chapter, the different test cases for examining the frequency response of the model, with and without ESS are evaluated. Different system architectures and configuration are put under test for the largest contingency, whereby their frequency dynamics are compared.

**Chapter 5- Discussion:** In this chapter, the derived results from the previous chapters are discussed. Observations from the simulations and calculated data are used to assess the impact of VSM and ESS in the power system.

**Chapter 6- Conclusion & Future Work:** The main conclusions of the thesis are presented together with suggestions for future work.

# Chapter 2

# Technical Background

The chapter will cover the basics of power system stability and guide through the different classifications. A brief introduction into frequency regulations from a few TSOs are also discussed in this chapter. Essential control of SGs and the equations governing them are analyzed. A detailed look into the GFL and GFM converters, along with an explanation of Type IV WT are also part of the chapter. The chapter also delves into different classification of GFM converters and basis of their classification. As a conclusion, potential barriers in the applications and how these could be addressed by introducing an ESS unit, is the scope.

## 2.1 Power System Stability

As per definition, power system stability is characterized as the ability of a power system to reach to an equilibrium state for a given initial condition, after being subjected to a physical disturbance[7]. Furthermore, certain classifications exist according to the impact on power system's aspects, namely: voltage, rotor angle and frequency stability. These aspects account for the dynamic behavior of the system, whose dynamic performance was predominantly so far relied on SG and loads. Different dynamics fall, in addition, to further categories of classification according to their nature, based on their time scale, ranging from milliseconds to minutes [7], [18]. These are: wave, electromagnetic, electromechanical, and thermodynamic phenomena. Specifically electromechanical phenomena are divided into long-term and short-term, where a phasor representation is implied.

Nonetheless, as discussed in Chapter 1, the increasing number of IBPS has led to significant transformation of power systems, with addition of technologies such as, wind and photovoltaic generation, high voltage direct current (HVDC) lines, and power electronic converters to name a few. Thus, the dynamic response of a power system, progressively becomes more dependent on fast-response power electronic devices. Overall, the increasing share of IBPS creates new types of power system stability problems[19]. Apparently, these problems stem from the different dynamic behavior of IBPS compared to the conventional SG, due to control, reduction in total system inertia, and limited short circuit current contribution. Two new aspects, resonance stability and converter-driven stability arise, mainly associated with electromechanical and electrical resonance s. All in all, the converter topology, the switching devices used in combination with the control algorithms for fast interaction, creates converter-driven stability. However, these two aspects are completely out of the scope of this thesis.

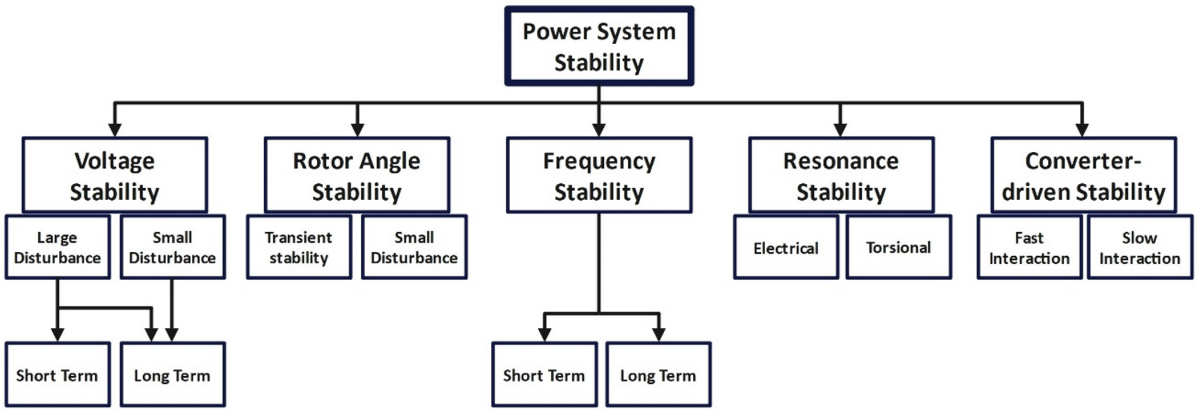


**Figure 2.1:** Stability aspects of traditional power systems, along with newly arising stability aspects due to converter topology interfaced power generation (resonance and converter-driven stability).

### Voltage Stability

The ability of a power system to maintain steady voltage at all nodes after a disturbance, is referred as voltage stability, and it is threatened when this disturbance increases the demand in reactive power beyond the capacity of the reactive power resources. Voltage instability could be the progressive drop in bus voltages, but the capacitive behavior of e.g., an EHV transmission line could risk an overvoltage as well [18], [19]. A system is voltage stable if the voltage magnitude increases, as the reactive power injection on the same bus increases. Adversely, a system is voltage unstable if the voltage magnitude decreases, as the reactive power injection on the same bus increases. Furthermore, short term voltage stability could refer to fast dynamics of rapid acting components as HVDC converters, while long term voltage stability involves slower acting equipment such as, tap-changing transformers[19].

### Rotor Angle Stability

The ability of interconnected synchronous machines to remain and regain synchronism after being subjected to a disturbance is defined as rotor angle stability. A synchronous machine will remain in synchronism based on its ability to maintain and restore the equilibrium between electromagnetic and mechanical torque. In a power system, this would reflect in the form of angular swings which might lead to loss of synchronism of one or more units. Thus, rotor angle stability involves the study of electromechanical oscillations. Rotor angle has a correlation with output power of the system[18], [19].

### Frequency Stability

When subjected to a substantial imbalance between generation and load, it is the ability of the power system to maintain a steady state frequency within a specified range. For example, in CE (Continental Europe), the frequency range is 47.5 Hz -48.5 Hz with a time duration not less than 30 minutes[20]. When a major load is suddenly connected or disconnected an imbalance is created.

#### *a) Frequency regulation*

Power imbalances result in a non-ideal state of the power system. TSO (Transmission system operators) ensure a safe and optimal operating frequency using frequency responses. As such an example from National Renewable Energy Laboratory (NREL), the frequency response could be classified into four categories[7],[21], as depicted in Figure 2.2.

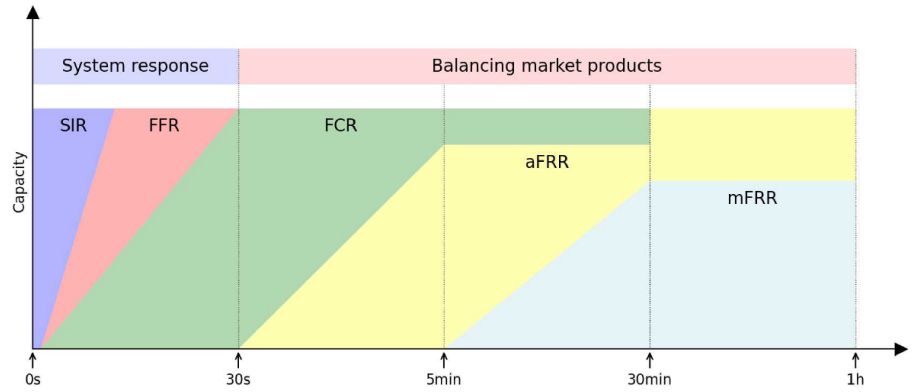


**Figure 2.2:** Approximate period of different frequency responses. (Figure source: [21]).

**Table 2.1:** Brief description of frequency responses illustrated in Figure 2.2.

| Name | Description | Control |
|---|---|---|
| IR: Inertial Response (SG). FFR: Fast Frequency Response (IBPS). | The RoCoF is reduced with an instant response by the inertia in the system. One form of FFR is synthetic energy. | Inherent SG characteristic(SG). Emulated inertia by dedicated units injecting active power (IBPS). |
| FCR: Frequency Containment Reserve, or PFR: Primary Frequency Response. | Governor action in case of SGs. Energy provision capability of dedicated storage units for IBPS and/or synchronous generation. | Primary |
| aFRR: Automatic Frequency Restoration Reserve. | Active power is produced by dispatching the balancing market. Frequency is restored by dispatching new set point automatically for generators. | Secondary |
| mFRR: Manual Frequency Restoration Reserve. | A manual dispatch is ordered if the frequency is not restored yet. | Tertiary |

Before proceeding it is important to highlight a few key differences regarding frequency control and reserves. As defined in [22] based on the ENTSO-E grid code regulations [23], FCR must be active for at least 15 minutes [24] and aFRR must be activated within 30 seconds. However, the classification and the activation times of different reserves may differ amongst European countries. For instance, the Nordic system has a further division of FCR defined as: Frequency controlled normal operation reserve (FCR-N) and Frequency controlled disturbance reserve (FCR-D) [25]. All in all, these differentiations involve socio-economic aspects as well, however, the sequence of activation is as follows: FCR shifts the burden to aFRR and then mFRR takes over.

During a system disturbance, the high RoCoF, which is a result of steadily declining system inertia calls for the need for immediate and faster energy injection to suppress the dropping frequency. This type of fast and immediate response to frequency change is called FFR [26], [10]. There are different

ways in which FFR can be provided such as inertial response from SGs, a portion of turbine governor response, controls from WT to extract extra energy from rotating blades, batteries with fast controls to name a few [26]. The usage of FFR is also mentioned in [27]. Generally, the requirements for FFR may also differ but according to [10], technical requirements as: a) full activation time of FFR, b) frequency triggering level of FFR, c) deactivation, d) avoiding overdelivery and e) recovery requirements, should be considered before designing.

With the steady increase in number of IBPS, the system inertia is reduced thus, frequency stability has become more of a challenge these days [19]. There is a drastic decline on rotational mass since the main sources of IBPS are HVDC, solar and wind power. Though for instance, WTs might have some kinetic energy, it is decoupled through the power converter interconnection resulting in a low inertia behavior [28]. Owing to this, high ROCOF, low frequency nadir will be the outcome, while the system is more prone to frequency changes. Inertia decline and its impact on frequency instability must be assessed [29].

While more and more IBPS are integrated to the system synchronous generators are replaced. Power system stability and its classification have their corresponding impact when more IBPS are added [19]. Due to proliferation of IBPS, the total inertia of the system gets reduced. For a system with lower inertia, its frequency is expected to have larger deviations when there is a sudden change in generation or load thus creating an imbalance in active power [30]. According to HPoPEIPS (High Penetration of Power Electronic Interfaced Power Sources) 2019, the reduction of total system inertia is ranked the major power system stability challenge as identified by European TSOs [1]. Frequency stability will be the focus of the thesis.

## 2.2 Operation of Synchronous Generators

So far SGs have been the backbone of power systems, providing frequency stability owing to their inherent characteristics. Thus, it is crucial to understand their dynamic behavior. Based on the power-angle curve [31], the ability of a power system to reach an equilibrium state, is directly related to mechanical and electrical power output relationship, a product of torque. The electrical power depends on the generator loading and may vary according to the generator parameters. The mechanical power is typically regulated by a prime mover, controlled by a governor controller [31]. The regulation of active power to recover frequency if any disturbance in the system occurs is adjusted by the governor who manages the turbine valves position and reflects on the acceleration or deceleration of the rotor shaft, in order to reach the equilibrium point. However, characteristics of the rotational mass such as inertia and damping should be considered too. The droop should typically be between 3%-5% [7], and is expressed as the percentage change in speed, required for 100% governor action. This principle is illustrated in the following block diagram.

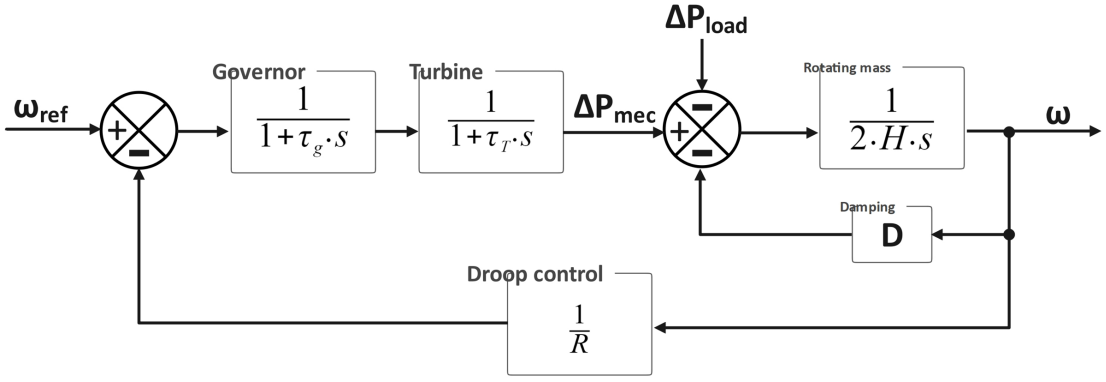


**Figure 2.3:** Block diagram representation of active power regulation in a SG considering inertia and damping.

Where, $\omega_{ref}$ is the reference angular velocity in rad/sec. The governor and the turbine are expressed each by a first order term, with $\tau_g$ and $\tau_T$ their respective time constants in seconds. Then the output mechanical power $\Delta P_{mec}$ is compared with the active power demand $\Delta P_{load}$, so that the new angular velocity is reached, considering the rotational mass model where H is the inertia constant in seconds and finally damping.

### Inherent characteristics mathematical representations

If an imbalance between the mechanical and the electrical torque occurs, oscillatory swings can affect the rotor speed. These swings are described as [18]:

$$\tau_{acc} = \tau_{mech} - \tau_{el} = J \cdot \frac{d\omega_m}{dt} \tag{2.1}$$

Where $\tau_{acc}$ is the accelerating torque, $\tau_{mech}$ is the mechanical torque and $\tau_{el}$ is the electromagnetic torque, all in $N \cdot m$. The acceleration or deceleration of the rotor, as seen from Equation 2.1, can be described as the combined moment of inertia J of the generator and turbine in $kg \cdot m^2$, where $\omega_m$ is the angular velocity of the rotor. The mathematical representation of combined moment of inertia is described as [7]:

$$J = \frac{2 \cdot H \cdot S_n}{\omega_0^2} \tag{2.2}$$

where, H is the inertia constant, $S_n$ is the apparent power of the machine and $\omega_0$ the rated angular velocity of the rotor. By rearranging Equation 2.2, the inertia constant defined as the kinetic energy with respect to nominal apparent power can be derived.

For complete mathematical representation of all the parameters, the classical swing equation can be obtained through Equation 2.1 and Equation 2.2, with the damping term and can be represented as:

$$\frac{2 \cdot H}{\omega_0} \cdot \frac{d^2\delta}{dt^2} = T_{mech} - T_{el} - \frac{K_d}{\omega_0} \cdot \frac{d\delta}{dt} \tag{2.3}$$

Where $T_{mech}$ and $T_{el}$ are the per-unit mechanical and electrical torque respectively, $\omega_0$ is the rated electrical angular velocity, $\delta$ is the rotor angle in electrical degrees and $K_d$ is the damping coefficient. Whenever the SG is subjected to system disturbance, it is the damping torque that helps the SG reach equilibrium faster [7]. Finally:

$$\frac{d\Delta\omega_r}{dt} = \frac{1}{2 \cdot H} \cdot (T_{mech} - T_{el} - K_d \cdot \Delta\omega_r) \tag{2.4}$$

Here the rotor angle is expressed in terms of angular rotor speed deviation $\Delta\omega_r$. The above reveals a relationship between inertia constant H and $\frac{d\Delta\omega_r}{dt}$. The term $\frac{d\Delta\omega_r}{dt}$ corresponds to the rate of change of frequency (RoCoF)and as the inertia constant is higher, the lower the RoCoF, indicating their inverse proportionality. SGs can inherently balance frequency stability by using the stored kinetic energy in the rotating masses of rotor [7].

## 2.3 Operation of Full Converter Type IV Wind Turbine

Double fed induction generator (DFIG), induction generators (IG), or synchronous generators are commonly used in WT to generate wind power. The generator of WT could be connected to the grid via a power converter or directly. There are four topologies of WT on the basis of arrangement of WT generator and converter. Type IV WT is focus of the project [32]. The basic assembly comprises of machine side converter (MSC), a DC link with shunt capacitor and the grid side converter (GSC).

GSC and MSC controls the active power and the DC link voltage respectively as shown in Figure 2.4 [33].

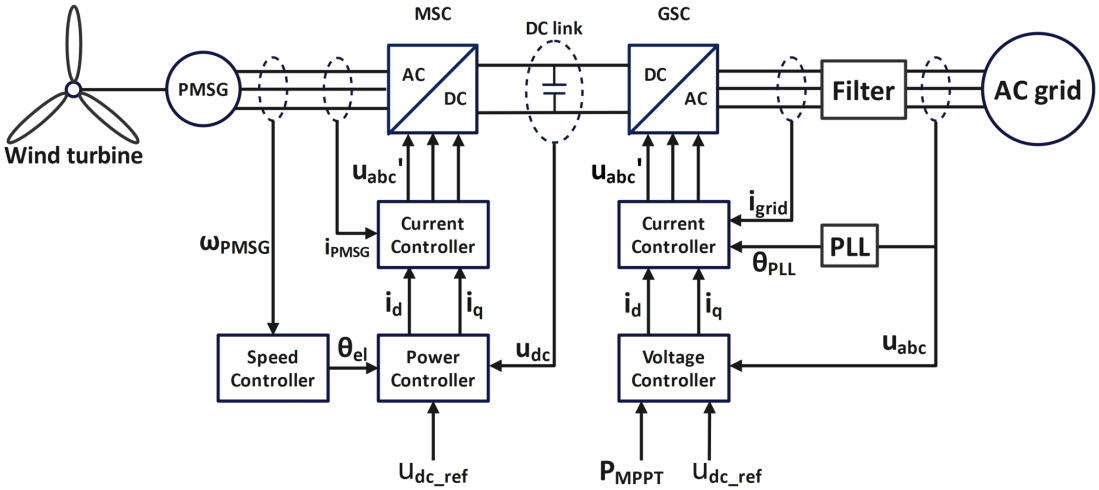


**Figure 2.4:** Type IV WT configuration.

The two control loops of the MSC are represented by the inner loop and the outer loop. The reference DC voltage $V_{ref,dc}$, is compared with DC link voltage $V_{dc}$. Thus, the outer loop controls the DC link voltage, while it also provides the reference values for the inner loop, and the d and q axis components of MSC which are controlled by the inner loop [33].

Under the assumption that there are no converter losses, the current flowing in and out of DC link capacitor has to be equal, while the GSC ensures the amount of current taken from the DC link capacitor [34].

The two control loops of the GSC are - an outer loop and an inner loop. Active power provided to the power grid is controlled with maximum power point tracker $P_{MPPT}$ using the outer loop. Based on rotor speed and measured wind speed $P_{MPPT}$ is calculated. The outer loop is used to control the reactive power flow by controlling the magnitude AC voltage of the converter [33], [34].

The outer loop provides the reference values for the inner loop and the current controller of GSC provides a reference voltage which is transformed into PWM signals for the power modules of the converter. To synchronize the converter to the grid, PLL (Phase Locked Loop) is used. By measuring the voltage phase angle of AC grid, a dq0 reference frame is created by PLL [33], [34].

Traditionally the WT converters are grid following (GFL). These converters inject active and reactive power into the grid and operate as current control converters. Control of active and reactive power can be achieved by calculating equivalent references and by "following" the grid voltage. By default, a type IV WT does not provide the same frequency and inertial response as that of synchronous generator during a system level event, due to the fact that full-scale converter completely decouples the WT generator from the grid [34].

## 2.4 Grid Forming & Grid Following Concept

Based on the assumption that synchronous generation sources will help regulate the frequency and voltage deviation, the IBPS are generally GFL [35]. Now with more and more penetration of IBPS, frequency stability is affected [19]. Using GFL control in WTs, the RoCoF during frequency events can be limited by having the WT respond to such events by controlling the frequency response according to RoCoF [35]. The method estimates the frequency from local voltage measurements by relying on PLL to calculate RoCoF. By doing so an additional power signal or torque which is proportional to

the estimated RoCoF could be added to the original power reference. Thus, the GFL WT can provide additional active power for frequency response during underfrequency events [35].

However, GFL also has its disadvantages as the method of calculating RoCoF, can have lot of time lag ranging from 0.1s to 5s, involving sampling, filtering and signal processing which affects the inertial response and FFR, which takes place in the range of 5-10s [36]. Furthermore, the frequency estimation becomes even more challenging in weak grids due to distorted voltage signals and GFL cannot operate as a power source in islanded mode or isolated microgrid [37], [38].

GFM control has been prevailing and introduced for islanded power systems and microgrids [39]. Definition and capability of GFM is still in an early phase. However, by analyzing the various requirements from ENTSOE's working group and TSOs, some of the capabilities which GFM should have are: generate system voltage, fault level contribution, total system inertia contribution, supporting system restoration, prevention of adverse control system interactions, need to act as a sink for harmonics and voltage unbalance in the system. In Figure 2.5 it is evident that the GFL and GFM takes current and voltage from PCC (Point of Common Coupling) as input and outputs a reference.

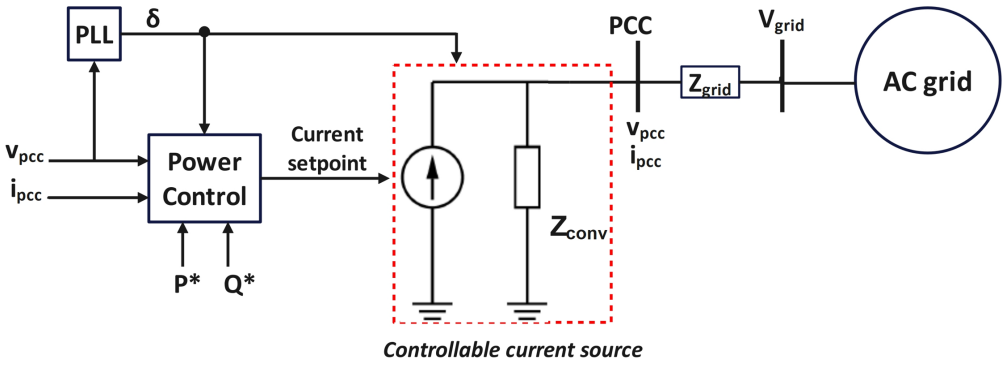


**(a)** Grid Following (GFL) control method for IBPS as controllable current sources.

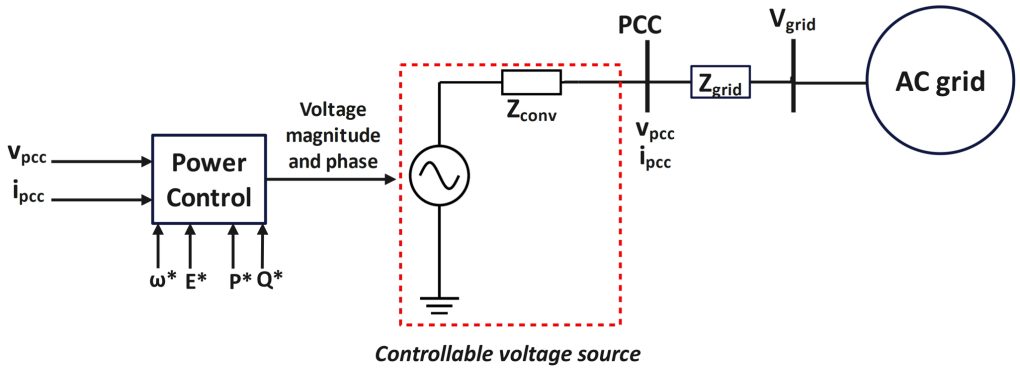


**(b)** Grid Forming (GFM) control method for IBPS as controllable voltage sources.

**Figure 2.5:** Simplified control method comparison of GFL and GFM.

In Figure 2.5 it is evident that the GFL and GFM takes current and voltage from PCC (Point of Common Coupling) as input and outputs a reference for PWM (Pulse width Modulation). A GFL converter can be considered to have an equivalent behavior of a controlled current source with a large parallel impedance, while GFM converter can be considered as a voltage source with a low series impedance. Both GFL and GFM have power control with the input measurements. In GFL, the active and reactive power set points for GSC is done using the d and q axis current set points which are the output of power control. While in GFM, it is the voltage amplitude and phase angle that governs the active and reactive power set points. Even with different working principles, under normal operating

conditions, both GFM and GFL control the active and reactive power injection into the grid, while adhering to the limitations of voltage and current in the converter [40].

As shown in Figure 2.6, different behavior of the GFL and GFM converter phasor diagrams, to a grid event is shown with their respective equations:

$$V_{conv} = V_{grid} + I_{conv} \cdot Z_{grid} \quad \text{(GFL)} \tag{2.5}$$

$$E = V_{grid} + I_{conv} \cdot (Z_{grid} + Z_{conv}) \Rightarrow$$
$$V_{conv} = E - I_{conv} \cdot Z_{conv} = V_{grid} + I_{conv} \cdot Z_{grid} \quad \text{(GFM)} \tag{2.6}$$

where, $V_{conv}$ the converter voltage, $Z_{grid}$ and $Z_{conv}$ the grid and the converter impedances, $E$ the internal voltage, the magnitude and angle of which is defined by the desired active and reactive power set points. Finally, the grid and converter current which are equal, $I_{conv} = I_{grid}$, based on Kirchhoff's current law.

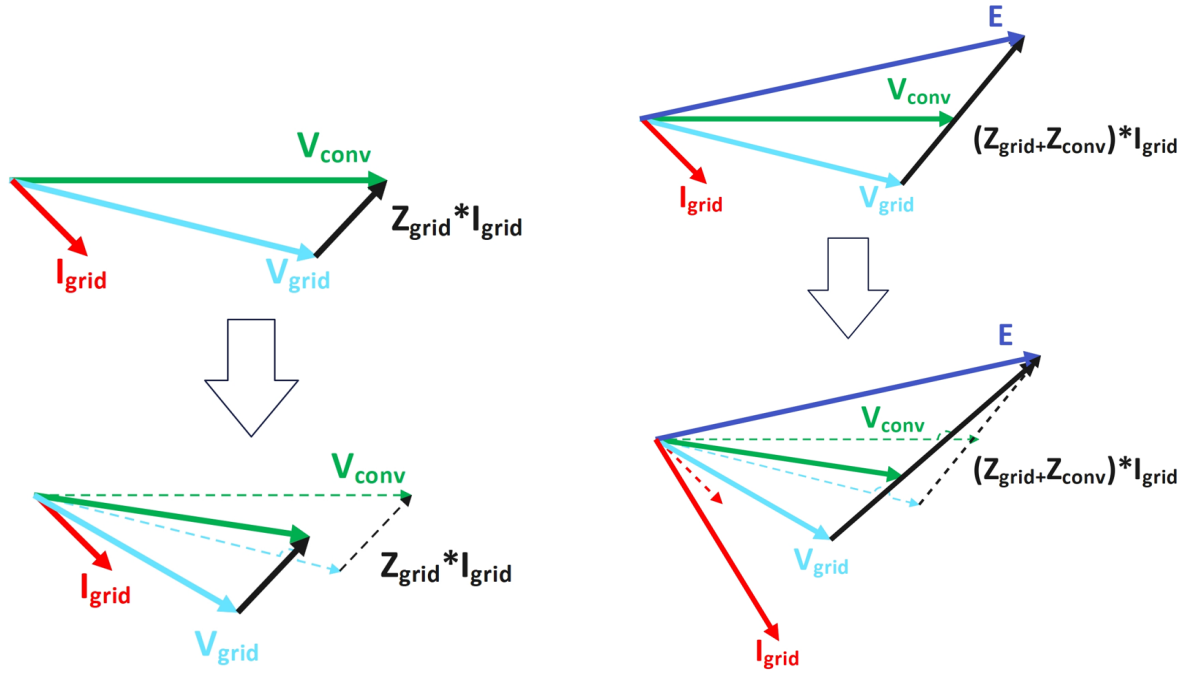


**(a)** Phasor diagram of a GFL converter according to perturbation of the grid voltage, Equation 2.5.

**(b)** Phasor diagram of a GFM converter according to perturbation of the grid voltage, Equation 2.6.

**Figure 2.6:** Phasor digrams comparison of GFL and GFM after a system disturbance.

Due to GFL Converter's current source behavior, the GFL converter tries to maintain the current phasor $I_{grid}$ constant in terms of magnitude and phase, causing a change of the converter voltage phasor $V_{conv}$; as a new phase angle for $V_{grid}$ is detected and hence a new current setpoint. While in GFM converter, due to its behavior as a voltage source behind impedance, the internal voltage phasor $E$ does not change initially due to disturbance, thus causing change in phasor $I_{grid}$ [40], [41].

This project will focus on GFM control, hence details of GFL control will not be analyzed and explored in detail. Next chapter will explain the different classifications of GFM control.

## 2.5 Control Based Classification of Grid Forming Converters

The operation of an inverter is to inject the necessary active or reactive power, while state-of-art literature analyzes and proposes methods regarding their extensive capabilities. Based on their synchronization methods [40], [41], GFM inverters are classified into different categories. Therefore, in

this section a classification of GFM control methods is made, and certain technical differences with their counterpart GFL control are mentioned. The power calculation equivalent single line diagram of a typical inverter is shown in Figure 2.7. The active and reactive power output of the converter can be expressed as:

$$P = \frac{V_{conv} \cdot V_{grid}}{X_{grid}} \cdot sin\delta \tag{2.7}$$

$$Q = \frac{V_{grid}}{X_{grid}} \cdot (V_{conv} \cdot cos\delta - V_{grid}) \tag{2.8}$$

where, $X_{grid}$ the grid reactance in ohms, $V_{conv}$ the inverter-side RMS voltage, $V_{grid}$ the grid-side RMS voltage in volts, and finally $\delta$ the phase angle difference between the grid and the inverter.

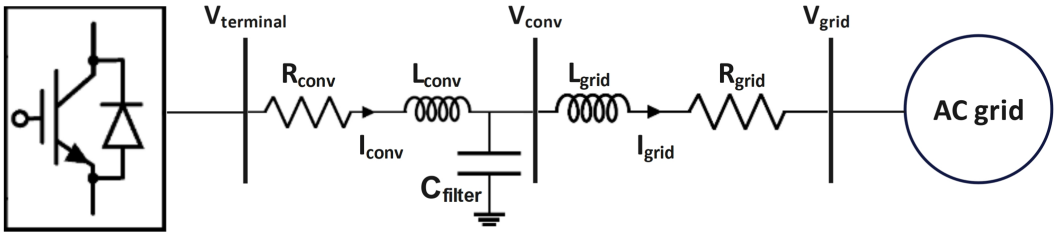


**Figure 2.7:** Typical single line diagram of inverter coupled with the grid and their respective network elements.

As discussed in the previous section, for current injection a GFL inverter requires a reference angle for synchronization, typically utilizing a PLL that uses the voltage phase angle measured at PCC [42].

Nevertheless, the synchronization processes are different when it comes to GFM control as presented in the following subsection, while studies [43], [44] have shown that interactions of GFL synchronization units operating in proximity, can become stronger under weak grid conditions. On the contrary under stiff grid conditions GFM control seems to be more prone to instability [45], [39]. GFM control methods offer a variety of techniques that can be implemented, where some designs aim to imitate the behavior of SGs by applying sophisticated mathematical models [46], [47], [48]. Others involve a simplified representation by employing the swing equation to approximate the dynamic behavior of a SG, while some control's voltage and current loops are based on variation of the active and reactive power [40], [41]. To this end, typically GFM inverter control might comprise of multiple levels of inner control loops, such as inner-current loop, virtual impedance loop, voltage control loop, active and reactive power controllers. In this section only droop and synchronous machine-based control methods are presented as shown in Figure 2.8, while the rest are beyond the scope of this thesis.

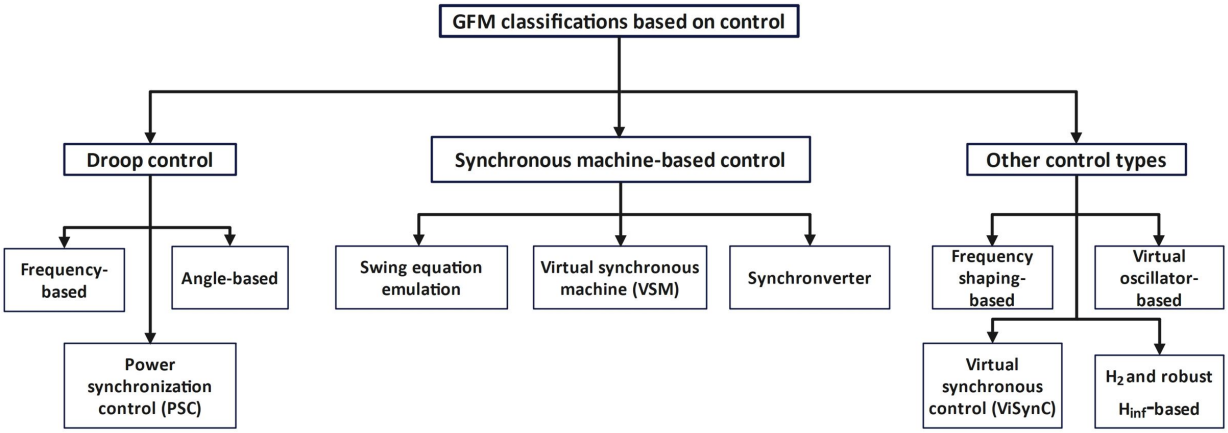


**Figure 2.8:** Typical single line diagram of inverter coupled with the grid and their respective network elements.

### Generalized model of GFM converters

The figure below represents a generalized control model of a GFM converter [40], [41]. As mentioned before the structure consists of different control levels such as an outer loop, responsible for power synchronization and voltage profile management, in addition to an inner loop where the modulation signal is calculated in order to form the output voltage of a GFM converter. The measured current and voltage at PCC are indicated as $i_{grid}$ and $u_{grid}$. Further inputs are the reference setpoint of active and reactive power $P_{set}$ and $Q_{set}$, along with the reference frequency $\omega_{ref}$ and the reference voltage $V_{ref}$. The outer control loop calculates the frequency $\omega$ and the rotor angle $\theta$, in addition to the amplitude $E$, of the virtual voltage source. The inner loop includes further control actions to produce the proper modulation signal $e$ for PWM. Based on the control approach the subsystems comprising power synchronization loop may differ and some are briefly analyzed.

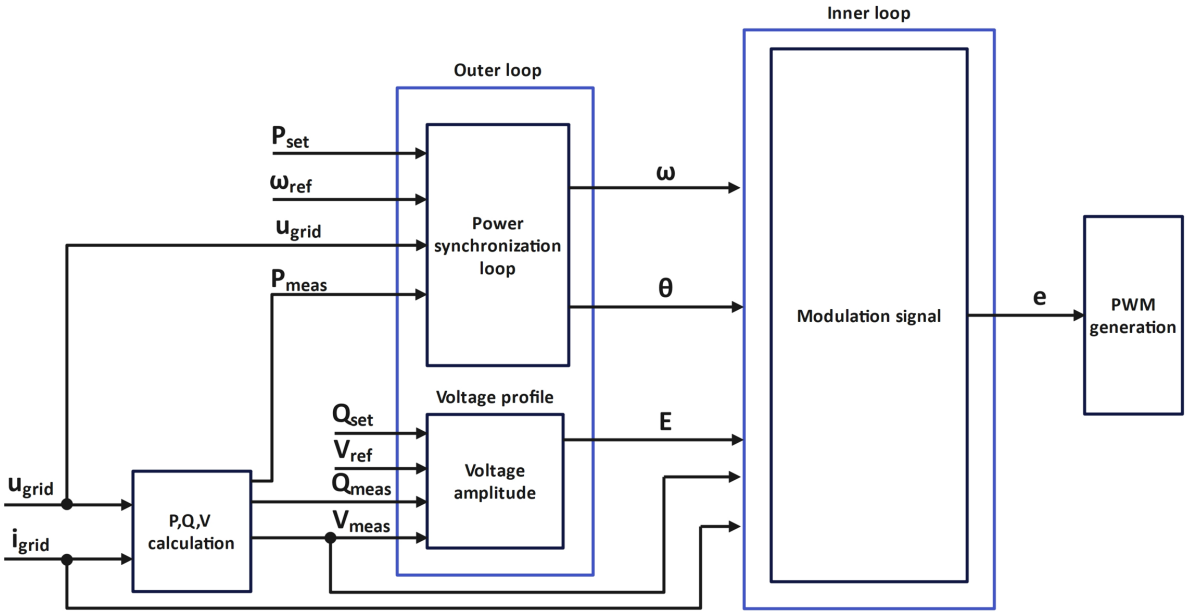


**Figure 2.9:** Generalized control model of GFM control with the respective subsystem level control loops.

### Droop Control

Droop control is one of the most mature control techniques with relative simplicity, while their concept originates from the governor action [49]. They were originally included in isolated AC power systems [50], but they are capable of operating in large interconnected power systems as well. Their reference values are based on the variation of measured active and reactive power and are used mainly assuming the grid impedance is inductive.

- Frequency based droop

Frequency droop control is based on the relationship between active power and frequency. The variation of the converter frequency $\Delta\omega$, is calculated based on the difference of the reference active power setpoint $P_{set}$ and the measured active power $P_{meas}$. The linear drooping relationship of decreasing frequency and increasing active power is represented by the droop coefficient $D_{coeff}$. Thus, as seen in Figure 2.10, the droop regulator expression (Equation 2.9) can be derived as:

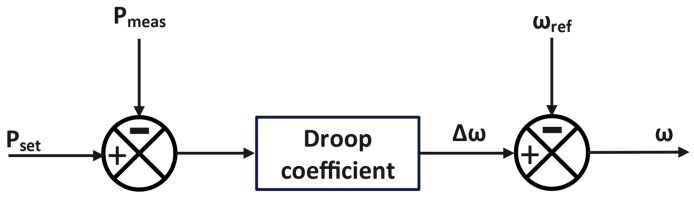


**Figure 2.10:** Frequency droop control block diagram.

$$\omega = \omega_{ref} - D_{coeff} \cdot (P_{set} - P_{meas}) \tag{2.9}$$

Likewise, the voltage droop can be implemented in the same manner, based on the voltage-reactive power relationship. The inner virtual voltage $E$, of the GFM converter is calculated as (Equation 2.10):

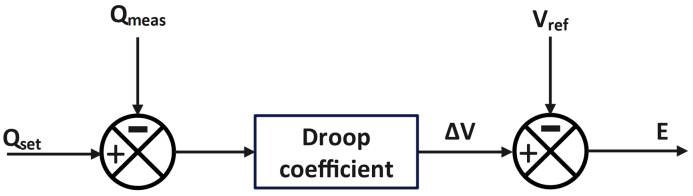


**Figure 2.11:** Voltage droop control block diagram.

$$E = V_{ref} - D_{coeff} \cdot (Q_{ref} - Q_{meas}) \tag{2.10}$$

where, $Q_{set}$ the reference reactive power setpoint, $Q_{meas}$ the measured reactive power. In order to attenuate high frequency components, the droop controller might operate in conjunction with a low pass filter.

- Angle based droop

The angle-based droop is similar in structure with frequency-based droop. However, by integrating Equation 2.9, the corresponding angle $\theta$ is obtained. The corresponding control equation is described as:

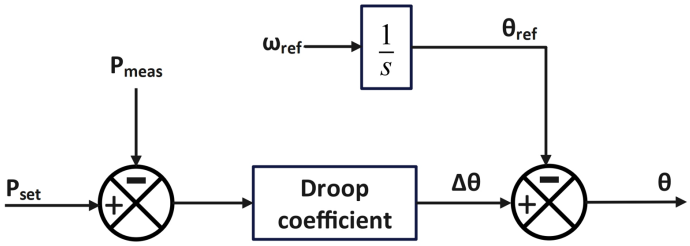


**Figure 2.12:** Angle based droop control block diagram.

$$\theta = \theta_{ref} - D_{coeff} \cdot (P_{set} - P_{meas}) \tag{2.11}$$

where, $\theta$ ref the reference angle as derived from the integration, $P_{set}$ the reference active power setpoint and the measured active power $P_{meas}$.

- Power synchronization control (PSC)

The PSC was initially proposed for HVDC applications and was developed in order to overcome the limitations of conventional synchronization methods (PLL) in weak AC systems [51], [52]. The power synchronization is achieved through emulation of SG power synchronization by means of transient power transfer, however, it is classified here due to the controller's resemblance to droop control. PSC again utilizes the phase angle, which is drooped based on power increment. Finally, it should be noted that even though under normal operation there is no requirement for a PLL unit, a back-up may be employed during severe grid faults, since there are certain limitations of the converter [52].

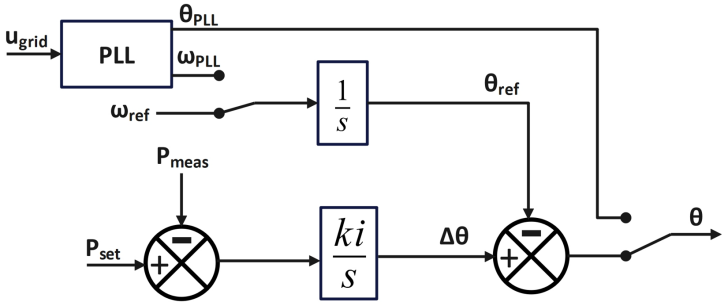


**Figure 2.13:** PSC block diagram.

The controller equation for deriving $\theta$ is described as:

$$\theta = \theta_{ref} + \frac{ki}{s} \cdot (P_{set} - P_{meas}) \tag{2.12}$$

where, $\theta_{ref}$ phase angle is obtained by integrating the reference signal $\omega_{ref}$. $P_{set}$ the reference active power setpoint and the measured active power $P_{meas}$ and $ki$ a control parameter.

### Synchronous Machine-Based Control

The control philosophy of synchronous machine-based control aims to emulate the dynamic behavior of a real SG, through power electronic components. Therefore, the new concept introduced called virtual synchronous machine (VSM) [46], [47], targets to implement a mathematical model describing SG dynamics by imitating their inherent characteristics. The different in complexity and accuracy models of representing a SG distinguish the different applications of VSM. Nevertheless, the basis of

a VSM model could include the stator windings, damper windings and excitation windings. Thus, the power synchronization control differs from one application to another. The primary concept though is that the machine currents are calculated based on measurement of grid voltage $u_{grid}$ at PCC, while the active and reactive power control is based on virtual inertia control and virtual excitation voltage respectively [40], [41].

- Swing equation emulation

The power synchronization loop in this mode is structured upon the principle of swing equation in Equation 2.4 where virtual inertia is emulated, while the damping effect is accounted too. The virtual inertia is supposed to be provided by units accommodating power reserve. For analyzing the dynamics, Equation 2.4 is expressed in terms of power by replacing torque multiplied with rotor frequency $\omega$. Thus:

$$\frac{d\Delta\omega_r}{dt} = \frac{1}{2 \cdot H} \cdot (P_{mech} - P_{el} - K_D \cdot \Delta\omega_r) \tag{2.13}$$

where, $\frac{d\Delta\omega_r}{dt}$ the RoCoF and $H$ the inertia constant as mentioned in section 2.2. $P_{mech}$ is mechanical power, but since VSM is analyzed, this term refers to the emulated mechanical power $P_{vir}$. $K_D$ is the damping coefficient and $\Delta\omega_r$ the difference between the virtual rotating speed and the reference speed. The virtual rotor angle $\theta$ of VSM can be derived from the integral of virtual rotating speed [53], [54]. The block diagram is illustrated in Figure 2.14.

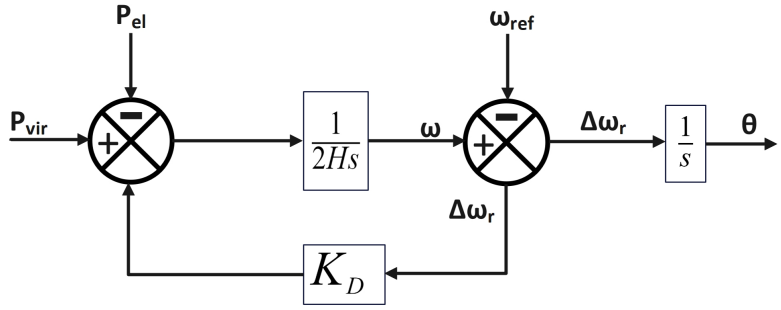


**Figure 2.14:** Block diagram of VSM emulating the swing equation.

- Synchronverter

Synchronverter is another approach for emulating a SG behavior. It entails a more sophisticated and detailed mathematical model of a machine, overcoming the need for a synchronization unit first proposed in [48], [55], including in addition parameters such as, damping, field inductance and mutual inductance [40]. The output of the controller is the frequency and angle based on virtual rotor motion, and the power synchronization is based on Newton's second law:

$$J\alpha(t) = T_m(t) - T_e(t) - D \cdot \omega(t) = T\alpha(t) \tag{2.14}$$

where, $J$ is the moment of inertia and $D$ the damping coefficient, which can be readily tuned based on the steady-state P-$\omega$ droop thus, the desired virtual inertia is provided. $T_m$ is the mechanical torque, in case of a converter, the virtual mechanical torque, and $T_e$ the electromagnetic torque. Finally, $\omega$ the virtual mechanical angular velocity and $T_a$ the acceleration torque. The synchronverter's virtual rotor angle $\theta$ is the output. If the grid's frequency is $\omega_{ref}$, thus $\theta_{ref}$ its rotor angle, then power angle $\delta = \theta - \theta_{ref}$ [40], [31]. The principle is illustrated in Figure 2.15.

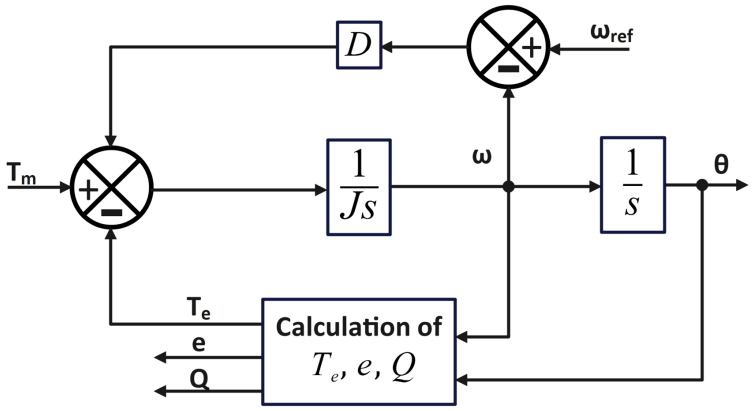


**Figure 2.15:** Block diagram of active power loop power synchronization of synchronverter.

As it is seen from the figure, the more detailed model of a synchronverter includes $T_e$ , $e$, $Q$, the electromechanical torque, the back electromotive force represented by the internal virtual voltage of the converter and reactive power. The above can be calculated as:

$$T_e = M_f \cdot i_f \cdot i\alpha \cdot cos(\theta - \phi) \tag{2.15}$$

$$e = \omega \cdot M_f \cdot i_f \cdot sin(\theta) \tag{2.16}$$

$$Q = \omega \cdot M_f \cdot i_f \cdot i_\alpha \cdot sin(\theta - \phi) \tag{2.17}$$

where, $M_f$ is the mutual inductance between the excitation winding and the stator winding, if the excitation current, $i_\alpha$ the stator phase currents, $\theta$ the rotor angle and finally $\phi$ the phase angle.

### 2.5.1 Comparison of Different GFM Controls

To develop GFM controls, there are different ways as each control has its own properties. On the basis of key features such as ,PLL for synchronization, tunable virtual inertia, communication-less control, dispatchability and overcurrent protection, various GFM controls have been assessed as shown in the following table [40].

| Category | Control structure | Tunable virtual inertia | PLL for synchronisation | Overcurrent Protection | Communication less | Dispatchable |
|---|---|---|---|---|---|---|
| Droop Based | Frequency Droop | × | √ | √ | √ | √ |
| | Angle Droop | × | √ | √ | × | √ |
| | PSC | × | √ | √ | √ | √ |
| Synchronous machine-based control | VISMA | √ | √ | √ | √ | √ |
| | VSG | √ | √ | √ | √ | √ |
| | Synchronverter | √ | √ | × | √ | √ |
| | eSM | √ | × | √ | √ | √ |
| Other topologies | VOC | √ | × | × | √ | × |
| | H2/Hinf | √ | √ | √ | × | √ |
| | ViSynch | √ | × | √ | √ | √ |
| | Frequency shaping | √ | √ | × | × | √ |

**Table 2.2:** Comparison of various GFM controls.

Since the project focuses more on frequency dynamics, provision of virtual inertia becomes an important parameter of GFM control. As compared to synchronous generators, virtual inertia is a control feature for GFM, and hence GFM converter control has the ability to adjust the inertia based on the needs of designer. The assessment also reveals that virtual inertia is not supported by droop-based, as they are mostly controllers of high bandwidth, however, the SM-based control can provide virtual inertia and is the focus of the project [40].

## 2.6 GFM Control & WT Generators

A major limitation that might be presented is the amount of energy that can be extracted from the WTG. Under the assumption that the GSC is a GFM converter, during a frequency disturbance it must support any increase or decrease in power. Subsequently, the disturbance will provoke the MSC to respectively regulate power in order to maintain steady DC-link voltage. In this way, the WTG will be coupled to system disturbances [21], [54].

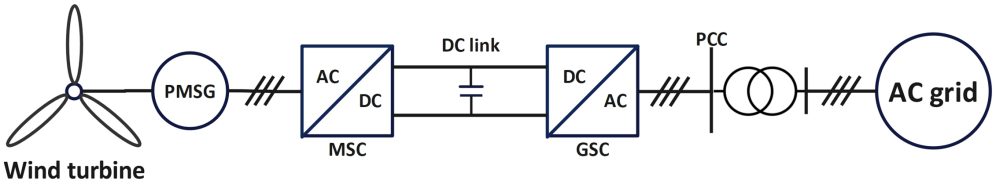


**Figure 2.16:** Type IV WTG in GFM mode under synchronization.

However, the dependability of WTs on wind conditions creates certain issues, that should be considered. A low wind speed WT subjected to negative RoCoF will have limited contribution, since there won't be energy stored in the WTG rotor. Likewise, during low wind speed and positive RoCoF, energy cannot be accumulated by the WTG rotor since it is close to cut-off speed [17], [56]. As per Figure 2.16, the only source to accommodate some energy would be the DC-link capacitor. However, additional energy could be acquired by curtailment of WTG, or similarly by following the deloading curve [17], [57].

According to [17], [58] a backup energy reserving scheme is a requirement for GFM-based WTs. In this fashion also, the WTG can follow the MPPT curve. Excess wind energy could be stored in the energy storage system (ESS) (e.g., Battery ESS), while it could be also used to support grid frequency.. As per the literature [58], [14] there could be two possible ways of connection and control of an ESS unit, as illustrated in Figure 2.17.

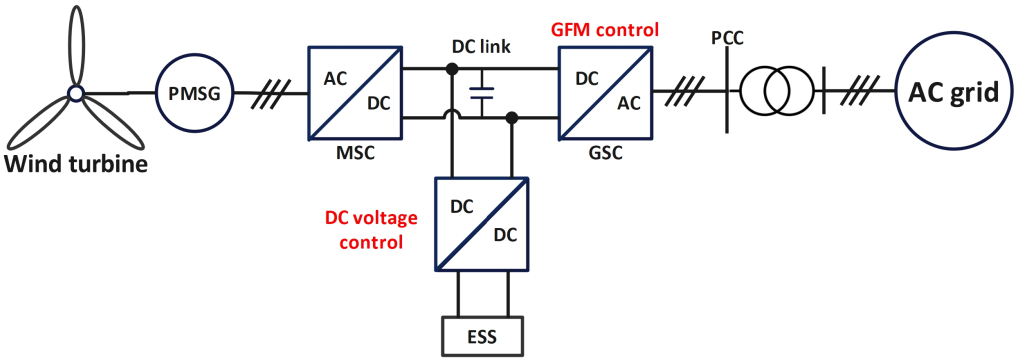


**(a)** Inner energy storage system on the DC-side.

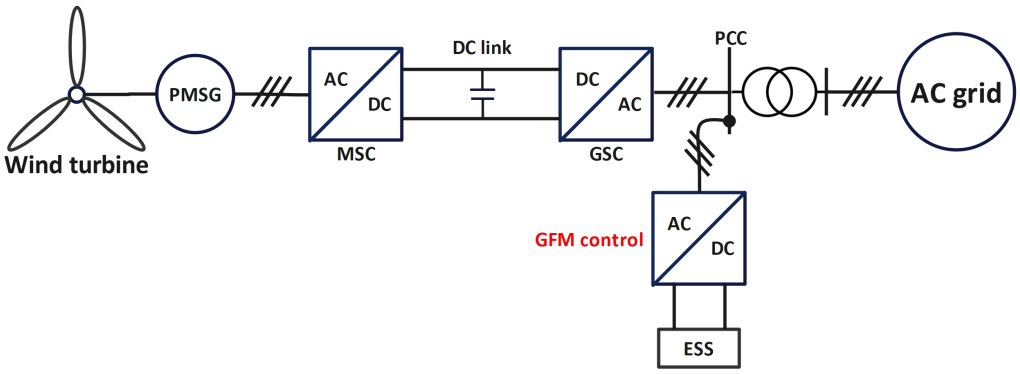


**(b)** Outer energy storage system on the AC-side.

**Figure 2.17:** Potential ESS connection on either AC or DC side of converter for GFM-based WTG.

As per Figure 2.17a, when the ESS is added on the DC-side, the GSC would be controlled as a GFM converter regulating active power injection to the grid and establishing the voltage at the converter terminals. The MPPT control could be performed on the MSC, while the DC-link voltage is controlled by the ESS DC/DC converter [58], [14]. However, this scheme may be limited by the capacity of the ESS since it should be a unit able to fit inside the WT, while it can damp the power supplied by the GFM converter.

In Figure 2.17b, the GFM control could be applied on the separate unit for frequency support. The injection of power to the grid would be the summation of WTG power and ESS power.. However, this application would require a large capacity of ESS, but spatial restrictions could be less [58]. Details about the choice of architecture for the project purpose will be discussed in the upcoming chapters.

## 2.7 Energy Storage Systems

ESS have gained more popularity on the market over the years, especially as the penetration of RES increases drastically. There are many reasons why ESS could be beneficial in wind power [59], [60], with a primary goal to account for an imbalance between energy demand and generation. Generally, power fluctuations from RES could be a challenge, however, their integration could be aided by energy storage devices which can improve power quality and reliability [61]. Specifically in wind generation, during high wind power but low demand, excess energy could be stored. In case of low wind power while demand is high, energy could be provided by storage. Nevertheless, according to the application requirements the selection of ESS may vary, but there are certain key characteristics to be considered. These key characteristics are immediately coupled with ancillary services provision [62]. These services refer to functions that enable the system operators to maintain a stable grid with

continuous power flow, addressing imbalances between generation and demand. The classification of different ESS based on rated power and discharge time is illustrated in Figure 2.18 [63].

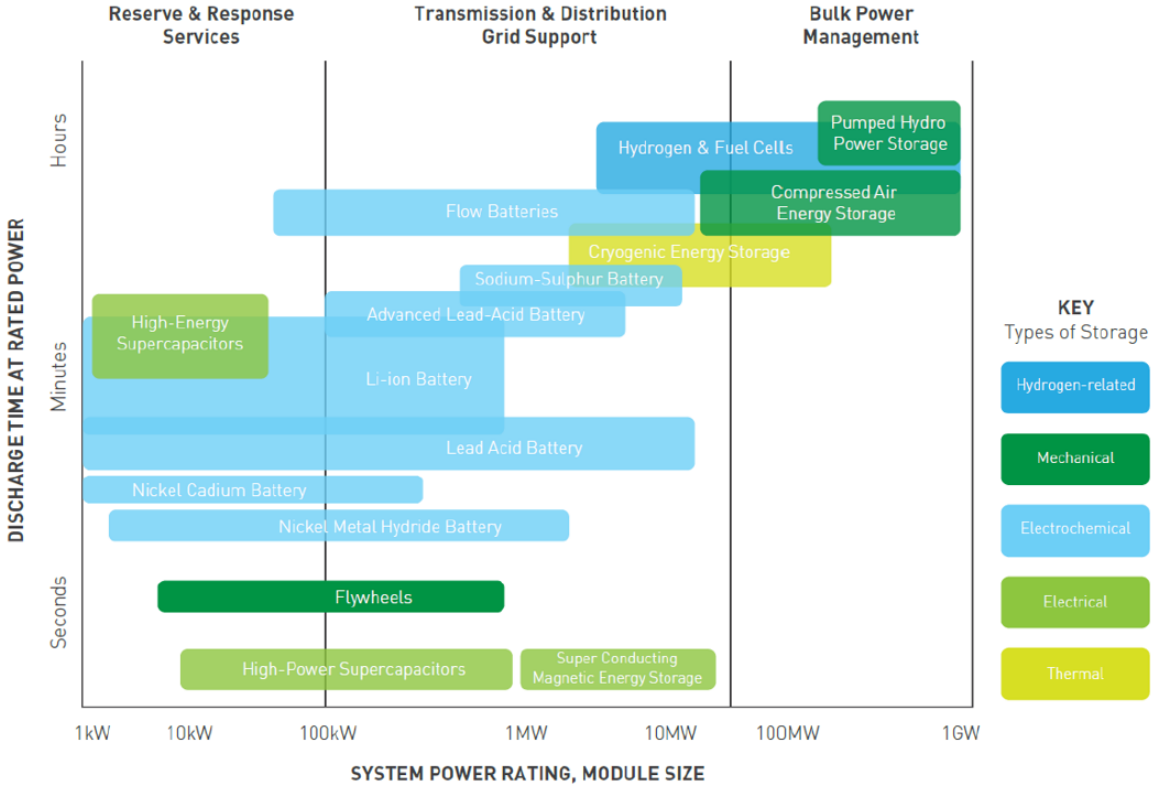


**Figure 2.18:** Rated power versus discharge time of different ESS for ancillary services.

From the figure, it can be seen that supercapacitors, super conducting magnetic energy storage (SMES), flywheel energy storage (FES) and batteries could be suitable for grid support at transmission and distribution levels. However, power and energy levels are not the only parameters for consideration. ESS suitability for a given ancillary service depends on other important parameters as well, such as specific power, specific energy, and efficiency, with a comparison of the aforementioned ESS presented in Table 2.3 [64].

**Table 2.3:** Characteristics of ESS suitable for transmission and distribution levels.

| Parameters | Supercapacitor | SMES | FES | Batteries |
|---|---|---|---|---|
| Specific energy (Wh/kg) | 2.5-15 | 0.5-75 | 5-100 | 75-200 |
| Specific power (W/kg) | 500-10000 | 500-2000 | 400-1500 | 150-2000 |
| Efficiency (%) | 85-97 | 95-98 | 90-95 | 90-97 |
| Self-discharge (%/day) | 5-40 | 10-15 | 100 | 0.1-0.3 |
| Discharge time | ms-s | ms-min | s-min | min-h |

Specific power describes the ability of the ESS to provide instantaneous power, while specific energy is their ability to provide continuous energy over longer periods of time. High specific power and specific energy, reflect on the ability of ESS to discharge a large amount of power, and energy for long periods respectively. Ideally, an ESS should be able to have both of its features at high levels, however, as per Table 2.3, usually ESS units with high specific power tend to have lower specific energy known as short-term storage. On the contrary, ESS with higher specific energy tend to have lower

specific power, described as long-term storage. Discharge time refers to the energy capacity-power rating ratio (E/P), meaning the duration a module can operate while delivering its rated output.

Regarding ancillary services provision for frequency stability, these characteristics play a crucial role while considering the different time frame each service takes place. For instance, FFR which requires high power for a short duration for synthetic inertia provision, a high specific power ESS would be more suitable, whereas frequency regulation in larger time frames could be accommodated by a high specific energy ESS.

## 2.8 Summary

Chapter 2 begins with power system stability and its different classifications. A glimpse into the frequency regulation and frequency response activation time are covered here. Section 2.2 begins with SGs and its basic control block. The basic mathematical equations of SGs during a power imbalance and the swing equation is derived. The inverse relationship between inertia and RoCoF is also coned in this subsection. Section 2.3 begins with converter control algorithms of GFL and GFM. The section begins with a detailed explanation of GFL type IV WT and its control system. Then, the difference between GFL and GFM covering the working principle and basic phasor diagrams during an event. As it was also examined through literature, the droop based GFM converter control cannot emulate and act on inertia, while the swing equation emulation algorithm can. Thus, the thesis also starts focusing its attention on VSM, a swing equation emulation based GFM control which will be used throughout the project. Section 2.5 gives a brief explanation of the advantages and challenges in operating WT in VSM mode. It is also briefly explained, the need for ESS and two possible architectures from various literature that can support the power system stability. Section 2.6 covers the ESS part of thesis. Different ESS technologies and parameters that are necessary are covered in this subsection. The thesis does not focus its attention on a specific ESS technology, however, will consider a generic ESS concept to model it and analyze the impact on frequency stability.

# Chapter 3

# VSM Control Evaluation & ESS Sizing Methodology

Chapter 3 will begin with a simplified power system which will be used to evaluate the performance of a WPP in VSM mode. The thesis uses DIgSILENT PowerFactory to analyze the frequency dynamics. From the previous section 2.4, it has been addressed that focus of interest will be VSM, while its control architecture is explained. To implement the VSM and analyze its impact for different system disturbances, various power system scenarios will be explained. Low RoCoF and high RoCoF events occurring in the power system and how it affects the VSM response differently will be analyzed. The chapter will conclude with introduction and need for ESS in the power system. The methodology and sizing of ESS will be explained. The ESS is also operating in VSM mode. The frequency response of the new power system with the addition of ESS owing to system disturbances will be evaluated.

## 3.1 Simplified Power System Model

This chapter will explain the dynamic response of wind turbine operating in GFM mode. As depicted in Figure 3.1, a simple power system architecture is used to evaluate the dynamic response of WT operating in GFM subjected to various system disturbances. The response from the WT will be analyzed and explained in detail.

The architecture consists of a wind farm with 23 WTs, with Type IV converter. Each of the wind turbines is rated at 3 MW. Thus, the entire output of wind farm is 69 MW/ 78 MVA [17]. The model has used an aggregated representation of the wind farm in DIgSILENT PowerFactory. The wind turbine is operating in GFM mode. The model initially considers only the wind farm to be the sole generation source and is feeding a load of 120 MW. The model consists of an external grid with short circuit power of 1800 MVA, inertia constant of 10s and X/R ratio of 10, thus representing a strong grid [18]. DIgSILENT PowerFactory uses a voltage source and an internal impedance to model the external grid. A synchronous machine's equivalent mechanical equations are used. The combined inertia of all synchronous machines in the system is represented using the acceleration time constant [65]. The parameter ratings of different elements are summarized in Table 3.1.

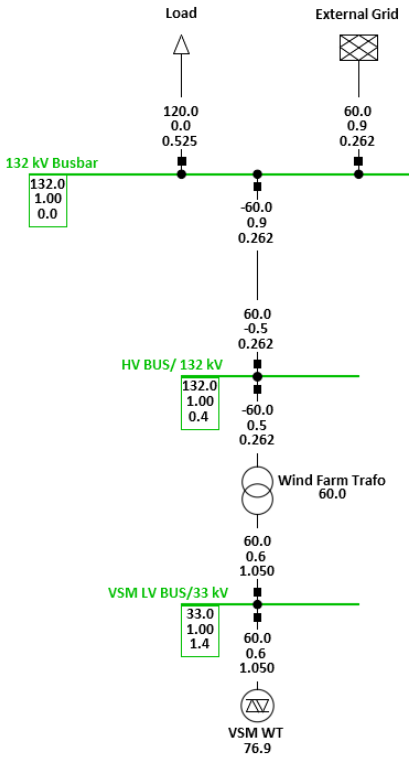


**Figure 3.1:** Simple system model for evaluation of VSM.

**Table 3.1:** Ratings of the component elements used in the current architecture.

| Components | Voltage (kV) | Rating (MVA) | Inertia (s) | Short circuit power (MVA) | Active power (MW) |
|---|---|---|---|---|---|
| External grid | 132 | 350 | 10 | 1800 | 51 |
| VSM WT | 33 | 78 | 4 | - | 69 |
| Transformer | 132/33 | 100 | - | - | - |
| Line | 132 | - | - | - | - |
| Load | 132 | - | - | - | 120 |

To understand the dynamic response of WT operating in GFM mode when subjected to system disturbances, it is quite important to understand the control aspects of GFM converter. Different classifications of GFM converters were explained in chapter 2, section 2.3. This project will focus its attention on implementing a GFM control based on swing equation emulation called virtual synchronous machine. Using this control scheme, the IBPS can emulate the behavior of a synchronous machine [40].

## 3.2 Control System of VSM

The control system that is used to emulate the synchronous machine behavior is a VSM where the block diagram in PowerFactory is depicted in Figure 3.2 and consists of: a voltage regulator, an SG model, a current limiter, and all of them comprise the generator model.

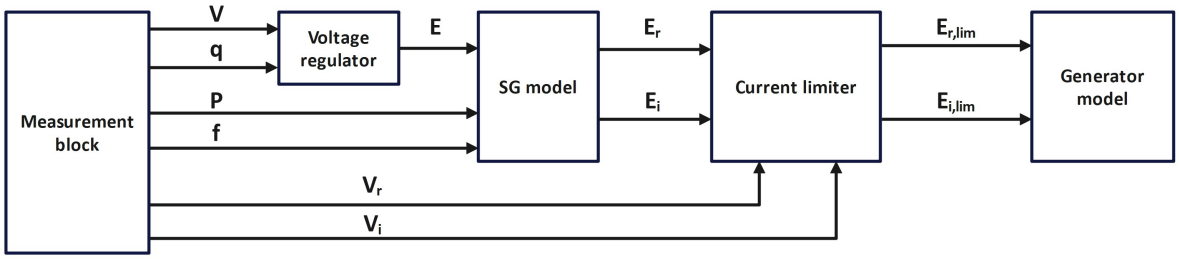


**Figure 3.2:** Control block diagram of VSM in PowerFactory.

Where, $V$ the measured voltage, $q$ the measured reactive power, $P$ the measured active power, $f$ the measured grid frequency, $V_r$ and $V_i$ the real and imaginary part of voltage component, $E$ the converter voltage with $E_r$ and $E_i$ its real and imaginary component, $E_{r,lim}$ and $E_{i,lim}$ the limited voltage reference sent to voltage source.

### Generator Model

To represent non-rotating generators like full scale wind turbines, a static generator model in PowerFactory is used as shown in Figure 3.3 [65].

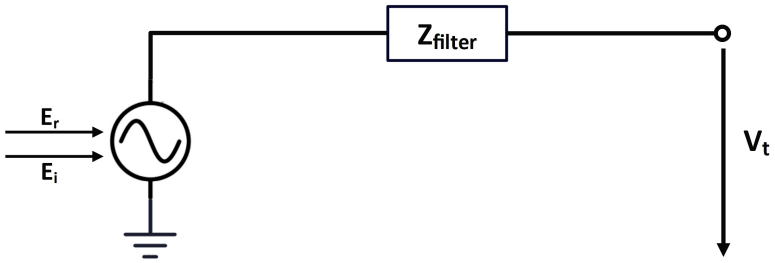


**Figure 3.3:** Schematic of the voltage source model of a static generator in PowerFactory.

### SG Model

SG block is used to obtain damping response and inherent inertia. It mimics the machine dynamics of a typical synchronous generator. SG model's block diagram implemented in PowerFactory is illustarted in Figure 3.4.

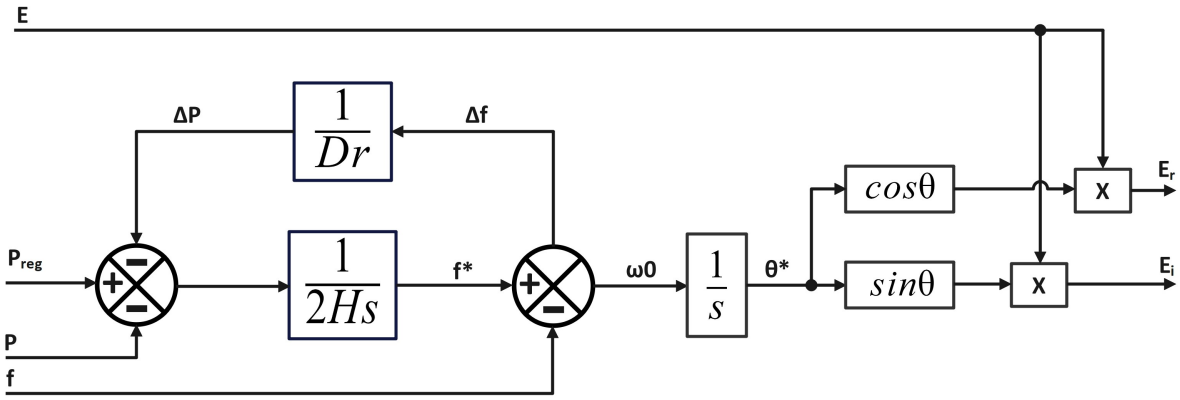


**Figure 3.4:** Block diagram of SG model implemented in PowerFactory.

As per the block, when there is a difference between $P_{reg}$ the reference power, and $P$ the measured output power, then an error prevails. This error is taken as input by the integrator term $(1/2Hs)$, where $H$ is the inertia constant. Output from the integrator term gives the estimated system frequency $f^*$. PLL block from Powerfactory is used to measure the system frequency $f$ [53].

Frequency deviation is given by the difference between the system frequency and measured frequency. If a frequency deviation exists, then damping term $K_d = \frac{1}{D_r}$, is added to the summation of power block. The damping term will hold a value of zero during steady state condition, but in the event of disturbance, $E_r$ the real part of AC voltage vector, and $E_i$ the imaginary part of AC voltage vector rotates based on $\theta^*$. So, the $\theta^*$ will not rotate if the system is in steady state and can provide necessary power $P_{reg}$. Owing to this, $\theta^*$ could be treated same as rotor angle of synchronous generator [53][66].

Rotor angle $\theta^*$ is given by the equation:

$$\theta^* = \frac{\omega_0}{s} \cdot [\frac{1}{2Hs} \cdot (P_{reg} - P - K_d \cdot \Delta f)] \tag{3.1}$$

For small disturbances, it can be linearized as:

$$\Delta\theta^* = \frac{\omega_0}{s} \cdot [\frac{1}{2Hs} \cdot (\Delta P_{reg} - K_s \Delta\theta^* - \frac{\Delta\theta^*}{\omega_0} s K_d)] \tag{3.2}$$

The electrical power output can be expressed as:

$$\Delta P = (\frac{dP}{d\theta^*}) \cdot \Delta\theta^* = (\frac{EV}{X_{tot}}) \cdot \cos(\theta^*) \cdot \Delta\theta^* = K_s \Delta\theta^* \tag{3.3}$$

Where, $E$ is the converter voltage, $V$ the external system voltage, and $X_{tot}$ is the total reactance in between the two bus voltages. Ks is known as the synchronising power coefficient [53], [66]. The two control blocks of voltage regulator and current limiting block are illustrated in Appendix A1. Knowledge of the SG control block is essential to understand the role of inertia and damping parameters and how the VSM provides it and is explained in SG Model.

## 3.3 Simulation Scenarios

### 3.3.1 Low RoCoF Events

For simulating low RoCoF events, the model explained in Figure 3.1 is used. The active power of the WT operating in VSM mode is set to 50 MW. The inertia constant of the VSM is set to 4s and Droop is 5%. In this scenario the project uses Siemens Gamesa direct drive D3 wind turbine. Data sheet of WT is attached in Appendix A.

Depending upon the initial rotor speed, the additional power from the extracted kinetic energy of WT can be released into the grid following a disturbance. Considering a negative RoCoF event, due to a decline in RPM (revolutions per minute), the change in rotor kinetic energy can be calculated as in [67]:

$$\Delta E = \frac{1}{2} \cdot J \cdot (\omega_0^2 - \omega_1^2) = \frac{1}{2} \cdot J \cdot (2 \cdot \omega_0 \cdot \Delta\omega + \Delta\omega^2) \tag{3.4}$$

Where J is rotor inertia in $Kg \cdot m^2$ and $\Delta\omega$ is change in rotor speed, where the power released can be calculated as:

$$\Delta P = \frac{\Delta E}{\Delta t} \tag{3.5}$$

in addition to:

$$P_{wind} = \rho \cdot v^3 \cdot A \tag{3.6}$$

where, $\rho$ the air density, $v$ the wind velocity, $A$ the swept area of D3 wind turbine, while Equation 3.6 calculates the available wind power. Equation 3.7 is used to calculate the output power of wind turbine.

$$P_{output} = \mu \cdot P_{wind} \tag{3.7}$$

where, $\mu$ the efficiency coefficient. Finally, Equation 3.8 can be used to calculate the RPM of wind turbine for the use active power:

$$RPM = 60 \cdot v \cdot (\frac{TSR}{Pi \cdot D}) \tag{3.8}$$

where, $TSR$ the tip speed ratio, and $D$ the diameter of the blades. The calculations yield an RPM for wind turbine close to 13 RPM before the event. Though the wind turbine mechanical dynamics have not been modelled, they have been computed using the Equations 3.4, 3.5 and 3.6. Considering a constant wind speed and knowledge of wind turbine parameters has helped the project calculate the inertia constant of WT. For a rotor speed of 13 RPM and mechanical parameters of 3 MW wind turbine and assuming a constant wind speed, energy stored in the rotor is calculated approximately to give and inertia constant of 4s. Low RoCoF events were created in the power system and dynamic response of the VSM was observed as shown in Figure 3.5.

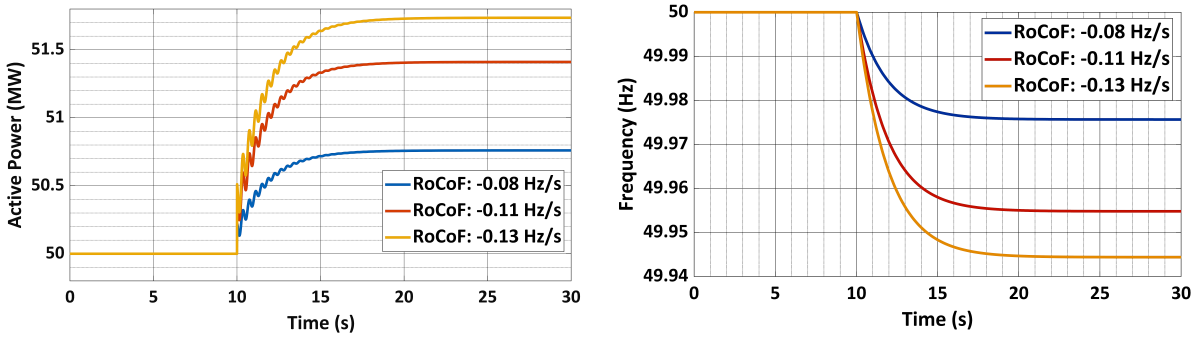


**(a)** Active power response of VSM for low RoCoF events.

**(b)** Frequency response of VSM for low RoCoF events.

**Figure 3.5:** Response from VSM WT.

Taking an example of -0.11 Hz/s RoCoF event, the calculated values correspond to approximately 1.2 MW, which can be obtained by rearranging the swing equation (Equation 2.3), and the simulated response in PowerFactory is approximately 1.3 MW . The case is also similar for other lower RoCoF events as the response from the wind turbine is also of the order of 600 kW - 1.3 MW. To understand the implication of smaller responses on WT the following equations must be analyzed.

Considering the case for -0.11 Hz/s event, using the Equations 3.5 and 3.6, the reduced RPM can be calculated and approximated. For the events with different lower RoCoF, corresponding new RPM post the event has been calculated as shown in Table 3.2.

**Table 3.2:** RoCoF and RPM table.

| RoCoF (Hz/s) | RPM before event | RPM after event |
|---|---|---|
| -0.08 | 13 | 12.88 |
| -0.11 | 13 | 12.76 |
| -0.13 | 13 | 12.71 |

The calculated results clearly show that during low RoCoF events, the response from VSM is small. Though the turbine mechanical dynamics was not included in the model, the mathematical

approximations were used to calculate the resultant drop in RPM during low RoCoF events. The results clearly show that RPM reduction in rotor is really small and insignificant. Considering the case -0.11 Hz/s event, the entire farm was responding close to 1.2 MW, meaning since there are 23 WTs, each turbine is responding approximately 53 kW for 5s or 265KJ.

### 3.3.2 High RoCoF Events

For analyzing the dynamic response of VSM during a high RoCoF event a step load increase of approximately 25 MW is given to the load. The inertia constant is set to 8s [17] and the active power output of WPP in steady state is reduced to 22 MW. This is done such that, as the inertia is increased in the VSM, during an event, the response from VSM will also be larger due to increased inertia. Hence the active power has been reduced, which could imply a curtailed operation of WPP, and the response is as shown in Figure 3.6.

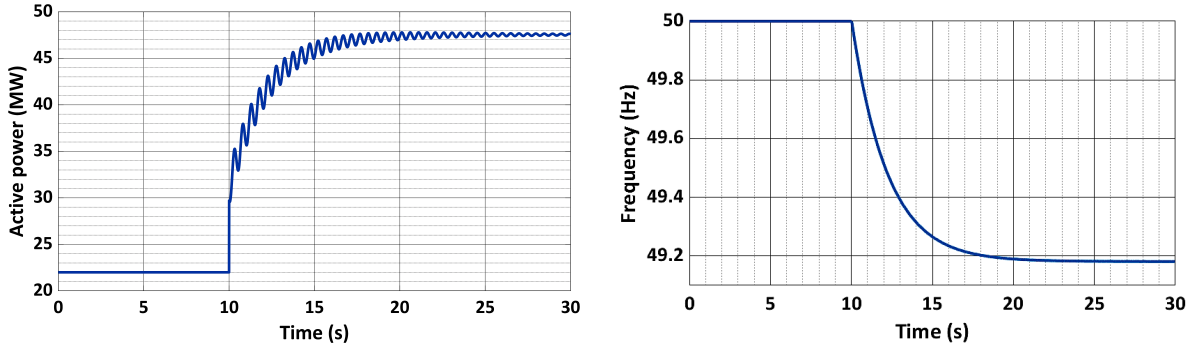


**(a)** Active power response of VSM for high RoCoF event.

**(b)** Frequency response of VSM for high RoCoF event.

**Figure 3.6:** Response from VSM WT for -1Hz/s RoCoF.

The response from the VSM clearly shows that during such high RoCoF events such as -1 Hz/s, each of 23 WT converters tries to respond with approximately 1 MW each. This response will have a significant decrease in rotor speed. The rotor speed is initially considered to be 13 RPM and using the Equations 3.4, 3.5 and 3.8 the reduced rotor speed is calculated to be 10.71 RPM. This reduction in rotor speed results in reduction of reference power [17].

Though not simulated, field experiments from Siemens Gamesa during 2019 reveal that such reduction rotor speed can also cause the turbine to produce reduced power during post event recovery period The situation can get even difficult when the wind conditions are fluctuating and different turbines in farm experience different wind speeds [17].

The simulation results reveal that considering severe events such as low wind speed and high RoCoF events, without additional energy storage, operating with higher values of inertia can be problematic in terms of appropriate response. The impact of adding ESS and the architecture used will be explained in the next chapter.

## 3.4 VSM & ESS

As discussed in Chapter 2, section 2.4, there are two major ways of integrating an ESS with the WTs. The first architecture 2.17a, where the ESS is connected to the DC side and GSC would be operating in VSM mode, while the second architecture referred to as architecture 2.17b, where the ESS is connected as a shunt to the main converter. The project has decided to use architecture 2.17b to represent and model ESS for the following two reasons:

- It is not recommended to connect anything to DC link of main power converter as it can create reliability challenges to the power flow from main converter to the grid.
- Power electronic hardware will have to be modified or additional components may be needed to supply the additional fault currents [14].

The project shall use architecture 2.17b hereafter to model the ESS operating in VSM mode and will be used to evaluate the dynamic response from ESS.

### 3.4.1 Methodology for ESS Sizing

Prior knowledge of system parameters such as power system rating and power system inertia are needed to size the required ESS. The term ESS will be used hereafter to represent a generic ESS and not a specific category of ESS as the aim of the project is to develop a generalized strategy to size the ESS required for the power system. The project uses the power imbalance $(\Delta P)$ and RoCoF to size the ESS and the sizing is used to provide inertial response (IR) service. This frequency service is categorized with high power and low energy with a capacity of fast response for a short duration of 5s. In later chapter requirement for PFR is also examined. Other frequency responses such as secondary frequency response and tertiary frequency response are considered out of scope for the project.

### 3.4.2 Inertial Response & Frequency Contribution

The power system under study for sizing the ESS is explained in section 3.1. However, to get a more realistic response two SG are used to represent the external grid. The SGs use a governor and an automatic voltage regulator controller presented in the Appendix A1. Worst case contingencies are considered while planning the power system [18]. A loss of a SG producing 40 MW in steady state, is assumed to plan and size the ESS. Based on a derivative control, the IR control of ESS is designed upon [68]. By reformulating the power swing equation, the IR contribution of ESS can be derived as:

$$H_{ESS} = P_{IR} \cdot \frac{f_0}{2} \cdot \frac{1}{RoCoF} \tag{3.9}$$

where, $H_{ESS}$ the inertia constant of ESS, $f_0$ the nominal frequency, and $P_{IR}$ the inertial power with max value of 1 p.u. The inertial power from the ESS is proportional to the RoCoF and can now be approximated as:

$$P_{IR} = K_{IR} \cdot RoCoF \tag{3.10}$$

where, $K_{IR}$ is a control gain. As the architecture is planning to use more than 50% of renewables penetration, which according to ENTSO-E requirements for RoCoF, should be 2 Hz/s [1], and for the ESS to provide nominal power for a RoCoF of 2Hz/s, the $K_{IR}$ should be 0.5. The inertia constant of ESS depends on the control gain of IR, and for $P_{IR} \leq 1 p.u.$, the $H_{ESS}$ can be approximated as:

$$H_{ESS} = \frac{f_0}{2} \cdot K_{IR} \tag{3.11}$$

Hence, the $H_{ESS}$ is calculated to be 12.5s, and will be used here to make a generalized ESS sizing approach. The ESS in this section designed only to provide IR and according to:

$$H_{sys} = \frac{\sum H_i \cdot S_i}{S_{sys}} \tag{3.12}$$

where, $H_{sys}$ the system inertia, and $H_i$ the inertia of $i_{th}$ unit, $S_i$ the nominal rating of $i_{th}$ unit, $S_{sys}$ the total power system rating. The initial power system comprises of two SGs (SG1, SG2), details of SGs are presented in Table 3.3. To incorporate the penetration of 50% of renewables, SG2 is replaced with a WPP operating in VSM mode and the parameters of WPP are given in Table 3.3.

**Table 3.3:** Parameters of system required for ESS sizing.

| Unit | Rating S (MVA) | Droop R (-) | Inertial constant H (s) |
|---|---|---|---|
| SG1 | 360 | 0.05 | 10 |
| SG2 | 78 | 0.05 | 6 |
| WPP | 78 | 0.05 | 4 |

The inertia of the power system, before the 78 MVA WT was introduced was calculated to be 9.2s. After, the inertia of the system was reduced. The WT is operating in VSM mode and is assumed to provide an inertia of 4s. The new system inertia after the introduction of WT is 8.9s. The major contingency $\Delta P$, for which ESS is designed is 40 MW. The sizing of ESS for the given parameters are:

$$S_{ESS} = S_{PS} \cdot \frac{H_{target} - H_{PS}}{H_{ESS} - H_{target}} = 30.8MW \tag{3.13}$$

where, $S_{PS}$ the rating of the power system after the contingency, $H_{target}$ the target inertia calculated based on the corresponding contingency, $H_{PS}$ the system inertia after the event.

The power injected into the grid due to inertia response is $P_{IR}$ represented with a maximum value of 1 p.u. and when multiplied with $S_{ESS}$, gives the power injected into the grid and is given by:

$$P_{ESS} = S_{ESS} \cdot P_{IR} \tag{3.14}$$

Considering the charging and discharging efficiency, the power injected into the grid, now referred as $P_{Eff}$ is given by [68]:

$$P_{Eff} = \frac{P_{ESS}}{\mu_d} \tag{3.15}$$

$$P_{Eff} = P_{ESS} \cdot \mu_c \tag{3.16}$$

where, $\mu_d$ the discharging efficiency and $\mu_c$ the charging efficiency of the ESS unit. When $P_{Eff} \geq 0$ the ESS gets discharged, while $P_{Eff} \leq 0$ it gets charged.

Another important property to consider for an ESS, is its state of charge (SoC). The power injected/absorbed will have an impact on the SoC of ESS. The relationship between initial SoC, final SoC and the effective power is given by:

$$SoC = SoC_{initial} - \frac{\int (P_{Eff})dt}{E_{ESS}} \cdot 100 \tag{3.17}$$

The project will consider the SoC range between 0 and 100 % and though there are multiple methods to reestablish the SoC every time after the ESS has provided service, the reestablishing strategy of SoC is not considered in this thesis [69], [70].

## 3.5 High RoCoF Event & Low Wind Speed Scenario

In section 3.3 a high RoCoF event was simulated and the challenges with operating the WT/farm in VSM mode was discussed. The chapter also concluded with the need and usage of ESS to address those challenges.

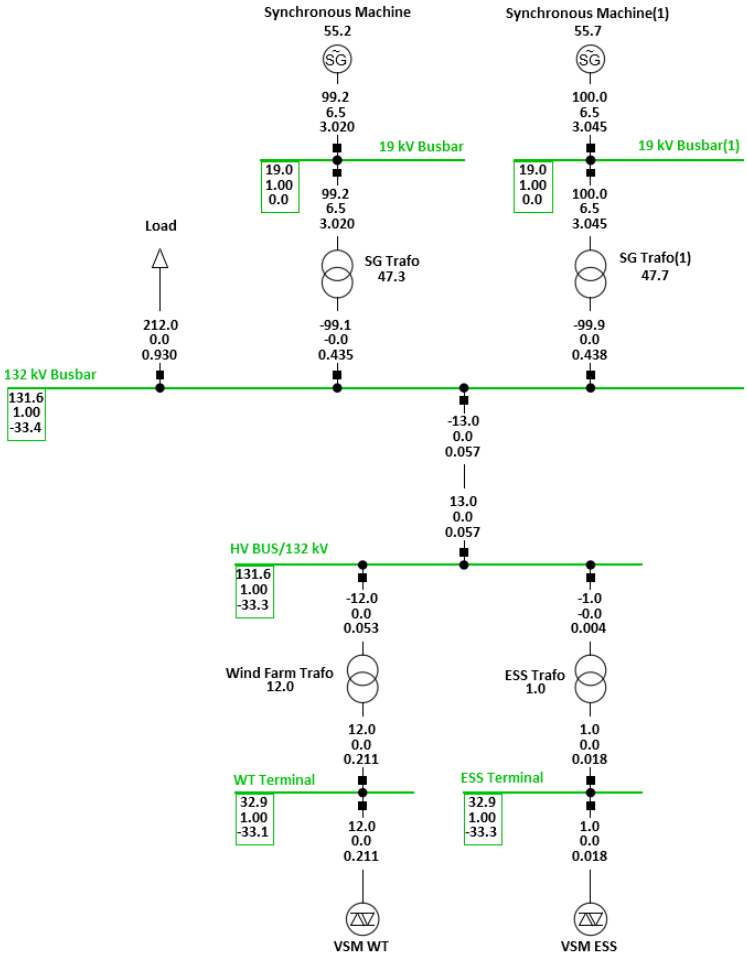


**Figure 3.7:** Architecture used for sizing of ESS.

The required ESS has been sized based on the equations and procedures as explained in the previous section. The architecture described implemented in PowerFactory can be seen in Figure 3.7. From Figure 3.8, the impact of adding the ESS into the power grid can be seen. There is a significant reduction in the inertial response from WT operating in VSM mode. In the absence of ESS, the WT operating in VSM mode had to provide the inertial response and the effect of inertial response on rotor speed reduction has been addressed before. Now with addition of ESS, while being the main contributor of inertia with 12.5s, the inertial response from WT is reduced significantly. A main point to understand is that the project uses the ESS to operate in VSM mode, as enabling the controller to operate in this mode, has multiple advantages such as operating in weak grid, emulate inertia and facilitate operation during islanding condition and support black start [30]. Though many of these parameters are not addressed and are out of scope the project, the project emphasize on provision of inertia from converter control by operating in VSM mode. The basic architecture is used to size the ESS and observe the response from ESS during a high RoCoF event and it can be seen in Figure 3.8 that the ESS provides close to 12 MW in the initial few seconds of event, and it can be calculated and

verified using Equation 2.3.

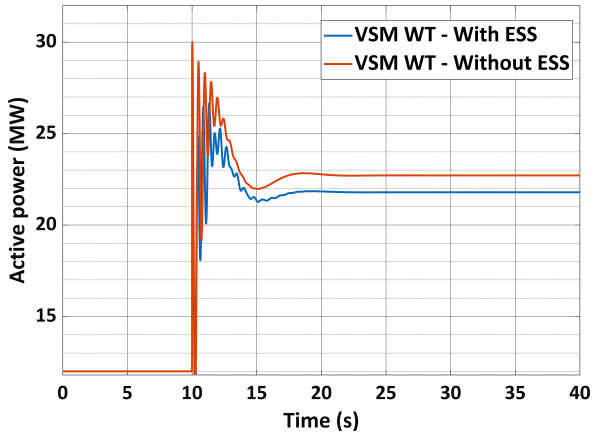


**(a)** Active power response of VSM WT for high RoCoF event with and without ESS.

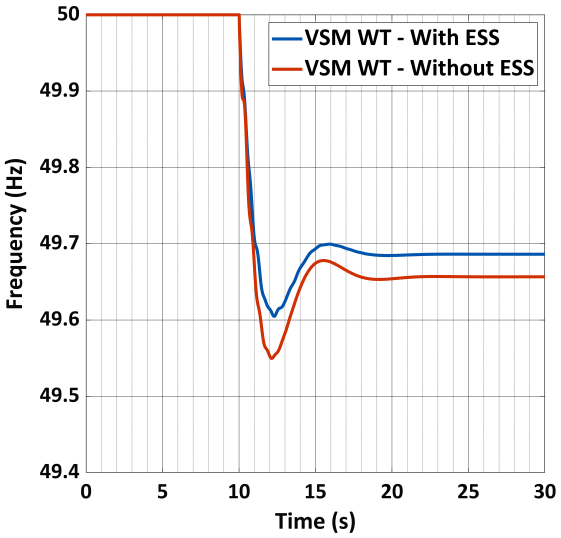


**(b)** Frequency response of VSM WT for high RoCoF event with and without ESS.

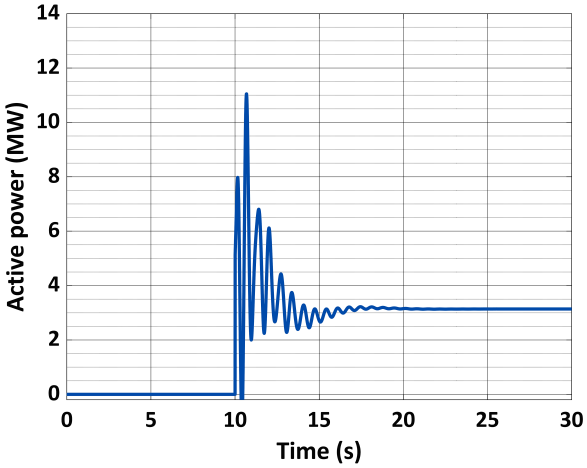


**(c)** Active power response of VSM ESS for high RoCoF event.

**Figure 3.8:** Response from VSM WT with and without ESS for -1Hz/s RoCoF.

During events such as generator outages or frequency fall, the ESS should have stored energy that can be used to discharge during the above-mentioned events. The ESS must also be capable of drawing power from the grid to recharge the storage capacity. As discussed, a generic model of ESS is used throughout the project and both during charging and discharging of ESS, losses are present. The round-trip efficiency can be treated to be 85% based on the assumption that the charging and discharging efficiency are the same. Applying the figures and analyzing the energy requirement for $\Delta P$ of 40 MW, the energy rating is found to be 0.08 MWh according to [68]:

$$E_{ESS} = \frac{t_{req} \cdot S_{ESS} \cdot \sqrt{\mu_c}}{3600} + \frac{t_{req} \cdot S_{ESS}}{3600 \cdot \sqrt{\mu_d}} \tag{3.18}$$

where, $t_{req}$ the required time for IR in this case, which is the first five seconds after the event.

Another important parameter for ESS is the SoC and with the charging and discharging property of the ESS, it gets affected. Using Equation 3.17, while only considering the discharging condition

and assuming the initial SoC was 100%, the SoC after the ESS has provided IR is calculated to be 24%. The choice of initial SoC to be 100% is very idealistic and is only used for calculation purposes.

## 3.6 Summary

A very simple model of an aggregated WPP operating in VSM mode is modelled using DIgSILENT PowerFactory. It has been decided that the project will focus its attention on VSM control and hence the operating principle, control diagram and major control blocks are explained in this chapter. It has been observed that for low RoCoF events, the response from WPP is lower and the inertial response by extracting kinetic energy from WT does not reduce the rotor speed drastically. However, when large events occur there is a significant reduction rotor speed. This response raises challenges as the situation could be bad in case of low wind speed scenario while the WPP tries to respond to such large RoCoF events, without additional energy storage or power curtailment. Chapter 3 begins with methodology, sizing and modelling of ESS that can provide necessary support to the power system. Detailed methodology including knowledge of system parameters, based on which ESS is designed is covered in this chapter. Test cases with high RoCoF event and low wind speed scenario were implemented, to analyze how the ESS largely contributes to inertial response. A simple model was examined that includes a VSM WPP, SG, external grid and load. The knowledge will be used to implement a VSM and ESS in a IEEE 9 bus model and the frequency dynamics for different test cases will be assessed.

# Chapter 4

# Case Study for Contingency Event

In this chapter, a power system study on the IEEE-9 bus system is performed. Frequency dynamics of three different power systems are analyzed for the largest contingency. The first power system consists of SGs only, while the second power system sees a penetration of WPP operating in VSM mode. The final power system is a modification of the second by introducing ESS operating in VSM mode. Based on the methodology developed in Chapter 3, the sizing of ESS required for inertial response for the above-mentioned system is assessed in this chapter. The impact of parameters that affect the ESS sizing and the frequency dynamics of the power system with the addition of ESS will be analyzed here. In addition to IR, a preliminary assessment of PFR, the sizing of ESS to provide both services and the impact on frequency stability will be analyzed.

## 4.1 Test Network

### 4.1.1 Base Power System

The power system in this chapter is modelled based on the IEEE -9 bus system. The initial model, however, is modified to a 12- bus system, where a generation unit is added on each respective bus, with the same characteristics as the initial ones. Thus, the base power system PS0 comprises of six SGs, and no WPP as shown in Figure 4.1. The nominal ratings of the elements are presented in Table 4.1. The total loading under which the evaluation is done is 870 MW.

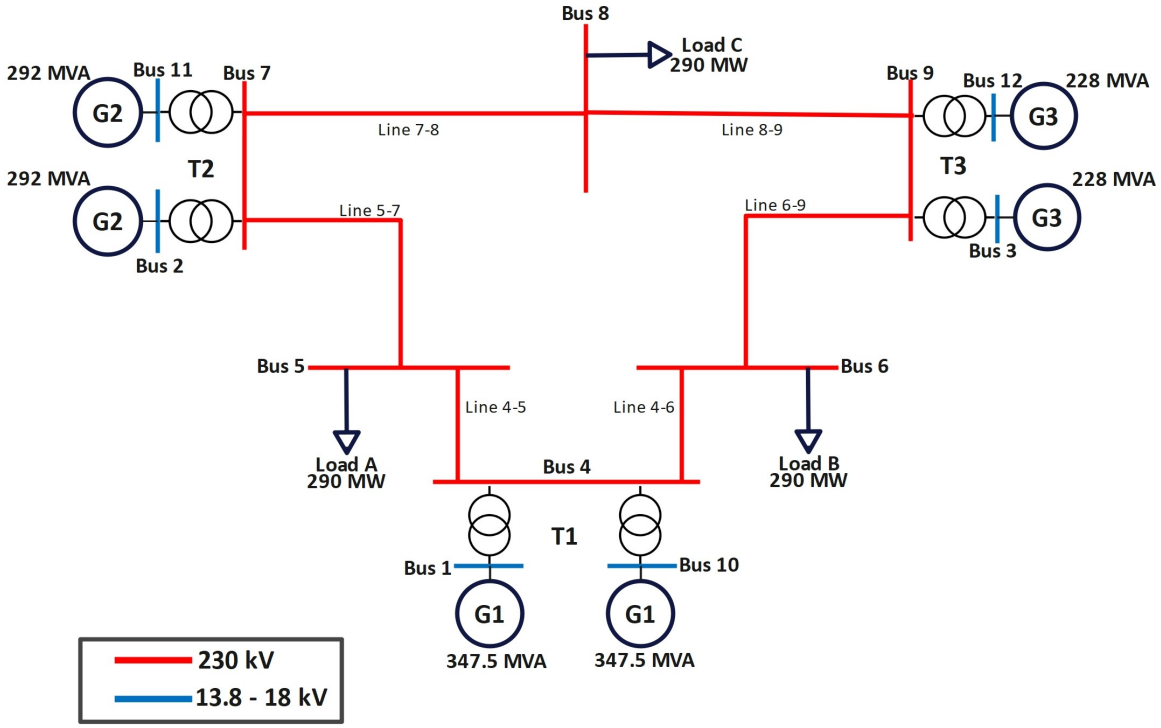


**Figure 4.1:** Single line diagram of base power system PS0.

**Table 4.1:** Element ratings of power system PS0.

| Unit | Power Rating S (MVA) | Voltage rating V (kV) | Number of units |
|---|---|---|---|
| G1 | 347.5 | 16.5 | 2 |
| G2 | 292 | 18 | 2 |
| G3 | 228 | 13.8 | 2 |
| T1 | 280 | 16.5/230 | 2 |
| T2 | 250 | 18/230 | 2 |
| T3 | 180 | 13.8/230 | 2 |

As a system should be designed in order to withstand a major component loss, a methodology in order to evaluate its response, and the sizing of an ESS unit is developed. A generator outage was simulated which involves the loss of one G1 unit. Subsequently, the event would lead to a frequency drop at a certain RoCoF related to the inertia level of the system, due to the power imbalance. Another important parameter related to the frequency stability is the frequency nadir level and steady state frequency, both function of the droop as discussed in Chapter 2, section 2.2.

### 4.1.2 Base Power System with WPP

The same outage event which was simulated in 4.1.1 is performed in 4.1.2. The architecture in the latter and former are same, However two G3 units of 4.1.1 are replaced with two VSM WPP of the same rating, operating in grid-forming mode in 4.1.2. The VSM algorithm uses the swing equation emulation as described in Chapter 2, section 2.4. This system is labeled as PS1 illustrated in Figure 4.2.

Important parameters for evaluating the response for each of the two systems are presented in Tables 4.2 and 4.3. The droop and inertial constant values are the predefined values of the IEEE 9 – bus model where both variables are between typical values of droop 3%-5% and inertial constant from 4-10s [18]. The governor and the automatic voltage regulator (AVR) controllers being used are from PowerFactory libraries namely: **gov_HYGOV** for generators G1 and G2, and **gov_IEEEG1** for generators G3. The AVR controllers are: **avr_IEEET1** for generators G1 and G2, and **avr_ESAC5A** for G3. The controller diagram and parameters are presented in the Appendix B. The system total inertia is calculated using Equation 3.12, while the overall droop is calculated based on Equation 4.1, where $f_0$ the nominal frequency, $S_i$ the nominal power of each unit, and $R_i$ the droop coefficient of each unit. The outage entails a loss of one 347.5 MVA G1 unit, which prior to the event was producing 200 MW active power in steady state.

$$R_{total} = \frac{f_0}{\sum_{i=1}^{n} \frac{S_i}{R_i}} \tag{4.1}$$

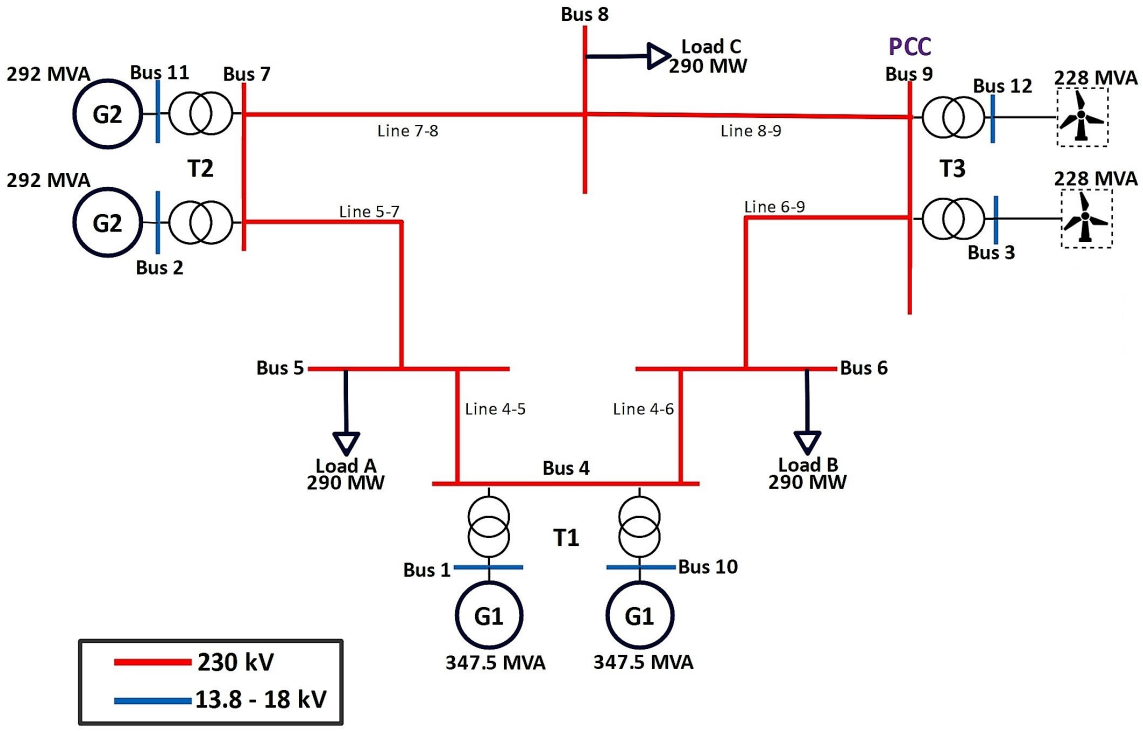


**Figure 4.2:** Single line diagram of power system PS1.

**Table 4.2:** Main parameters of PS0.

| Power plant | Power rating S (MVA) | Active power P (MW) | Droop R (-) | Inertial constant H (s) | Number of units |
|---|---|---|---|---|---|
| G1 | 695 | 400 | 0.05 | 9.55 | 2 |
| G2 | 584 | 300 | 0.05 | 5.92 | 2 |
| G3 | 456 | 170 | 0.05 | 4.76 | 2 |
| **Total** | 1735 | 870 | 0.0014 | **7.07/6.45 *** | - |
| *Recomputed inertia after G1 loss | | | | | |

**Table 4.3:** Main parameters of PS1.

| Power plant | Power rating S (MVA) | Active power P (MW) | Droop R (-) | Inertial constant H (s) | Number of units |
|---|---|---|---|---|---|
| G1 | 695 | 400 | 0.05 | 9.55 | 2 |
| G2 | 584 | 300 | 0.05 | 5.92 | 2 |
| WPP | 456 | 170 | - | - | 2 |
| **Total** | 1735 | 870 | 0.0019 | **5.8/4.88*** | - |
| *Recomputed inertia after G1 loss | | | | | |

As seen from Table 4.3 the WPP is assumed not to provide inertial response. However, as discussed in Chapter 3 and based on the field measurements referred to, the aggregated inertial constant of a WPP could be higher. Typical values of approximate inertia constant for a Type IV wind turbine is 3.5s [71]. As a result, the total inertia calculated in Table 4.3 for PS1, 5.8s is the lowest the system could have without contribution of inertia from the WTs. The system is feeding three loads of 870 MW total, 290 MW each.

The design criteria the system follows are proposed by UCTE for the continental Europe [22], [24], [27], [72]. Therefore, the frequency nadir limit is 48.8 Hz, while the RoCoF limit will be 0.5 Hz/s negative drop. According to ENTSO-E for the Nordic power system operation automatic load shedding occurs from a frequency below 48.8 Hz, thus the limit. The measurements for the RoCoF are calculated based on a 500 ms window. Finally, the maximum steady-state frequency deviation $f_{ss}$, should be at 200 mHz, if accounting for provision of PFR for 15 minutes [24]. The comparison results from the initial simulations yield the following.

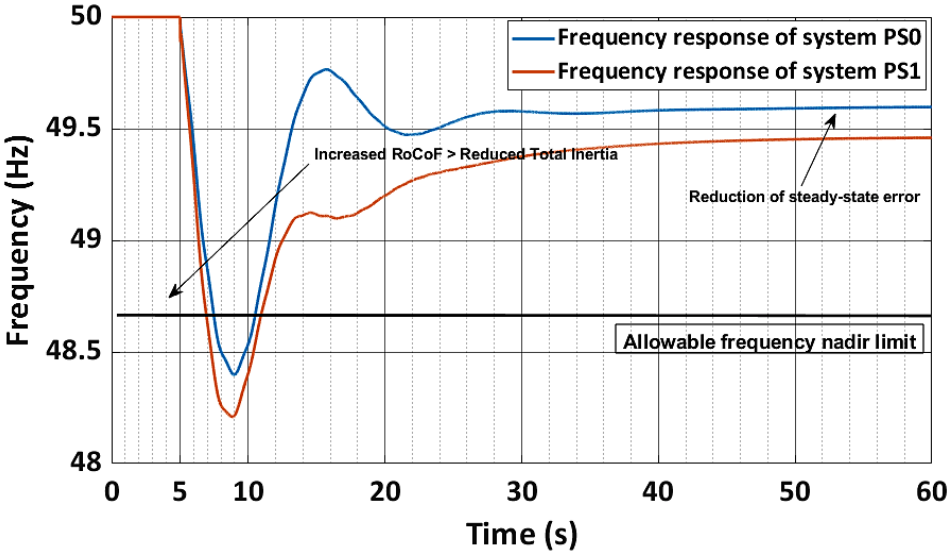


**Figure 4.3:** Frequency response during outage of G1, comparison of PS0 and PS1 system.

Table 4.4, includes the result based on measurements for the two systems.

**Table 4.4:** Results comparison for the two systems for generator G1 outage.

| System | RoCoF (Hz/s) | Frequency nadir (Hz) | Steady state error $\Delta f_{ss}$ (Hz) |
|---|---|---|---|
| PS0 | -0.5 | 48.4 | -0.4 |
| PS1 | -0.68 | 48.2 | -0.55 |

The results indicate that as the total system inertia has decreased, the RoCoF presents an increment in value as expected. The frequency nadir decrease is related to the droop. It has been mentioned that inertia contribution of the WPP is not provided for this case. Let us remember that for virtual inertia provision [40], what could be potentially utilized is some kinetic energy from the WT blades, where here there is none. When comparing the total droop of the system based on Tables 4.2 and 4.3, it is seen that the coefficient for system PS1 has increased. This would imply an increased active power demand for the generation units, while a steady-state error increase would affect frequency.

As mentioned in [40], the desired steady state P-$\omega$ droop, relies on the droop coefficient. If one compares the control diagram in Chapter 2, section 2.2 (SG basic power regulation control), and the one in Chapter 2, section 2.5, Figure 2.14 (VSM swing equation emulation active power loop), it is clear that the damping coefficient expressed in a gain, is related to the $\frac{1}{R}$ droop coefficient of a conventional SG [73]. However, in a case of a SG the droop is typically 3%-5%, whereas in a VSM may vary, based on the capability of the power source and the rating of the converter. In addition, as also mentioned in [73] an ideally small droop would be beneficial for frequency support, but the problem lies to the power needed to be extracted from the WT and restore frequency, considering the availability of power delivery from the wind. For this study case, the assumption is that there is low readily available power dispatch from the WPP, where power delivery could be achieved either by curtailment and/or using an energy buffer as explained in Chapter 2, section 2.4. Therefore, the inertia and damping coefficient decrease.

Figure 4.4 illustrates the active power output of the SGs for PS0 system. As per Tables 4.2 and 4.3, when looking at the inertial constants of the generators, the remainder G1 unit has the biggest inertia contribution to the event. The mechanical power is adjusted by the governor who after the IR period brings the system to a new steady state, where ideally the steady state frequency error should be low. Nonetheless, the mechanical and electrical power curves are complimentary to each other as the system tries to balance and reach the new equilibrium.

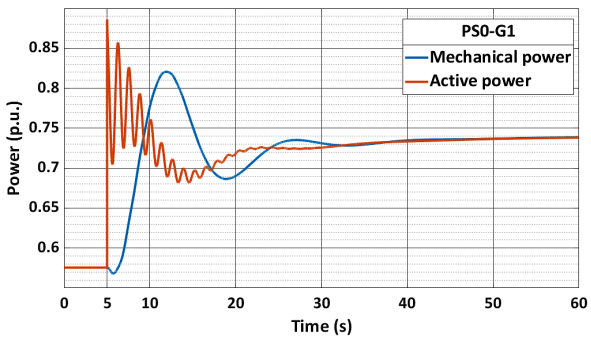


**(a)** Active power response of G1 in PS0.

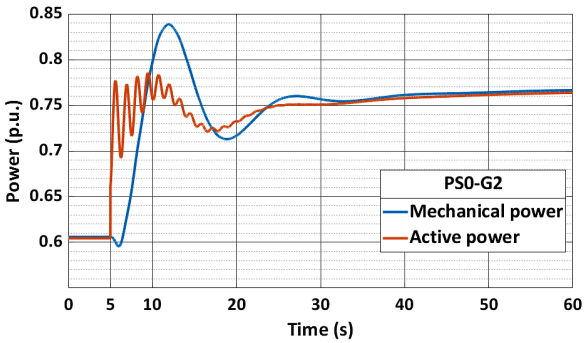


**(b)** Active power response of G2 in PS0.

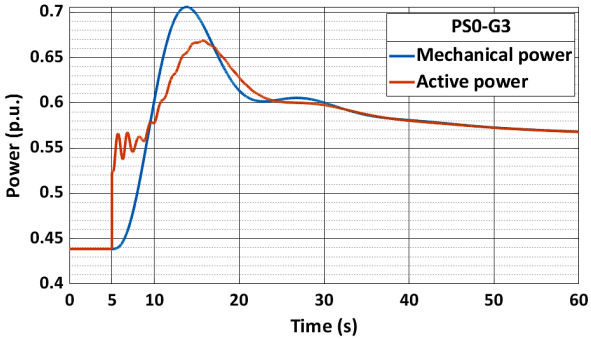


**(c)** Active power response of G3 in PS0.

**Figure 4.4:** Active power response of generation units of PS0.

In Figure 4.5 the active and mechanical power of SGs in PS1 system are illustrated. As mentioned in this scenario the inertia contribution from the WPP is absent, therefore there is increased response from the remainder G1 unit and G2 units. Considering the WT operates at MPPT, it is questionable if the required power can be provided, always depending on rating limitations of WT and power converter. The result of the droop increase is reflected not only in the frequency deviation error described in Figure 4.3, but from the increase in active and mechanical power outputs.

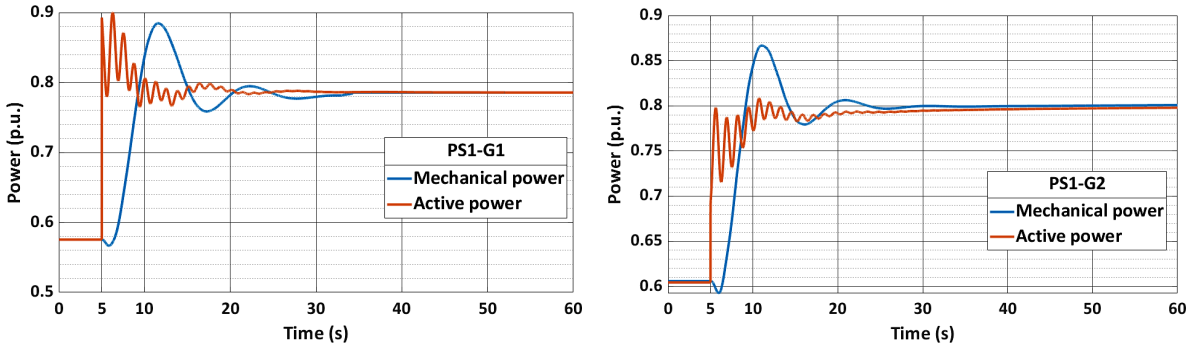


**(a)** Active power response of G1 in PS1.

**(b)** Active power response of G2 in PS1.

**Figure 4.5:** Active power response of generation units of PS1.

The active power response of the two systems comparison is summarized in Table 4.5. The loading of each set of the transformers is noted down too.

**Table 4.5:** Loading of components prior and after the event for PS0 and PS1 system.

| | PS0 | | PS1 | |
|---|---|---|---|---|
| **Unit** | **Active power p.u. (Prior outage)** | **Active power p.u. (Post outage)** | **Active power p.u. (Prior outage)** | **Active power p.u. (Post outage)** |
| G1 | 0.56 | 0.74 | 0.56 | 0.78 |
| G2 | 0.6 | 0.76 | 0.6 | 0.8 |
| G3/VSM | 0.44 | 0.57 | 0.44 | 0.48 |
| | **Loading in percentage** | **Loading in percentage** | **Loading in percentage** | **Loading in percentage** |
| T1 | 72% | 96% | 72% | 105% |
| T2 | 61% | 78% | 61% | 85% |
| T3 | 49% | 61% | 47% | 51% |

Finally, Figure 4.6 summarizes the active power response for the two systems, for the remainder units. Generator G3 response was illustrated in Figure 4.5, while it is removed in PS1 system. As mentioned the WPP does not contribute to inertia and droop. Thus, since the WT dynamics are not concerned the active power response for now is omitted. As per the dynamics, it was discussed in Chapter 3 the effect on rotor speed. In addition, the IR activated in a time window of 5 seconds, and the new steady state active power for PFR is marked on the graph.

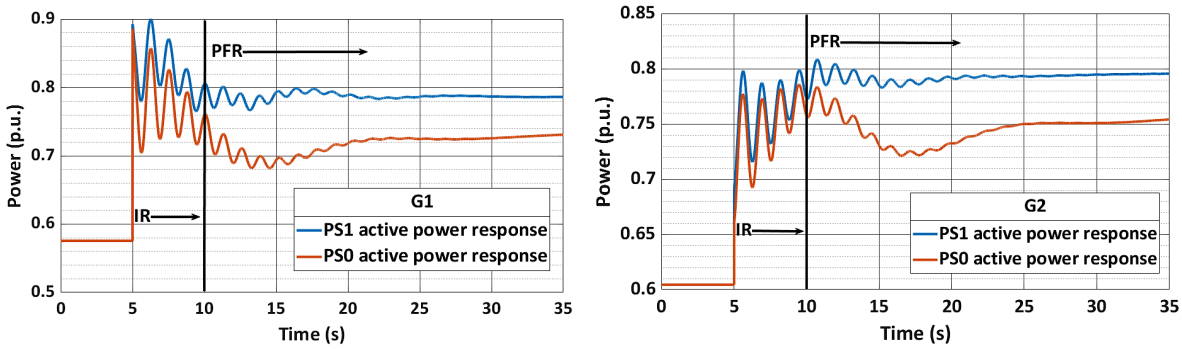


**(a)** Active power response of G1 for both systems.

**(b)** Active power response of G2 for both systems.

**Figure 4.6:** Active power response comparison of generation units for both system.

## 4.2 Inertia Contribution from WPP

In the previous scenario, a system with a certain level of inertia was compared with a modified system where two SGs have been decommissioned. They were replaced by two WPP operating in GFM VSM mode, and the effects of reduced inertia and damping, under the assumption that the system operates in MPPT unable to dispatch any power during the outage, were examined. However, a WT as per literature [71] can provide up to 3.5s of inertia. As seen also from actual field measurements [17] it is possible that the aggregated inertia could be at higher levels. Nevertheless, for this scenario, it is assumed that the WPP can provide 2.5s of aggregated inertia. In reality, to achieve this, some kinetic energy from the wind should be utilized. As a result, this would not only contribute to arresting the falling RoCoF, but the new active power set point of the WT would imply a higher damping coefficient, thus a lower droop meaning lower steady state frequency deviation. The parameters of the power system under study for this scenario are presented in Table 4.6, meanwhile the system is labelled as PS2.

**Table 4.6:** Main parameters of system PS2.

| Power plant | Power rating S (MVA) | Active power P (MW) | Droop R (-) | Inertial constant H (s) | Number of units |
|---|---|---|---|---|---|
| G1 | 695 | 400 | 0.05 | 9.55 | 2 |
| G2 | 584 | 300 | 0.05 | 5.92 | 2 |
| WPP | 456 | 170 | 0.09 | 2.5 | 2 |
| **Total** | 1735 | 870 | 0.0016 | **6.4** | - |

The total inertia of the system has increased. The droop coefficient of VSM in this case was set to 0.09, 0.03-0.05 being optimal according to literature. Yet, it would still reduce the steady-state error and increase the frequency nadir compared to PS1. The frequency response is illustrated in the following figure.

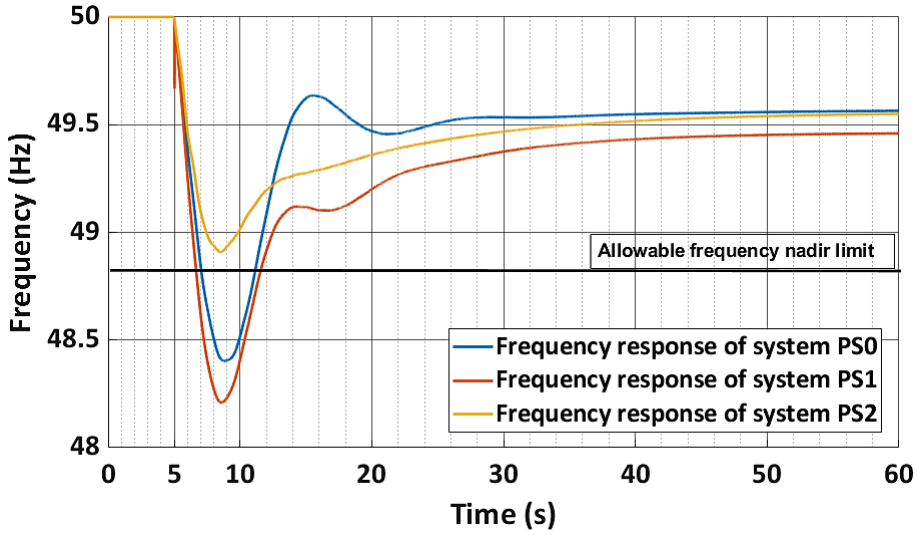


**Figure 4.7:** Frequency response of the systems.

As discerned from Figure 4.7, the WPP responds faster when operating in VSM mode. Also, the RoCoF for PS2 was measured at -0.48 Hz/s. The improved frequency nadir, in addition to the decreased steady state frequency compared to system PS1 is a result of a smaller droop. The steady state frequency error is included in Table 4.7. Still the steady state frequency error when compared to PS0 is higher, while the nadir establishment is higher, since there is no governor or mechanical parts and delays, and the control is through power electronics.

**Table 4.7:** Summary of simulation results from the three systems.

| System | RoCoF (Hz/s) | Frequency nadir (Hz) | Steady state error $\Delta f_{ss}$ (Hz) |
|---|---|---|---|
| PS0 | -0.5 | 48.4 | -0.4 |
| PS1 | -0.68 | 48.2 | -0.55 |
| PS2 | -0.48 | 48.9 | -0.45 |

As per Table 4.7 the RoCoF of PS2 is lower than PS0, and the system complies with the reference requirement of 0.5 Hz/s constraint. However, the VSM allows the fast provision of IR, yet not significant reduction observed, since the inertial strength of the system is still lower. The active power response of PS2 system is shown in Figure 4.8 in the blue curve. The other two curves are a quick experimentation to confirm the response of VSM. As the damping of the WPP can offer to the system is reduced, the droop increases, resulting in a higher error. The effect of the droop has minimal effect on RoCoF. On the other hand the change in inertia affects the IR and the energy needed to be extracted if one integrates the area under the curve for required time frame for IR provision, without affecting the droop.

In addition, there are certain considerations in this case. Assuming the WPP has 40 WT of 5.6 MW rating each, the 45 MW active power demand during inertial response period would require 1.12 MW power extraction from each, if all 40 operate producing 2.12 MW during steady-state. Again, the impact on the rotor speed based on WT characteristics has been addressed in Chapter 3. But supposedly the rotor speed reduction would not be significant, if in the same case the WTs were producing 4.5 MW each, while 20 are in operation, the demand would exceed their rated capability. Apart from the IR, if policies for provision of PFR of 15 minutes [24] apply, then the capability of the WT turbine to provide this power by operating at the new set point is something that cannot be guaranteed.

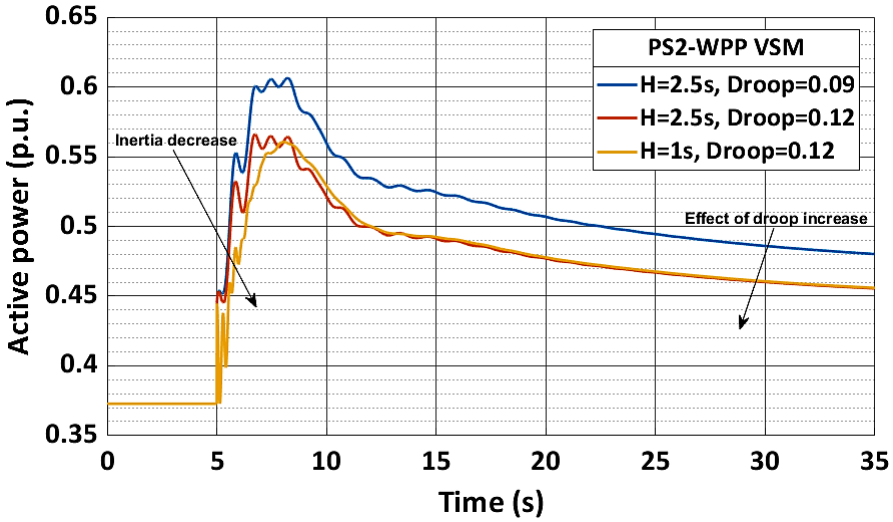


**Figure 4.8:** Active power response of WPP with inertia contribution.

The following figure illustrates the active power response of the system's SGs. As expected, the WPPs inertial contribution has led to reduced IR from the SGs, the period of IR shown in the graph. The active power dispatch from the WPP has also an effect on the new steady state power output of the SG, which has decreased.

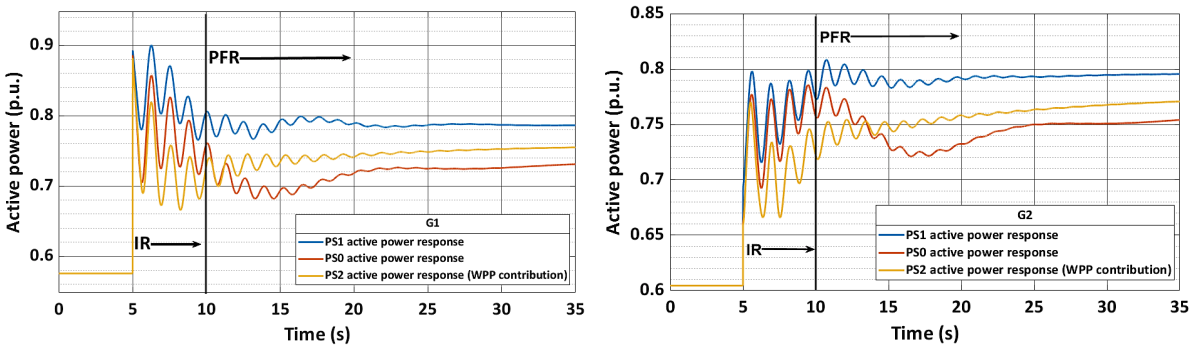


**(a)** Active power response of G1 for all systems.

**(b)** Active power response of G2 for all systems.

**Figure 4.9:** Active power response of G1 and G2 for all systems.

As seen in this case, even though the response of VSM is better, the varying conditions of operation of a WPP cannot guarantee the desirable overall system state, bearing in mind the challenges mentioned in Chapter 3. Therefore, in order to explore the response of the system further, an ESS unit is introduced, the sizing of which is calculated for the required services while certain tradeoffs are noted.

## 4.3 Sizing of ESS for IR

For the sizing of the ESS for IR, the RoCoF limit is 0.5 Hz/s as per reference grid code requirements. Only if the penetration of non-synchronous generators crosses beyond 50%, the RoCoF limits need to be raised [74], [75]. As far as the largest contingency is considered, a loss of 200 MW is considered the major outage in the power system.

Depending on the power system configuration, the contingency level also changes. Based on the power system explained in Figure 4.2 and Table 4.2, the generator's G1 (347.5 MVA) loss causing

a deficit of 200 MW and considered the largest contingency, the ESS is designed. As mentioned in Chapter 2, section 2.5 different potential coupling methods of ESS units were introduced. Here the ESS is connected as shunt to the main converter as per architecture (b)2.17b. The sectional also uses a generic representation of ESS and the round-trip efficiency considering the charging and discharging state is assumed to be 85% [68].

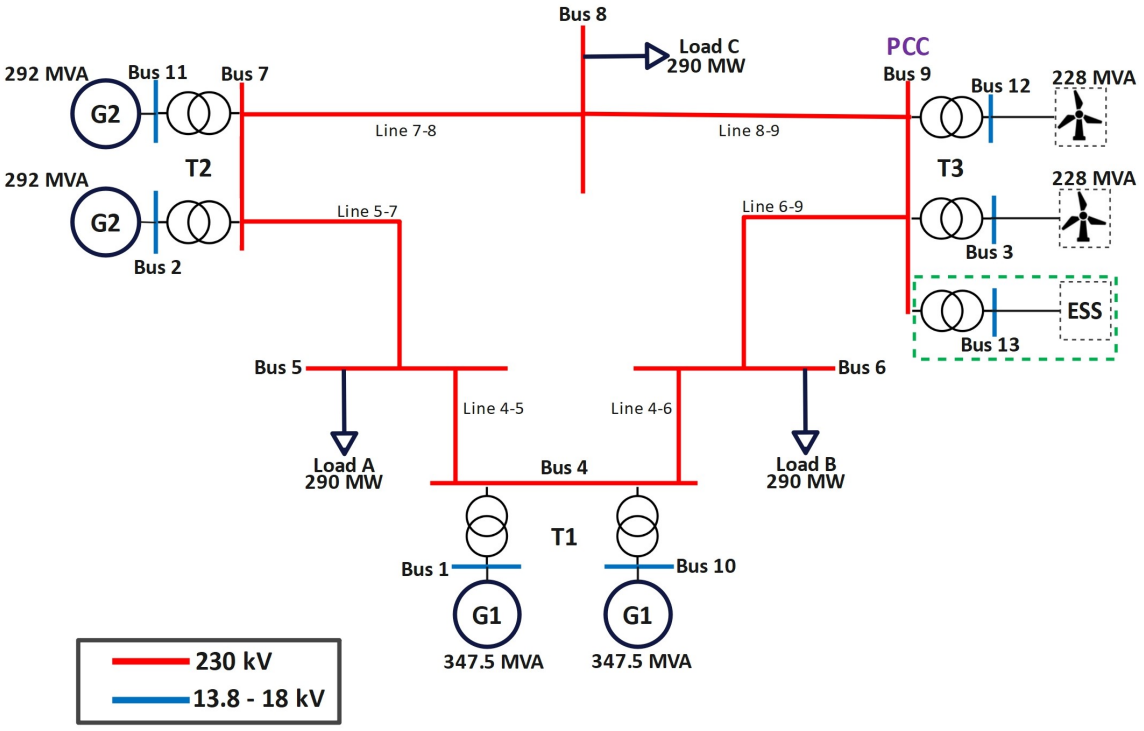


**Figure 4.10:** Single line diagram of base case power system with the addition of ESS unit.

### 4.3.1 System without Inertia Contribution from WPP

As explained in previous chapters, IEEE-9 bus has been modified to a 12 bus with two WPP (228 MVA each) replacing the two G3 units. The single line diagram and element parameters have been explained in Figure 4.2 and Table 4.3. For the initial study of the sizing of ESS in PS1, the WPP is assumed to provide no inertia to the power system. This is done to analyze and calculate the ESS sizing without inertial contribution from WPP and the knowledge will be used to analyze and size the ESS, when WPP operates in VSM mode and contributes to inertia. With the inputs such as power imbalance $\Delta P = 200MW$, RoCoF limit to 0.5 Hz/s, using the modified swing equation the target inertia using Equation 2.4 is found to be 7.2s. After the contingency, the power rating of PS1 has dropped from 1735 MVA to 1387.5 MVA and the new system inertia after the contingency is 4.88 s. Based on Equation 3.9, the inertia from the ESS is calculated to be 50s, based on which the sizing of ESS for IR can be calculated using Equation 3.13:

$$S_{ESS} = S_{PS1} \cdot \frac{H_{target} - H_{PS1}}{H_{ESS} - H_{target}} = 1387.5 \cdot \frac{7.2 - 4.88}{50 - 7.2} = 75MW \tag{4.2}$$

Considering the fact that ESS discharges and charges the same amount of energy from the grid and by using Equation 3.18, the energy rating of ESS is calculated to be 0.2 MWh. The SoC is another important parameter that indicates the performance of the ESS. Using Equation 3.17, assuming the

initial SoC was 75%, after the response from ESS, the final SoC has dropped to 49%. The usage of high value of inertia of the ESS close to 50s creates challenges within the physical provision of such enormous amount of storage. The impact of varying the inertia of storage and therefore, its impact on ESS sizing will be assessed on the upcoming sections. This section does not consider the inertia contribution from WPP.

### 4.3.2 System with Inertia Contribution from WPP

The two aggregated models of wind farms rated at 228 MVA each are operating in VSM mode. The project hereafter will consider the inertia contribution from WPP operating in VSM mode to explore the sizing of the ESS. From the previous chapter it was well established that for the studied contingency without inertia contribution from WPP leads to an ESS size close to 75 MW. GFM control algorithm such as VSM helps WPPs to mimic the behavior of SG and contribute to system inertia. The provision of inertia through VSM WPP also comes with a crucial advantage for ESS sizing, as for the same power deficit, a reduced ESS sizing can be made. The main parameters of the power system are shown in Table 4.6.

Again, as inputs a deficit of 200 MW, and a RoCoF limit of 0.5 Hz/s using the modified swing equation, the target inertia is found to be 7.2s. After the contingency, the power rating of PS1 had dropped from 1735 MVA to 1387.5 MVA, and the new system inertia after the contingency is 5.71s. Based on Equation 3.9, the inertia from the ESS is calculated to be 50s, based on which the sizing of ESS for IR can be calculated using Equation 3.13:

$$S_{ESS} = S_{PS1} \cdot \frac{H_{target} - H_{PS1}}{H_{ESS} - H_{target}} = 1387.5 \cdot \frac{7.2 - 5.71}{50 - 7.2} = 48MW \tag{4.3}$$

Using Equation 3.18, the energy rating of ESS is calculated to be 0.1 MWh and assuming a 75% initial SoC, the final SoC can be calculated using Equation 3.17, and found to be 61%. Table 4.8 summarizes the results.

**Table 4.8:** Comparison of ESS parameters with and without WPP inertia contribution.

| Category | Active power P (MW) | Energy rating E (MWh) | Initial SoC (%) | Final SoC (%) |
|---|---|---|---|---|
| WPP without inertia | 75 | 0.2 | 75 | 49 |
| WPP with inertia | 48 | 0.1 | 75 | 61 |

Based on Equation 3.11, keeping a 0.5 Hz/s RoCoF limit has given the inertia constant of 50s. This large value of inertia poses both technical and economic challenges [76]. From a technical front, provision of 50s of inertia would mean that an enormous storage capacity would be needed. Only with such a large amount of stored energy, such high values of inertia can be attained. On the economic front, provision of inertia is only a technical requirement, meaning that such high value of inertia would bring great advantage to frequency stability in power system. But, the providers of such high inertia are not rewarded with incentives [77] [78]. This raises a question if such large value of inertia is needed or not, to support sufficiently frequency stability.

## 4.4 Impact of Parameters

In the previous section, project highlighted the challenges with respect to large inertia values provided by ESS. In this subsection, the impact of varying parameters such as inertia of storage and the power imbalance/largest contingency will be assessed and how the sizing of ESS affects when the parameters are varied will be analyzed.

### Inertia of Storage

To analyze the impact of parameters and how it affects the ESS sizing for IR, the inertia of storage is varied, keeping the largest contingency in the power system constant ($\Delta P = 200MW$) as shown in Table 4.9 and Table 4.10. The RoCoF based on which the ESS is designed is fixed at 0.5 Hz/s. It can be clearly understood from the table that keeping the power imbalance constant and the inertia of storage is reduced, causes the increase in the sizing of storage.

**Table 4.9:** Storage sizing with reducing inertia and constant power imbalance, without WPP contribution.

| Power imbalance ΔP (MW) | ESS inertia $H_{ESS}$ (s) | ESS size $S_{ESS}$ (MW) | ESS energy $E_{ESS}$ (MWh) |
|---|---|---|---|
| 200 | 50 | 75 | 0.2099 |
| 200 | 40 | 98 | 0.2739 |
| 200 | 30 | 141 | 0.394 |
| 200 | 20 | 251 | 0.7021 |

**Table 4.10:** Storage sizing with reducing inertia and constant power imbalance, with WPP contribution.

| Power imbalance ΔP (MW) | ESS inertia $H_{ESS}$ (s) | ESS size $S_{ESS}$ (MW) | ESS energy $E_{ESS}$ (MWh) |
|---|---|---|---|
| 200 | 50 | 48.6 | 0.1356 |
| 200 | 40 | 63.5 | 0.177 |
| 200 | 30 | 91.3 | 0.2547 |
| 200 | 20 | 162.7 | 0.4537 |

Though the trend on both the tabular columns are same, there is significant difference in the rating of the ESS. It can be clearly seen that for the same power imbalance, the sizing of ESS is smaller in Table 4.10 compared to Table 4.9. This can be directly attributed to the fact that in the latter case, the WPP is operating in VSM mode and providing an aggregate inertia of 2.5 sec. With the integration of WPP, more SGs are being replaced and even with WPP operating in VSM mode and contributing to inertia, the challenges of such mode were explained in previous chapters. However, the limited inertia contribution from VSM WPP can significantly reduce the size of ESS.

### Power Imbalance

The next important parameter for analysis is power imbalance. So far, the basis of all the studies and simulations performed were based on largest contingency in the power system. This subsection explores a different approach by keeping the ESS sizing fixed. The reason for choosing this approach is:

1. The current simulation uses a 228 MVA WPP. An ESS sizing of 45 MW would enhance the possibility of having the ESS within the WT.
2. Fixing an ESS sizing as parameter, in this case 45 MW, will also help the understand what the largest contingency is which ESS can support and how inertia of storage may affect the contingency.

It can be observed from Table 4.11 and Table 4.12 that keeping the ESS sizing constant and reducing the inertia creates a negative trend in the power imbalance. In other words, as we reduce the inertia of storage but keeping the constraint that the ESS sizing is fixed, will result in a lower value of the largest contingency. Though both tabular columns show a decreasing trend in the power imbalance as inertia is reduced, from Table 4.12 it can concluded that for the same storage sizing, the largest contingency ESS can support is also larger compared to values in Table 4.11. This can be directly attributed to the inertia contribution from VSM WPP in the power system.

**Table 4.11:** Power imbalance with fixed storage sizing and reducing inertia, without WPP contribution.

| Power imbalance ΔP (MW) | ESS inertia $H_{ESS}$ (s) | ESS size $S_{ESS}$ (MW) | ESS energy $E_{ESS}$ (MWh) |
|---|---|---|---|
| 175 | 50 | 45 | 0.1258 |
| 166.5 | 40 | 45 | 0.1269 |
| 142.2 | 12.5 | 45 | 0.1257 |
| 137.4 | 7 | 45 | 0.126 |
| 134.8 | 4 | 45 | 0.1214 |

**Table 4.12:** Power imbalance with fixed storage sizing and reducing inertia, with WPP contribution.

| Power imbalance ΔP (MW) | ESS inertia $H_{ESS}$ (s) | ESS size $S_{ESS}$ (MW) | ESS energy $E_{ESS}$ (MWh) |
|---|---|---|---|
| 197 | 50 | 45 | 0.1256 |
| 188 | 40 | 45 | 0.1244 |
| 164.3 | 12.5 | 45 | 0.1261 |
| 159.5 | 7 | 45 | 0.1283 |
| 158.6 | 4 | 45 | 0.1239 |

This study also reveals that there is a tradeoff between power imbalance, inertia of ESS and their sizing. If the ESS sizing must be decided based on largest contingency and the available inertia, then it has to be increased with reduced inertia of storage. The availability of inertia value of the storage would depend on its type, power system application for which it is used and grid code requirements. The penetration of WPP operating in VSM mode has a significant reduction in ESS sizing for same power imbalance.

On the other hand, it is also possible that after preliminary studies, the TSOs plan to fix a size of storage. This may be due to the fact that, after having discussed with wind turbine OEMs, there is possibility to fit the ESS inside the nacelle of the wind turbine. Choice of the ESS sizing with reduced inertia comes with reduced value of power imbalance. Hence a tradeoff exists between the power imbalance, Inertia and ESS sizing. Figure 4.11 coins a relationship between power imbalance, inertia of storage and ESS sizing for the values in Tables 4.9 and 4.10. It can be clearly seen how each parameter affects the other.

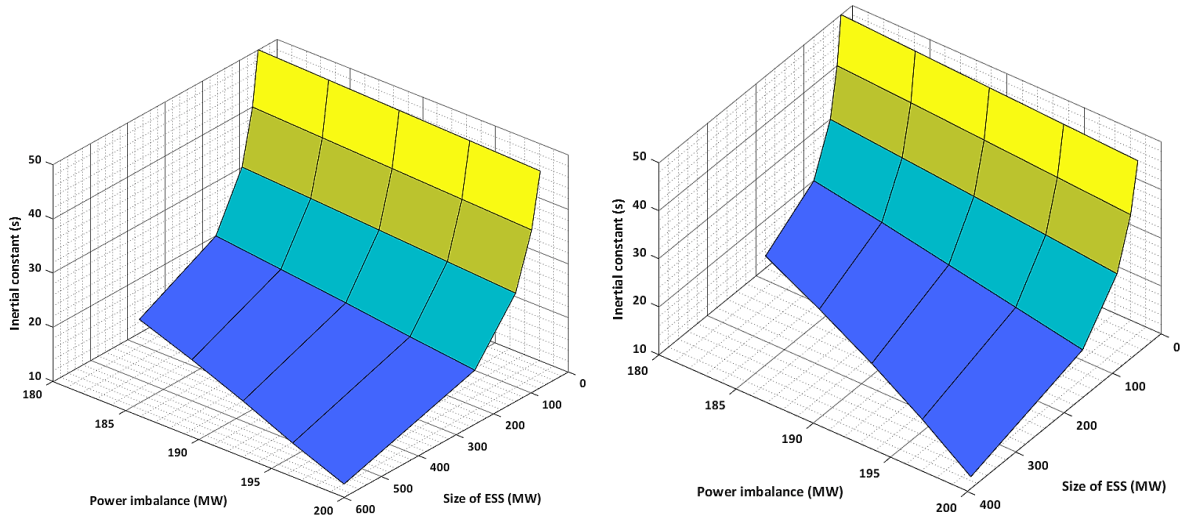


**(a)** Relationship between inertia of storage, power imbalance and ESS sizing according to Table 4.9.

**(b)** Relationship between inertia of storage, power imbalance and ESS sizing according to Table 4.10.

**Figure 4.11:** Comparison between inertia of storage, power imbalance and ESS sizing.

## 4.5 Response of the System with ESS

Based on Table 4.9, when computing the required size for ESS, the theoretical calculations showed that as the size in MW of storage increases, the required inertia provision for the system should be lower for the same power imbalance. However, the simulations revealed that a unit of 75 MW/ 50s, and 98 MW/ 40s of ESS comes to saturation during an outage of 200 MW. Thus, even though theoretically it can be easily calculated, practically the ability of a unit to provide such enormous amounts of inertia is not viable since they might get limited by their rated capacity. In addition, the unit's SoC is crucial in order to provide this response. As naturally there could be no rotating parts to provide kinetic energy e.g., a supercapacitor or a battery rely on the amount of stored energy to provide proper response. If also limitations apply to the SoC like e.g.: minimum discharge level 10%, and maximum charge level 90%, which is beneficial for prolonging the life of the ESS , it could probably have implications when it comes to services provision [79]. Figure 4.12 illustrates the active power response of the ESS in system PS1 during IR period, within 5 seconds after the disturbance. The cases shown are the first three cases from Table 4.9.

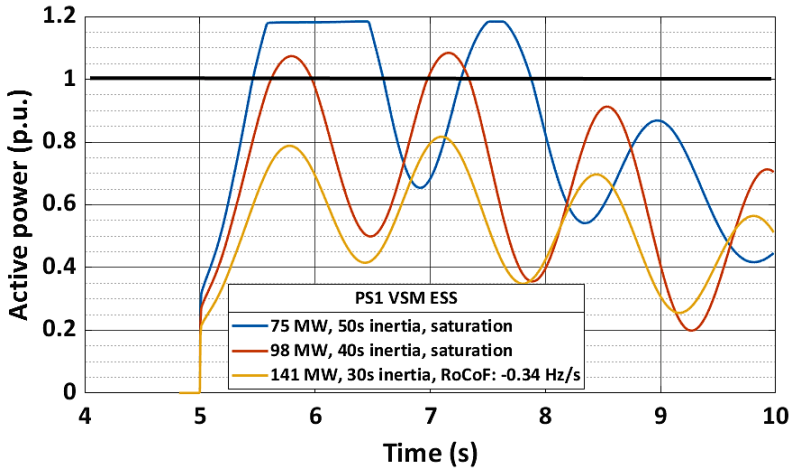


**Figure 4.12:** ESS active power response in PS1 for the first three cases according to Table 4.9.

In the case of PS2 where the WPP provides 2.5s of inertia, it was inferred according to Table 4.10, that the size of the ESS could be decreased. The simulations confirm the finding, where a 91.3 MW/30s storage could provide the necessary support without reaching saturation as illustrated in Figure 4.13.

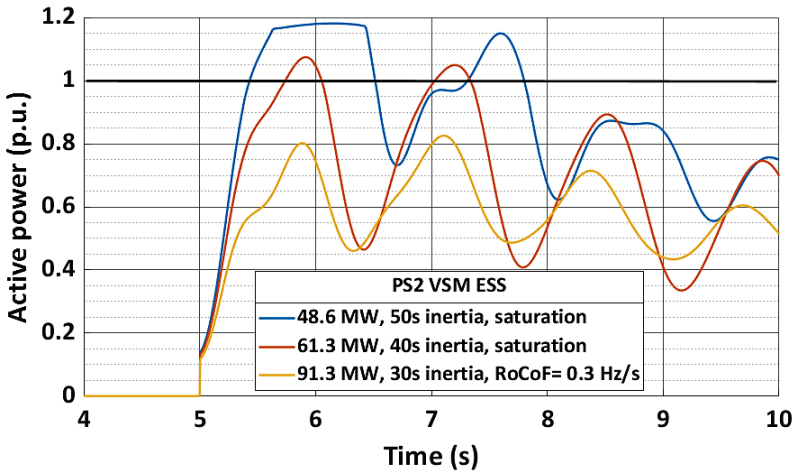


**Figure 4.13:** ESS active power response in PS2 for the first three cases according to Table 4.10.

The calculations according to Table 4.11, where the ESS size is kept constant and the inertia is lowered, showed that the power imbalance should be less, accounting for a 0.5 Hz/sec RoCoF limit. Figure 4.14 illustrates the frequency response of the different power systems configuration, while 141 MW/30s ESS is used for system PS1 with ESS, as the unit won't saturate. Table 4.13 shows the data comparison. As in PS2 and PS1 with ESS there is provision of inertia and both systems when compared to PS0 showed improved response. Furthermore, PS1 with ESS exhibited a very much improved RoCoF for the outage of 200 MW as 30s of inertia are provided. The droop of the ESS was set at 0.06. The steady state error in this case is definitely less when comprared to PS1 where there was no droop response from WPP. However, as computed with Equation 4.1, the total droop of the system is 0.0017 for PS1 with ESS, while PS2 as per Table 4.6 is smaller. Thus, the slightly higher steady state frequency error in case of PS1 with ESS. Measurements are listed in Table 4.13.

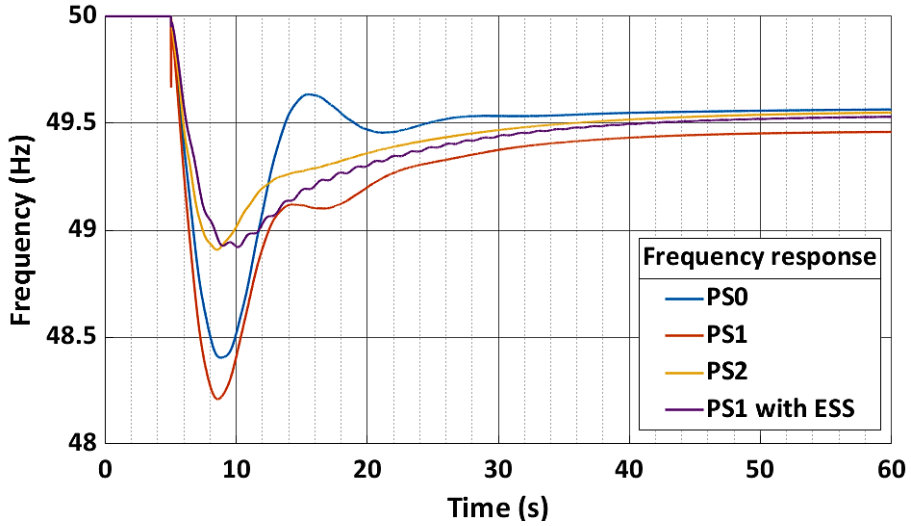


**Figure 4.14:** Frequency response of the different systems simulated.

Finally, PS2 with ESS response was assessed. In the scenario where there is inertia contribution from both WPP and ESS, the result reflects in the improved RoCoF which is the lowest recorded compared to the other cases complying with the grid code requirements. The smaller droop value reflects in the decreased steady-state frequency error. The values are presented in Table 4.13 while the final frequency response of all the cases is shown in Figure 4.15.

**Table 4.13:** Listed measurements of the systems simulated.

| System | RoCoF (Hz/s) | Frequency nadir (Hz) | Steady state error $\Delta f_{ss}$ (Hz) | Steady state frequency $f_{ss}$ (Hz) |
|---|---|---|---|---|
| PS0 | -0.5 | 48.4 | -0.4 | 49.6 |
| PS1 | -0.68 | 48.2 | -0.55 | 49.45 |
| PS2 | -0.48 | 48.9 | -0.45 | 49.55 |
| PS1+ESS | -0.34 | 48.9 | -0.48 | 49.52 |
| PS2+ESS | -0.3 | 49.2 | -0.38 | 49.62 |

From Table 4.13 results it can be inferred that, if inertia is provided from the WPP in case of PS2, or the ESS in PS1+ESS neither of the systems violates the imposed RoCoF restrictions. Apparently, the difference in the derivative of frequency between PS2 and PS1+ESS is sensible since the ESS provides 30s of inertia. However, that does not mean mandatory usage of ESS, since the 2.5s aggregated inertia considered in PS2 case for each VSM WPP, could keep the system within limits for an imbalance of 200MW. The effect of inertia and droop for the VSM in frequency response was discussed in section 4.2 shown in Figure 4.8.

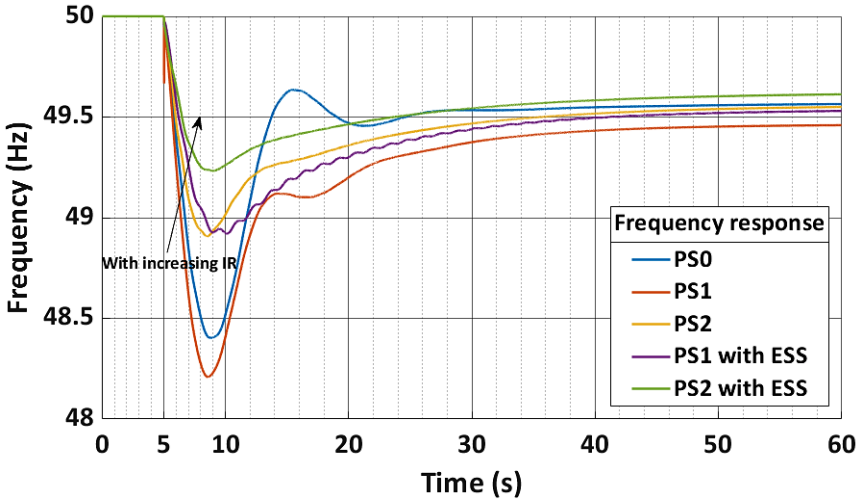


**Figure 4.15:** Frequency response of all the systems simulated.

## 4.6 ESS Sizing for IR & PFR

### 4.6.1 ESS for PFR

As described in Chapter 2 section 2.2, SGs have two roles in frequency restoration. The first role, inertial response was analyzed in the previous subsection. It was discussed how the VSM can imitate the SG behavior and provide virtual inertia, offering flexibility by manipulating this control parameter, while conventional power plants offer a small range of variation typically 2-10s [18], [73]. The second role of SGs is to bring the system frequency to a new steady state condition. This is determined by the prime mover of an SG. The parameter referred to as droop coefficient or speed regulation is equal to the ratio of steady state frequency deviation to change in active power. In Chapter 3 section 3.2, the VSM controller utilized in this thesis was presented. Apart from the emulation of swing equation for virtual inertia, the controller includes a droop control for PFR. PFR is another service that could be provided by the ESS. Unlike IR, PFR service requires large power and energy rating for the ESS to be able to support the power system for up to 15 mins with maximum steady state frequency deviation of 200 mHz for Continental Europe [24]. After the IR, the stabilization of frequency to a steady state value with a permissible range of error from its normal value is done by PFR, within 30 seconds after the occurrence of frequency event. Frequency nadir, which is the point of minimum frequency in the grid frequency response depends on magnitude and time of deployment of PFR. The above power-frequency characteristic is described by the following equation [22]:

$$\lambda = -\frac{\Delta P}{\Delta f} = \sum_{i=1}^{n} \cdot \frac{1}{R_i} \cdot \frac{S_i}{f_0} \tag{4.4}$$

where, $\Delta P$ the power imbalance, $\Delta f$ the steady state frequency, $f_0$ the nominal frequency, $R_i$ is the droop coefficient and $S_i$ the nominal rating of the i-th generation unit.

#### 4.6.1.1 No Droop from WPP

A target steady state frequency deviation of 0.2 Hz, considering a power deficit of 200 MW yields the following target power frequency characteristic:

$$\lambda_{target} = -\frac{\Delta P}{\Delta f} = -\frac{200}{-0.2} = 1000 MW/Hz \tag{4.5}$$

For system PS1, the value of $\lambda_{PS1}$ where before the event was calculated to be 511.6 MW/Hz using Equation 3.9 and after the loss of one unit of G1, dropped to 372.6 MW/Hz. One can observe that the $\lambda_{target}$ is higher than $\lambda_{PS1}$ after the event. In order for the ESS to enable PFR service, the $\lambda_{PS1}$ has to be increased. To deliver the ESS's nominal power for a frequency deviation $\pm 200mHz$, the droop value of ESS, $R_{ESS}$ has to be 0.004. This value is only reached in the regulated area. The power rating of ESS was computed as:

$$S_{ESS} = (R_{ESS} \cdot f_0) \cdot (\lambda_{target} - \lambda_{PS1}) = (0.004 \cdot 50) \cdot (1000 - 372.6) = 125.4MW \tag{4.6}$$

An ESS is not just defined by its power rating, but also by its energy rating. Both upward and downward regulation can be done by ESS and considering a round trip efficiency ($\mu_c$ and $\mu_d$) of 85%, the energy requirement for $t_{req}$ equal to 15 minutes of the ESS is calculated as:

$$E_{ESS} = \frac{t_{req} \cdot S_{ESS} \cdot \sqrt{\mu_c}}{3600} + \frac{t_{req} \cdot S_{ESS}}{3600 \cdot \sqrt{\mu_d}} = 62.9MWh \tag{4.7}$$

#### 4.6.1.2 Droop from WPP

Now we are considering the case where the WPP provides the droop of 0.09. The value of $\lambda_{PS2}$ before the event was calculated to be 612.9 MW/HZ and after the loss of one unit of G1, dropped to 473.9 MW/Hz. One can observe that the $\lambda_{target}$ is higher than $\lambda_{PS2}$ after the event. In order for the ESS to enable PFR service, the $\lambda_{PS2}$ has to be increased. $R_{ESS}$ is treated fixed and taken to be 0.004. The power rating and energy of ESS was computed according to Equation 3.9 as:

$$S_{ESS} = (R_{ESS} \cdot f_0) \cdot (\lambda_{target} - \lambda_{PS2}) = (0.004 \cdot 50) \cdot (1000 - 473.9) = 105.2MW \tag{4.8}$$

$$E_{ESS} = 52.7MWh \tag{4.9}$$

## 4.7 ESS for IR & PFR

As shown in Figure 2.2, looking in the time domain scale, both IR and PFR are separated. However, there are possibilities that both IR and PFR may overlap. For the ESS size determination only the power requirement is considered here. From 4.6.1, the power requirement for PFR is 125.4 MW based on the power frequency characteristic. While we can take the case with ESS that has been sized for IR rated to 75 MW from Table 4.9 for PS1, the difference in energy and sizing is evident. As per 4.6.1, the ESS sizing for PFR amounts to 105.2 MW and 48.6 MW ESS computed from Table 4.10 for PS2, the observations are the same. The new energy requirement of both IR and PFR is a sum of energy requirements from each.

**Table 4.14:** ESS sizing and comparison for both IR and PFR.

| System | Service | ESS size $S_{ESS}$ (MW) | ESS energy $E_{ESS}$ (MWh) |
|---|---|---|---|
| PS1 | IR | 75 | 0.2 |
| PS1 | PFR | 125.4 | 62.9 |
| PS1 | IR + PFR | 125.4 | 63.1 |
| PS2 | IR | 48.6 | 0.13 |
| PS2 | PFR | 105.2 | 52.7 |
| PS2 | IR + PFR | 105.2 | 52.83 |

Table 4.14 clearly summarizes the service provided along with the power and energy rating required for ESS. It can be observed that the IR is a high power with less energy oriented, while PFR is attributed with high power and high energy. Both IR and PFR can be provided by the same ESS and is depicted in the table. It can be clearly observed that for a $\Delta P$ of 200 MW, the energy contribution from IR and PFR can be separated and observed.

## 4.8 PFR Simulations

Sections 4.6 and 4.7 explain the theoretical calculations behind the sizing of ESS required to provide PFR. The sizing calculation is now used to model the ESS providing PFR in DIgSILENT PowerFactory. The power system used for the model only considers architecture PS2. The sizing of the ESS is provided in Table 4.15 which covers both the power and energy rating of different services. From section 4.5, it was concluded that the ESS was sized to be 91.3 MW with inertial constant $H_{ESS}$ equal to 30s, as the ESS would not saturate during a 200 MW deficit.

**Table 4.15:** ESS sizing for both IR and PFR for PS2+ESS.

| System | Service | ESS size $S_{ESS}$ (MW) | ESS energy $E_{ESS}$ (MWh) |
|---|---|---|---|
| PS2+ESS | IR | 91.3 | 0.2547 |
| PS2+ESS | PFR | 105.2 | 52.7 |
| PS2+ESS | IR + PFR | 105.2 | 52.9 |

The simulations presented for the selected ESS, where there is a droop of 0.09 provided by each of the WPP, and according to sizing calculations for PFR in 4.6.1 based on power frequency characteristic, that the system can meet the grid code requirements. The new steady state condition, 30 seconds after the frequency drop due to the event has been deployed, and at 35 seconds the system is heading to steady state. The impact of PFR to the frequency nadir of the system is also shown and compared with the previous cases in Table 4.16. Even though inertia has almost no effect on frequency extremum level and droop has almost no effect on RoCoF [73], it was confirmed by observations in section 4.2; that the significantly small droop value selected for the ESS according to grid code regulations, caused a slight improvement in RoCoF.

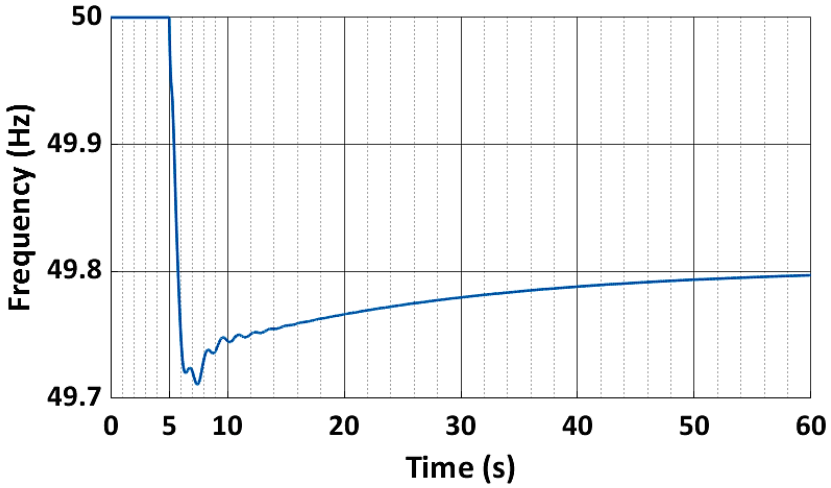


**Figure 4.16:** Frequency response of system PS2 with ESS based on section 4.6.1.

Figure 4.17 illustrates the active power response of the ESS. The first five seconds after the event,

the IR period, the calculated size of the ESS can provide the necessary inertial response without reaching saturation. Now, as the system reaches the steady state, the active power of ESS is measured at 0.59 p.u. provided by the PFR keeping the frequency within the desired margin. However, in this thesis a detailed model of specific ESS e.g., BESS was not accounted, thus the ability to provide the required energy for 15 minutes has not been simulated. But this depends on the SoC level of the designated storage unit, and its current SoC during the occurrence of the event. The parameters such as Soc and its impact on ESS provision of PFR has not been addressed in this thesis and could be considered for future work.

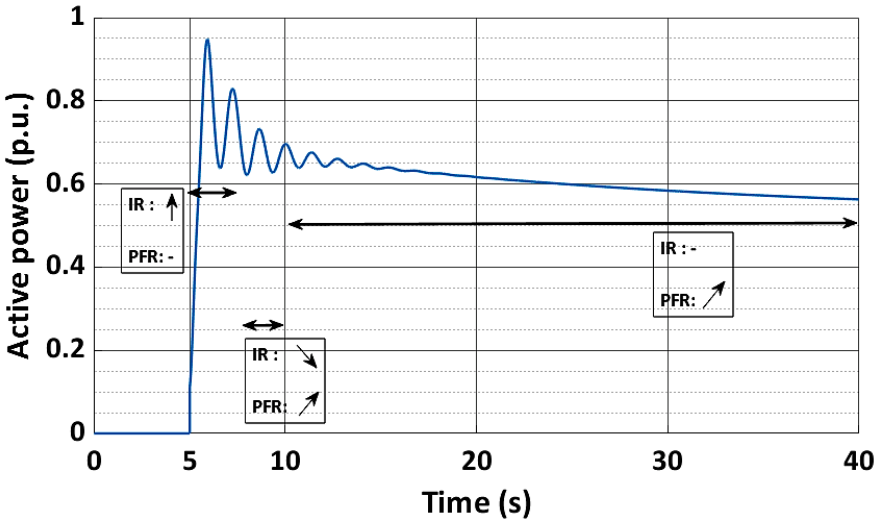


**Figure 4.17:** Active power response of ESS based on section 4.6.1.2.

**Table 4.16:** Data comparison of all simulations.

| System | Service | ESS size (MW) / H (s) | ESS energy $E_{ESS}$ (MWh) | RoCoF (Hz/s) | Frequency nadir (Hz) | Steady state frequency $f_{ss}$ (Hz) |
|---|---|---|---|---|---|---|
| PS0 | IR | - | - | -0.5 | 48.4 | 49.6 |
| PS1 | IR | - | - | -0.68 | 48.2 | 49.45 |
| PS2 | IR | - | - | -0.48 | 48.9 | 49.55 |
| PS1 + ESS | IR | 141/30 | 0.394 | -0.34 | 48.9 | 49.52 |
| PS2 + ESS (a) | IR | 91.3/30 | 0.2547 | -0.3 | 49.2 | 49.62 |
| PS2 + ESS (b) | IR + PFR | 105.2/30 | 52.9 | -0.26 | 49.7 | 49.8 |

In PS2+ESS (b) with 30s inertia, ESS provides PFR and IR is additionally provided by a 105.2 MW ESS unit. The frequency nadir and the RoCoF have improved to 49.7 Hz and -0.26 Hz/s when compared to PS2+ESS (a). The latter scenario has the ESS requirement up to 105.2 MW of nominal power and 52.9 MWh of nominal energy, thus providing the better results in terms of different frequency parameters.

### Analysis of PFR

It can be observed that in VSM control, due to the presence of droop control, the PFR is activated and the active power corresponding to 0.004 droop is dispatched immediately. This also means that the steady state frequency deviation of 49.8 Hz would be attained much faster. However, when the

frequency deviation exceeds $\pm 20mHz$ from nominal value known as the dead band, PFR is activated. For a frequency deviation of $\pm 200mHz$, the PFR has to be linearly deployed and the ESS must be able to provide the service up to 15 minutes. Thus, the droop of ESS reaches 0.004 only in the regulated area. The ESS gets constrained according to maximum power rating and $R_{ESS}$ could vary according to Figure 4.18, when a frequency deviation exists more than $\pm 200mHz$. The droop in this region would be larger than that of the regulated area and the active power dispatched would be more than the rating of ESS, thus reaching saturation. Later, the secondary frequency reserves (SFR) will activate and relieve the PFR, however, SFR and other services after PFR are not considered for the thesis.

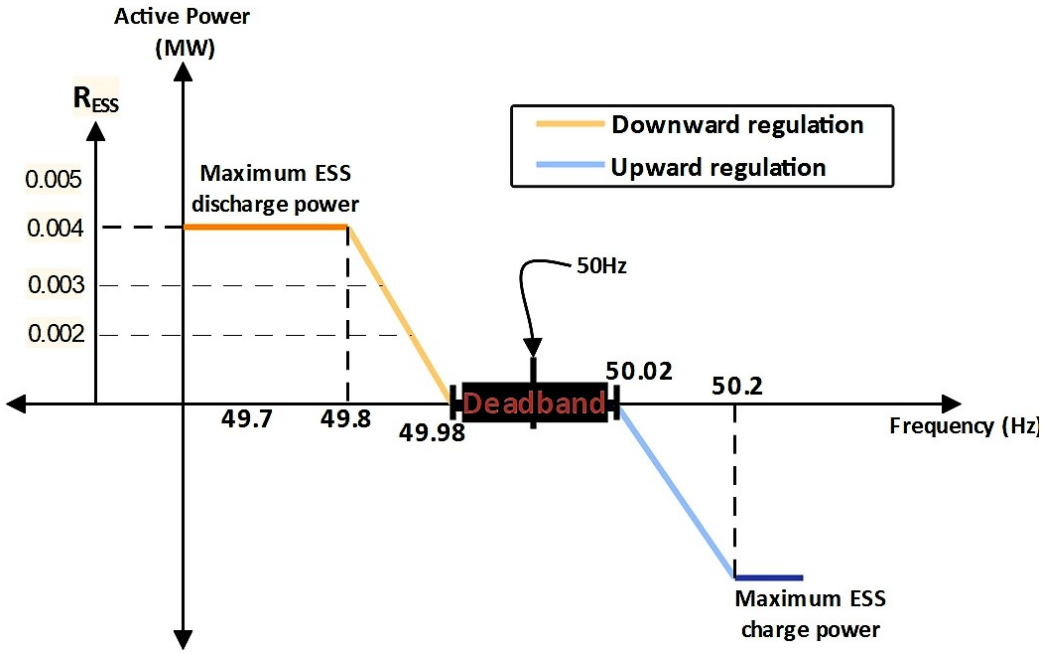


**Figure 4.18:** Effective value of the ESS droop.

## 4.9 Summary

Chapter 4 uses an IEEE 9 bus which was modified to a 12-bus system to evaluate the frequency response. The chapter uses a complete SG based power system and transitions by allowing the penetration of WPP. The WPP is initially assumed not to provide Inertia and droop and later the WPP are operating in VSM mode. During the largest contingency, the traditional power system with SG was able to arrest the RoCoF within specified limits while the system with WPP penetration had crossed the limit. It was observed that the architecture with WPP operating in VSM mode had faster response, lower RoCoF and lower steady state frequency deviation. Though the capability of WPP operating in VSM mode has been analyzed, to provide the right response and by staying within the WT and converter rating capability, the WT/WPP must be curtailed or provided with energy buffer. Section 4.3 commences with the sizing of ESS considering different cases. Section 4.4 takes into account parameters such as inertia of storage and the power imbalance. Relationship between these two parameters and size of ESS is coined. The addition of ESS is evaluated in section 4.5 and simulations clearly reveal the enhancement of frequency stability. Section 4.6 begins by sizing the ESS for PFR, and using the design parameters, the ESS sizing to accommodate both IR and PFR is done. The simulations were carried out for some seconds until steady state condition was reached. Complete PFR provision for 15 minutes was not evaluated. The effect of SoC, provided a detailed model of ESS and even restoration of frequency back to 50 Hz could be potential future work.

# Chapter 5

# Discussion

The thesis aims at investigating the ability of a wind farm operating in GFM control to enhance frequency stability and how the addition of ESS will facilitate frequency stability.

To meet the fundamental objectives, the thesis begins with state-of-the-art literature review and covers power system stability and its classification. The thesis only focuses its attention on frequency stability and how concepts like GFM control and ESS can be used to improve frequency stability. In section 2.2 a good understanding of synchronous generators and equations governing SGs were analyzed. Inertia is an inherent characteristic of SG and using swing equation the inverse relationship between inertia and the RoCoF was understood.

In section 2.3 the thesis enters the converter control and discusses about GFL and GFM control. Traditionally the IBPS are GFL based on the assumption that inertial sources will help regulate the frequency and voltage deviation. However, GFL also has its disadvantages as the method of calculating RoCoF, can have lot of time lag which affects the inertial response and FFR. Challenges with GFL control with weak grids and islanded condition have been analyzed in literature.

Section 2.4 provides a detailed classification of different GFM controls. There are mainly three different classifications:

1. Droop based - is one of the most mature control techniques with relative simplicity, while their concept originates from the governor action.
2. Synchronous machine based - The control philosophy of synchronous machine-based control aims to emulate the dynamic behavior of a real SG, through power electronic components.
3. Other types.

It was analyzed that the droop based GFM do not provide inertia while the synchronous machine based GFM control does. The project also focuses its interest on VSM, a synchronous machine based GFM control.

Section 2.5 discusses type IV WT where the mechanical part is decoupled from the electrical side. To implement a VSM GFM control and provide inertia from WT one of best options is to use a kinetic Energy of the blades or utilize the limited storage in DC link capacitance or both [17].

In section 2.6 it is highlighted that the inertial response from WT can be enhanced by integrating an ESS into the DC link capacitance or connecting the ESS as shunt to the main power converter. The challenges of connecting the ESS to DC link of WT has been addressed and thesis decides to connect the ESS as shunt to the main power converter. Since ESS and VSM are the focus of the thesis, the ESS will be operating in VSM mode.

Chapter 3 begins with a simple power system architecture involving load, SG, external grid and WPP operating in VSM mode. The chapter also explains the control system of VSM, and it clearly shows how VSM emulates the behavior of SG providing inertia and damping. The architecture was inspired from SGRE's test trial on a 23 MW farm in Scotland to investigate the inertia contributions.

It was found that during low RoCoF events, the response from VSM WPP was very small. However, during high RoCoF events, it was observed that the inertial response from WPP was large. It was studied that such responses will have drastic reduction in rotor speed. If the rotor speed goes below the cut in speed, the WT could trip. This is also one of the major challenges with renewables like wind, where there is unpredictability in availability of resources. The simulations for high RoCoF, low wind speed scenario also revealed a drastic reduction in rotor speed and high probability for the WTs to trip. A potential solution to such challenges is curtailment or operating with ESS. The latter portion of Chapter 3 explores the methodology and sizing of ESS operating in VSM mode and the simulation in section 3.4 clearly shows how the ESS operating in VSM mode can support the frequency stability.

In Chapter 4 the case studies are performed on the IEEE 9-bus model. An outage event of 200 MW of a generation unit is assumed. Based on the reference grid code requirements, the limit in RoCoF should be 0.5 Hz/s with 48.8 Hz frequency nadir. Three different power system were analyzed in sections 4.1 and 4.2. It was found that the power system architecture with WPP operating in VSM mode had significant improvement in terms of frequency stability and simulations clearly reveal the benefit of VSM in providing IR. As a prerequisite, however, the ability of the WPP to contribute with kinetic energy extracted from the blades would definitely have an impact, considering the response times of blade pitch control and MPPT to achieve this. Thus, it is possible to provide the necessary support to the grid's demand, if the power imbalance will not cause the WT to drop below cut in speed. In order to avoid this, WTs would be expected to operate in curtailment or an ESS could be introduced.

In section 4.3 the sizing of ESS is analyzed for scenarios with penetration of WPP. The scenario was subdivided into two: where WPP do not provide inertia and one with inertia provision. The former scenario is more prominent as traditional WPP integrated into the power system is based on the assumption that the SGs will provide the inertial response. However, the latter represents the scenarios such as Wind farms in Dersalloch Scotland operating in VSM mode and providing inertia. The two scenarios were well analyzed and used to size the ESS. While the former needed a larger ESS, for the same power imbalance a lower ESS sizing was only needed for the latter.

In section 4.4 the impact of varying parameters such as inertia of storage and the power imbalance/largest contingency were assessed and how the sizing of ESS affects when the parameters are varied were analyzed. If the ESS sizing is based on power imbalance, then with reduced inertia of storage, the power rating of ESS will increase. On the other hand, if the ESS sizing is fixed then, choice of the ESS sizing with reduced inertia comes with reduced value of power imbalance. Hence a tradeoff exists between the power imbalance, Inertia of storage and ESS sizing.

In section 4.5 it was elaborated showed how the addition of ESS can improve the frequency stability. The architecture with WPP operating in VSM mode and ESS in VSM is considered to be the ideal architecture. There is significant room for improvement of VSM control as it help optimize the ESS sizing and by doing so the 2 VSMs can have a complimentary behavior during system disturbances. This could be considered for future work. In addition, the simulations indicated that it might be physically unattainable to provide very large inertia from an ESS with low size, as it might saturate.

Besides IR, another service provided by ESS is PFR. Unlike IR, PFR is high power and energy oriented. The ESS with PFR is expected to provide service up to 15 mins. The sizing of ESS to provide both were also calculated. It was observed in simulations that the ESS sized for both IR and PFR had significant improvement in RoCof, frequency nadir and steady state frequency. Chapter 4 also reveals that with architecture were WPP is operating in VSM mode, the sizing of the ESS can be reduced. This shows the possibility of integrating the ESS that can provide both services inside the WT. However, a detailed evaluation of implementation of PFR could be considered for future work.

# Chapter 6

# Conclusion & Future Work

### Conclusion

Traditional power systems were built around SGs, and they have their advantages in terms of system inertia and system strength. However, with the penetration of renewables, the total system inertia is reducing and creates challenges to power system stability. IBPS operate in GFL mode based on the assumption that the inertial response will be provided by SGs face challenges with decommissioning of SGs.

Making the IBPS operate in GFM mode is considered a viable option to improve the power system stability. Though GFM control has been used over more than decade and has found its place in microgrids and small islands, the concept is still in the infancy stage. Examples from GE's investment in PV inverters, Dalrymple BESS, Australia and Dersalloch wind farm in Scotland are example of emergence of GFM control in IBPS on a commercial scale. This has been an inspiration for the thesis and in Chapter 3, WPP is operating in VSM mode, and the inertia contributions are explored. The VSM model is made in DIgSILENT PowerFactory. The simulations show that WPP in VSM mode without energy buffer, can provide necessary inertial response by extracting the kinetic energy of the blades, however, with very large events and low wind speed scenarios could leading to a drastic reduction of rotor speed and finally WT tripping. These simulations were also backed up by the trials on Dersalloch wind farm, where WPP operating in VSM mode without energy buffer, during severe events, the turbine speeds were drastically reduced and lead to turbine tripping.

To avoid such scenarios, the IBPS are mostly operated with curtailment. By doing so the IBPS power is not fully utilized, and curtailment can also have economic drawbacks. This is where the thesis focuses its attention on ESS to support the frequency stability. When integrating an ESS into an architecture with WT, there are potential possibilities, with one being integrated directly into the DC link, while the other by connecting ESS as a shunt to the main converter. From a WT point of view, the latter architecture is considered the best and thesis uses the latter architecture through the remainder of the project. In 2021, Siemens Gamesa launched a Brande Hydrogen project where the ESS (hydrogen storage) is used. The ESS's DC/AC converter is connected as a shunt to the WT main converter.

The simulations in Chapter 4 clearly make a comparison of the frequency response from different power system architecture. The traditional power system with SGs as main source of power generation are getting replaced with penetration of IBPS. The frequency response also shows that the traditional power system with SGs have better frequency response compared to the power system with penetration of IBPS. However, with concepts like VSM, the IBPS can mimic the behavior of SGs and contribute to inertia and damping. The kinetic energy from blades of WT could be used to provide inertia and thus the WPP can operate in VSM mode. It was observed the VSM had much better frequency response compared to traditional SGs.

Recent implementation of VSM BESS in Australia such as ESCRI Dalrymple 30MW/8MWh, the

largest commercial scale connected GFM BESS [80] are examples on how ESS can support frequency stability and has been a source of inspiration for the thesis. The ESS has been sized based on the power imbalance and RoCoF. Through numerical calculations, different combinations of ESS sizing were obtained based on size of power imbalance and inertia of storage. It was observed that a tradeoff exists between the power imbalance and the inertia of storage and ESS sizing. It was observed that the addition of ESS improves the frequency stability.

The thesis concludes that traditional power grids were designed using SGs. With the penetration of IBPS using GFL control, power system stability is facing challenges. When viewed from frequency stability point of view, there is a declining inertia. VSM control, is considered a viable option as it provides inertia and damping. Enabling WPP to operate in VSM mode is feasible, however, when it comes large disturbance and low wind speed, IR without energy buffer will be challenging. ESS can be considered to complement renewables and from a thesis point of view ESS can support the WPP during severe events and low wind speed. During high wind and low electricity demand, the ESS could be charged, while the WPP could respond to events during small disturbances. When the wind speed is low and severe disturbances occur, the controllers can allow the ESS operating in VSM mode to respond instead of WPP and support frequency stability.

### Future Work

Though thesis is able to give brief glimpse into the dynamic response of VSM and ESS, it opens doors to different aspects which could be considered for future work and some of them are:

- An improved VSM control in WT – the thesis has clearly shown the dynamic response of WPP in VSM mode. An improved controller of VSM that provide dynamic response during large events and limitations could be analyzed.
- Specific ESS – the thesis mainly looks into a generic ESS model. Instead, a specific ESS like BESS or supercapacitor could be analyzed based on the intended application. The power and energy ratings, SoC and integration of ESS into the power system, techno-economic analysis and size optimization could be investigated.
- Black start, islanding operation – with new emerging grid requirements, it is expected that the GFM control can provide black start capability. By using ESS operating in VSM mode, how well it can support during islanding condition and provide black start capability could be analyzed.
- Weak grids – the simulations only consider renewable penetration up to 30%. However, in the future with higher levels of penetration, weak grids become more prominent and how the addition of ESS in VSM mode can support their healthy operation could be explored.

# Bibliography


[1] Peter Christensen et al. "High penetration of power electronic interfaced power sources and the potential contribution of grid forming converters". In: (2020).

[2] Hannah E Murdock et al. "Renewables 2021-global status report". In: (2021).

[3] Michael Renner, Celia Garcia-Banos, Arslan Khalid, et al. "Renewable energy and jobs: annual review 2022". In: (2022).

[4] Global Wind Energy Council. "GWEC Global Wind Report 2020". In: *Global Wind Energy Council: Brussels, Belgium* (2020).

[5] Tech. Rep. ""Denmark's climate and energy outlook 2020,"". In: (2020).

[6] Emmanuel S Karapidakis et al. "Impact of increased RES generation on power systems dynamic performance". In: *Materials Science Forum*. Vol. 721. Trans Tech Publ. 2012, pp. 185–190.

[7] Prabha S Kundur and Om P Malik. *Power system stability and control*. McGraw-Hill Education, 2022.

[8] European Network of Transmission System Operators for Electricity. *Inertia and Rate of Change of Frequency (RoCoF)*. `https://eepublicdownloads.azureedge.net/clean-documents/SOC%20documents/Inertia%20and%20RoCoF_v17_clean.pdf`. 2020.

[9] Ujjwol Tamrakar et al. "Virtual inertia: Current trends and future directions". In: *Applied sciences* 7.7 (2017), p. 654.

[10] Niklas Modig et al. "FFR Design of Requirements–External document". In: *ENTSO-E, Nordic TSOs, Inertia2020 Working Group, Tech. Rep* (2020).

[11] NationalGridESO. *Minimum Specification Required for Provision of GB Grid Forming (GBGF) Capability (formerly Virtual Synchronous Machine/VSM Capability)*. `https://www.nationalgrideso.com/document/189381/download`. 2021.

[12] Helge Urdal, Richard Ierna, and Andrew J. Roscoe. "Stability challenges & solutions for power systems operating close to 100% penetration of power electronic interfaced power sources: exchange of experience between hybrid and major power systems". In: 2018.

[13] Liang Lu and Nicolaos Cutululis. "Virtual synchronous machine control for wind turbines: a review". In: *Journal of Physics: Conference Series* 1356 (Oct. 2019), p. 012028. DOI: `10.1088/1742-6596/1356/1/012028`.

[14] Junru Chen et al. "Co-ordinated grid forming control of AC-side-connected energy storage systems for converter-interfaced generation". In: *International Journal of Electrical Power & Energy Systems* 133 (2021), p. 107201.

[15] Khalid Mehmood Cheema et al. “Modification in active power-frequency loop of virtual synchronous generator to improve the transient stability”. In: *International Journal of Electrical Power & Energy Systems* 128 (2021), p. 106668.

[16] Andrew Roscoe et al. “Response of a grid forming wind farm to system events, and the impact of external and internal damping”. In: *IET Renewable Power Generation* 14.19 (2020), pp. 3908–3917.

[17] A Roscoe et al. “Practical experience of operating a grid forming wind park and its response to system events”. In: *Proceeding of the 18th Wind Integration Workshop, Dublin, Ireland*. 2019, pp. 16–18.

[18] Prabha Kundur et al. “Definition and classification of power system stability IEEE/CIGRE joint task force on stability terms and definitions”. In: *IEEE transactions on Power Systems* 19.3 (2004), pp. 1387–1401.

[19] Nikos Hatziargyriou et al. “Definition and classification of power system stability–revisited & extended”. In: *IEEE Transactions on Power Systems* 36.4 (2020), pp. 3271–3281.

[20] StG CNC. *ENTSO-E guidance document for national implementation of frequency ranges for network codes on grid connection*. 2021.

[21] Benjamin Vilmann. “Frequency Stability of Offshore Wind Farms in Weak Grids with Grid-forming Wind Turbines”. In: (2022).

[22] Charis S Demoulias et al. “Ancillary services offered by distributed renewable energy sources at the distribution grid level: An attempt at proper definition and quantification”. In: *Applied Sciences* 10.20 (2020), p. 7106.

[23] ENTSO-E. *“Operations Handbook of the Union for the Coordination of Transmission of Electricity (UCTE)”*. 2018.

[24] Continental Europe Operation Handbook. *P1—Policy 1: Load-Frequency Control and Performance [C], Union for the Co-ordination of Transmission of Electricity (UCTE)*. Tech. rep. Technical Report, 2009.

[25] Julia Merino et al. “Ancillary service provision by RES and DSM connected at distribution level in the future power system”. In: *SmartNet project D* 1 (2016), p. 1.

[26] NERC Inverter-Based Resource Performance Task et al. “Fast frequency response concepts and bulk power system reliability needs”. In: *NERC* (2020), p. 1.

[27] Erik Ørum et al. “Future system inertia”. In: *ENTSOE, Brussels, Tech. Rep* (2015), pp. 1–58.

[28] Jon O’Sullivan et al. “Studying the maximum instantaneous non-synchronous generation in an island system—Frequency stability challenges in Ireland”. In: *IEEE Transactions on Power Systems* 29.6 (2014), pp. 2943–2951.

[29] Helge Urdal et al. “System strength considerations in a converter dominated power system”. In: *IET Renewable Power Generation* 9.1 (2015), pp. 10–17.

[30] Liang Lu and Nicolaos A Cutululis. “Virtual synchronous machine control for wind turbines: a review”. In: *Journal of Physics: Conference Series*. Vol. 1356. 1. IOP Publishing. 2019, p. 012028.

[31] Jan Machowski et al. *Power system dynamics: stability and control*. John Wiley & Sons, 2020.

[32] P Rodriguez and NB Lai. "Grid-following and grid-forming PV and wind turbines". In: *Control of Power Electronic Converters and Systems*. Elsevier, 2021, pp. 499–521.

[33] Bin Wu et al. "Variable-speed wind energy systems with synchronous generators". In: (2011).

[34] Qiuwei Wu and Yuanzhang Sun. *Modeling and modern control of wind power*. John Wiley & Sons, 2018.

[35] Yashen Lin et al. *Research roadmap on grid-forming inverters*. Tech. rep. National Renewable Energy Lab.(NREL), Golden, CO (United States), 2020.

[36] C Broderick. "Rate of change of frequency (RoCoF) withstand capability". In: *ENTSOE, Brussels, Belgium, Tech. Rep* (2018).

[37] Martyn Durrant, H Werner, and Keith Abbott. "Model of a VSC HVDC terminal attached to a weak AC system". In: *Proceedings of 2003 IEEE Conference on Control Applications, 2003. CCA 2003.* Vol. 1. IEEE. 2003, pp. 178–182.

[38] Lennart Harnefors, Massimo Bongiorno, and Stefan Lundberg. "Input-admittance calculation and shaping for controlled voltage-source converters". In: *IEEE transactions on industrial electronics* 54.6 (2007), pp. 3323–3334.

[39] Xiongfei Wang et al. "Grid-synchronization stability of converter-based resources—An overview". In: *IEEE Open Journal of Industry Applications* 1 (2020), pp. 115–134.

[40] Dayan B Rathnayake et al. "Grid forming inverter modeling, control, and applications". In: *IEEE Access* 9 (2021), pp. 114781–114807.

[41] Roberto Rosso et al. "Grid-forming converters: Control approaches, grid-synchronization, and future trends—A review". In: *IEEE Open Journal of Industry Applications* 2 (2021), pp. 93–109.

[42] Xiao-Qiang Guo, Wei-Yang Wu, and He-Rong Gu. "Phase locked loop and synchronization methods for grid-interfaced converters: a review". In: *Przeglad Elektrotechniczny* 87.4 (2011), pp. 182–187.

[43] Jenny Z Zhou et al. "Impact of Short-Circuit Ratio and Phase-Locked-Loop Parameters on the Small-Signal Behavior<? Pub _bookmark="" Command="[Quick Mark]"?> of a VSC-HVDC Converter". In: *IEEE Transactions on Power Delivery* 29.5 (2014), pp. 2287–2296.

[44] Roberto Rosso et al. "Analysis of the interaction among power converters through their synchronization mechanism". In: *IEEE Transactions on Power Electronics* 34.12 (2019), pp. 12321–12332.

[45] Yicheng Liao et al. "Sub-synchronous control interaction in grid-forming VSCs with droop control". In: *2019 4th IEEE Workshop on the Electronic Grid (eGRID)*. IEEE. 2019, pp. 1–6.

[46] Hans-Peter Beck and Ralf Hesse. "Virtual synchronous machine". In: *2007 9th international conference on electrical power quality and utilisation*. IEEE. 2007, pp. 1–6.

[47] Salvatore D'Arco and Jon Are Suul. "Virtual synchronous machines—Classification of implementations and analysis of equivalence to droop controllers for microgrids". In: *2013 IEEE Grenoble Conference*. IEEE. 2013, pp. 1–7.

[48] Qing-Chang Zhong and George Weiss. "Synchronverters: Inverters that mimic synchronous generators". In: *IEEE transactions on industrial electronics* 58.4 (2010), pp. 1259–1267.

[49] Karel De Brabandere et al. "A voltage and frequency droop control method for parallel inverters". In: *IEEE Transactions on power electronics* 22.4 (2007), pp. 1107–1115.

[50] Mukul C Chandorkar, Deepakraj M Divan, and Rambabu Adapa. "Control of parallel connected inverters in standalone AC supply systems". In: *IEEE transactions on industry applications* 29.1 (1993), pp. 136–143.

[51] Lidong Zhang, Lennart Harnefors, and Hans-Peter Nee. "Power-synchronization control of grid-connected voltage-source converters". In: *IEEE Transactions on Power systems* 25.2 (2009), pp. 809–820.

[52] Lidong Zhang, Lennart Harnefors, and Hans-Peter Nee. "Interconnection of two very weak AC systems by VSC-HVDC links using power-synchronization control". In: *IEEE transactions on power systems* 26.1 (2010), pp. 344–355.

[53] Abdullah Albalali. *Frequency Stability of Power Electronic Based Power System with 100% Renewable Energy.* 2022.

[54] Nikolaj Stig Stoltenborg. "Investigation of applying grid-forming converter control on wind turbines and its influence on power systems". In: (2020).

[55] Qing-Chang Zhong et al. "Self-synchronized synchronverters: Inverters without a dedicated synchronization unit". In: *IEEE Transactions on power electronics* 29.2 (2013), pp. 617–630.

[56] P Brogan et al. "Experience of grid forming power converter control". In: *17th Wind Integration Workshop, Stockholm, Sweden*. 2018.

[57] KV Vidyanandan and Nilanjan Senroy. "Primary frequency regulation by deloaded wind turbines using variable droop". In: *IEEE transactions on Power Systems* 28.2 (2012), pp. 837–846.

[58] Liang Huang et al. "Challenges and potential solutions of grid-forming converters applied to wind power generation system—An overview". In: *Frontiers in Energy Research* 11 (2023), pp. 1–14.

[59] WindEurope. *""Wind energy and on-site energy storage", Exploring market opportunities"*. 2017.

[60] Anant Narula. "Grid-forming wind power plants". In: (2023).

[61] David Connolly. "A review of energy storage technologies: for the integration of fluctuating renewable energy". In: (2010).

[62] Hannele Holttinen et al. "Ancillary services: technical specifications, system needs and costs. Deliverable D 2.2". In: (2012).

[63] Abraham Alem Kebede et al. "A comprehensive review of stationary energy storage devices for large scale renewable energy sources grid integration". In: *Renewable and Sustainable Energy Reviews* 159 (2022), p. 112213.

[64] Cong-Toan Pham. "Assessment of energy storage systems for power system applications based on equivalent circuit modeling". PhD thesis. KTH Royal Institute of Technology, 2019.

[65] DIgSILENT. *Digsilent powerfactory version 2018 user manual.* 2018.

[66] Bojana Barać et al. "Modeling and initialization of a virtual synchronous machine for power system fundamental frequency simulations". In: *IEEE Access* 9 (2021), pp. 160116–160134.

[67] Eduard Muljadi et al. *Understanding inertial and frequency response of wind power plants*. IEEE, 2012.

[68] Vaclav Knap et al. "Grid inertial response with Lithium-ion battery energy storage systems". In: *2014 IEEE 23rd International Symposium on Industrial Electronics (ISIE)*. IEEE. 2014, pp. 1817–1822.

[69] Maciej Świerczyński et al. "Field experience from Li-ion BESS delivering primary frequency regulation in the Danish energy market". In: *Ecs Transactions* 61.37 (2014), p. 1.

[70] Egill Thorbergsson et al. "Primary frequency regulation with Li-ion battery based energy storage system-evaluation and comparison of different control strategies". In: *Intelec 2013; 35th International Telecommunications Energy Conference, SMART POWER AND EFFICIENCY*. VDE. 2013, pp. 1–6.

[71] A Žertek, G Verbič, and M Pantoš. "Participation of DFIG wind turbines in frequency control ancillary service by optimized rotational kinetic energy". In: *2010 7th International Conference on the European Energy Market*. IEEE. 2010, pp. 1–6.

[72] Henrik Nordström. *Fast Frequency Reserves to Ensure Frequency Stability Regarding N-1 Criteria: Individual project report in FEG3214 Power System Stability and Control*. 2022.

[73] L Lu, O Saborío-Romano, and NA Cutululis. *Reduced-Order-VSM-Based Frequency Controller for Wind Turbines. Energies 2021, 14, 528*. 2021.

[74] Eirgrid. *DS3: rate of change of frequency (RoCoF) workstream*. 2011.

[75] Shuang Xu, Yaosuo Xue, and Liuchen Chang. "Review of power system support functions for inverter-based distributed energy resources-standards, control algorithms, and trends". In: *IEEE Open Journal of Power Electronics* 2 (2021), pp. 88–105.

[76] Tohid Rahimi et al. "Inertia response coordination strategy of wind generators and hybrid energy storage and operation cost-based multi-objective optimizing of frequency control parameters". In: *IEEE Access* 9 (2021), pp. 74684–74702.

[77] Jennie L Jorgenson and Paul L Denholm. *Modeling primary frequency response for grid studies*. Tech. rep. National Renewable Energy Lab.(NREL), Golden, CO (United States), 2019.

[78] Matthieu Paturet et al. "Economic valuation and pricing of inertia in inverter-dominated power systems". In: *arXiv preprint arXiv:2005.11029* (2020).

[79] Xin Jiang et al. "Optimization of battery energy storage system capacity for wind farm with considering auxiliary services compensation". In: *Applied Sciences* 8.10 (2018), p. 1957.

[80] Stephen Sproul, Stanislav Cherevatskiy, and Hugo Klingenberg. “Grid Forming Energy Storage: Provides Virtual Inertia, Interconnects Renewables and Unlocks Revenue”. In: *Hitachi ABB and ElectraNet* (2020).

# Appendix A

# Appendix 1

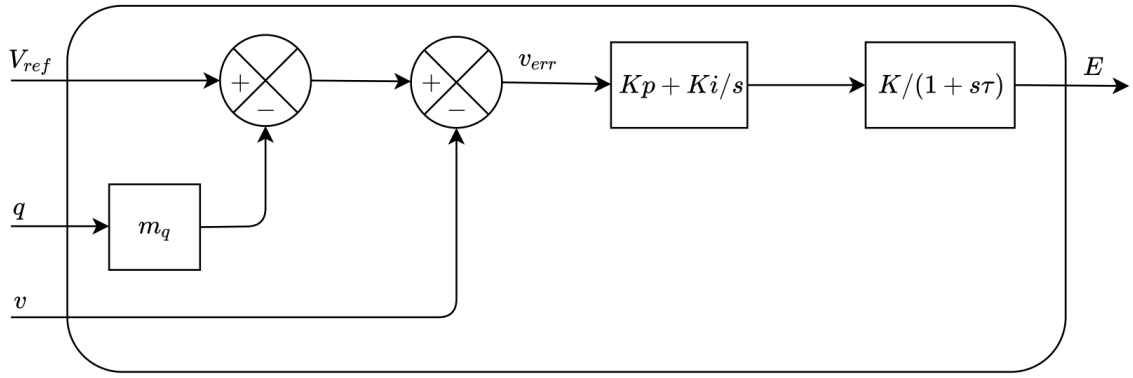


**Figure A.1:** Control block diagram of voltage regulator.

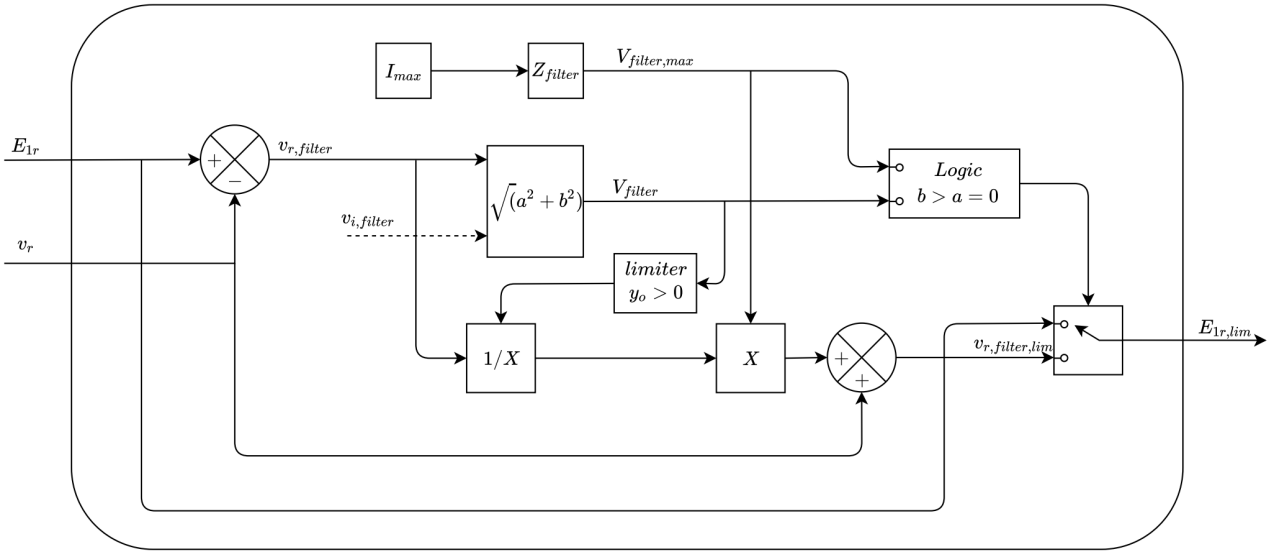


**Figure A.2:** Control block diagram of current limiter.

## SWT-DD-120

| General details | |
|---|---|
| Flexible power rating | 3.9-4.3 MW |
| Wind class | IEC IA/S/T |
| Control | Pitch regulation with variable speed |
| Standard operating temperature | Range from -20ºC to 40ºC |

| Rotor | |
|---|---|
| Diameter | 120 m |
| Swept area | 11,300 $m^2$ |
| Power density | 380.53 $W/m^2$ |

| Blades | |
|---|---|
| Length | 58.6 m |
| Airfoils | Siemens Gamesa proprietary airfoils |
| Material | Fiberglass reinforced with epoxy |

| Tower | |
|---|---|
| Type | Tubular steel tower |
| Height | 85 m and site-specific |

| Generator | |
|---|---|
| Type | Synchronous, PMG |
| Voltage | 690 V AC |
| Frequency | 50 Hz or 60 Hz |
| Power factor | 0.93 CAP-0.93 IND throughout the power range |

**Figure A.3:** Datasheet of Siemens Gamesa D3 WT.

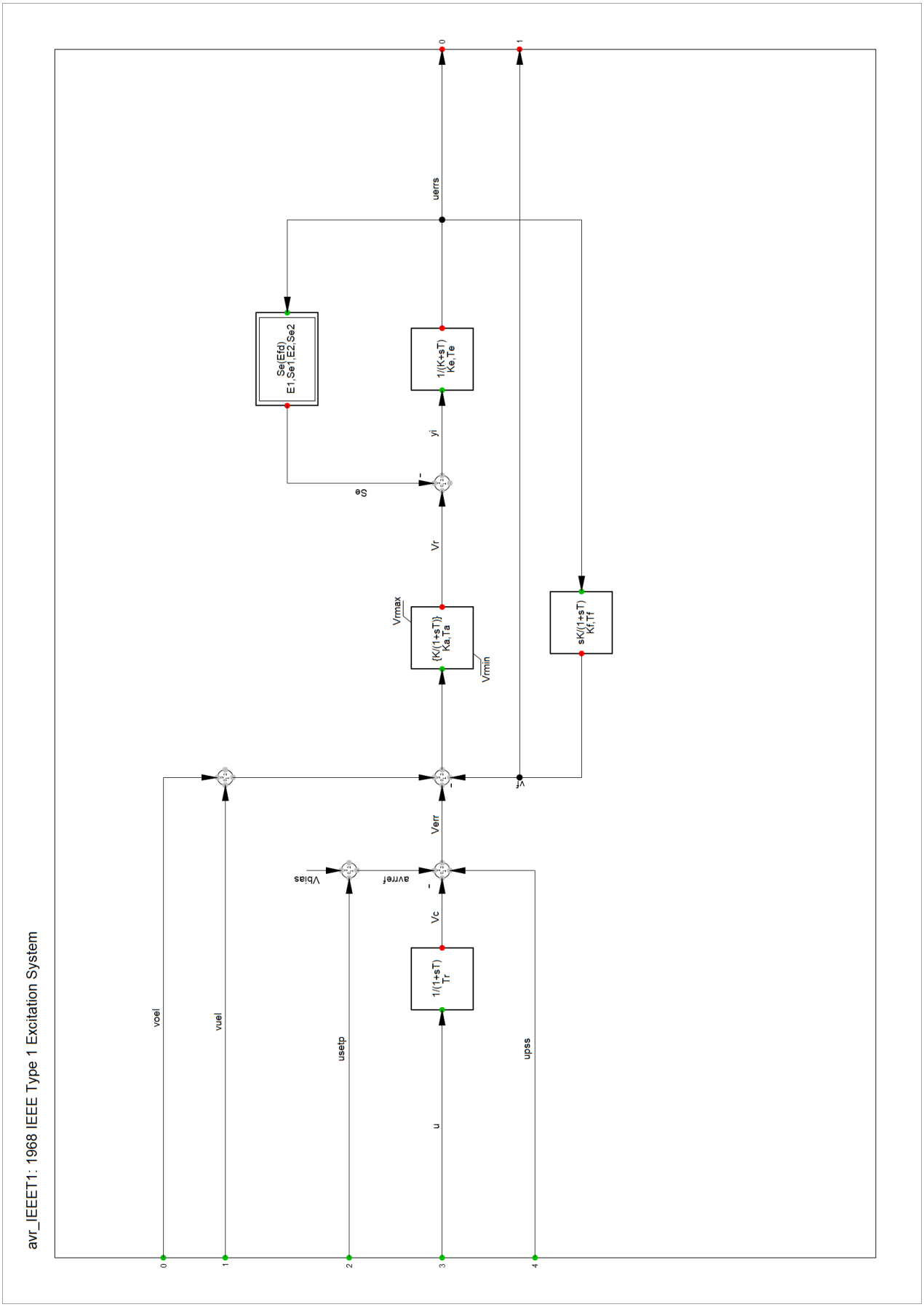


**Figure A.4:** Automatic voltage regulator control diagram in PowerFactory.

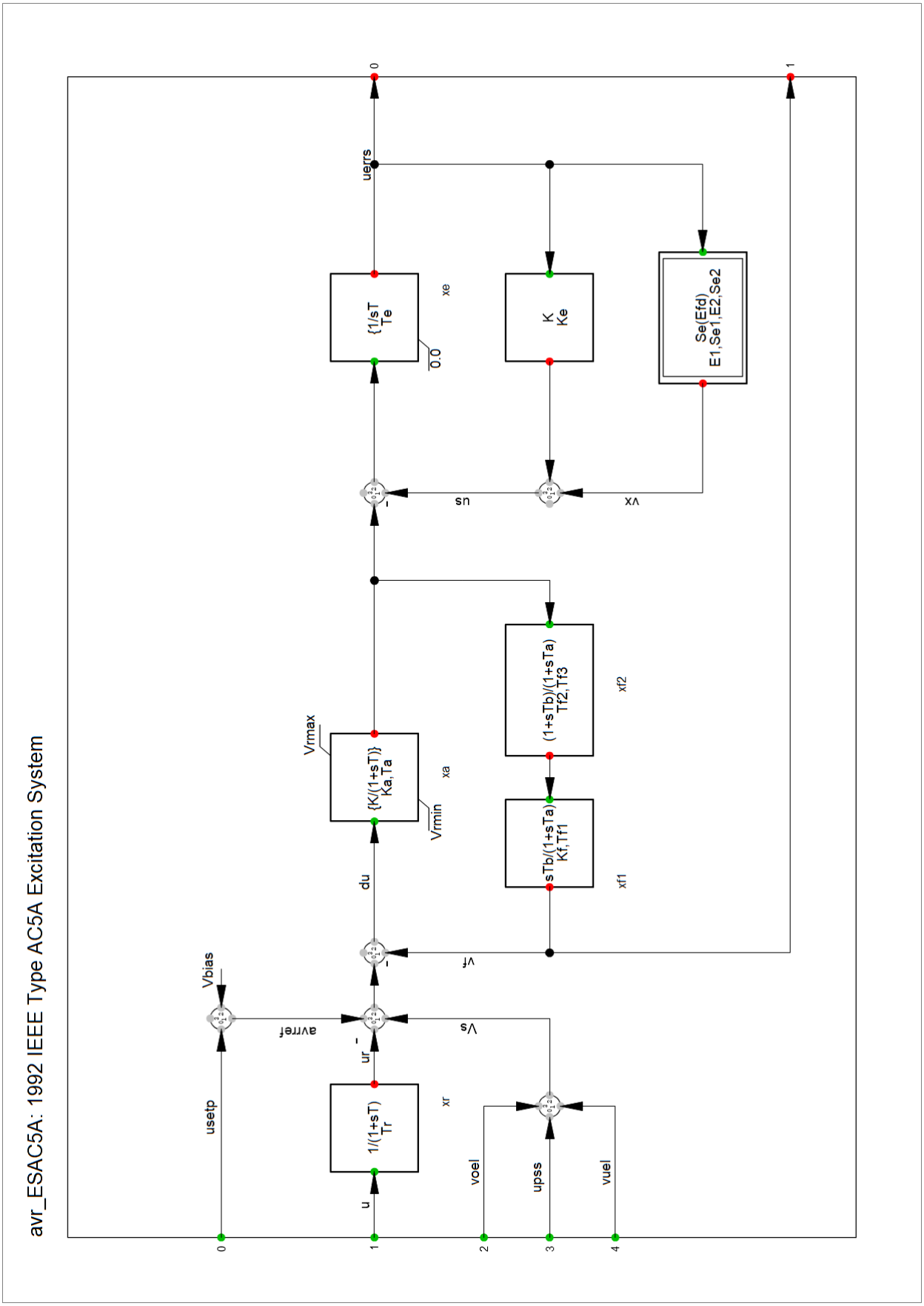


**Figure A.5:** Automatic voltage regulator control diagram in PowerFactory.

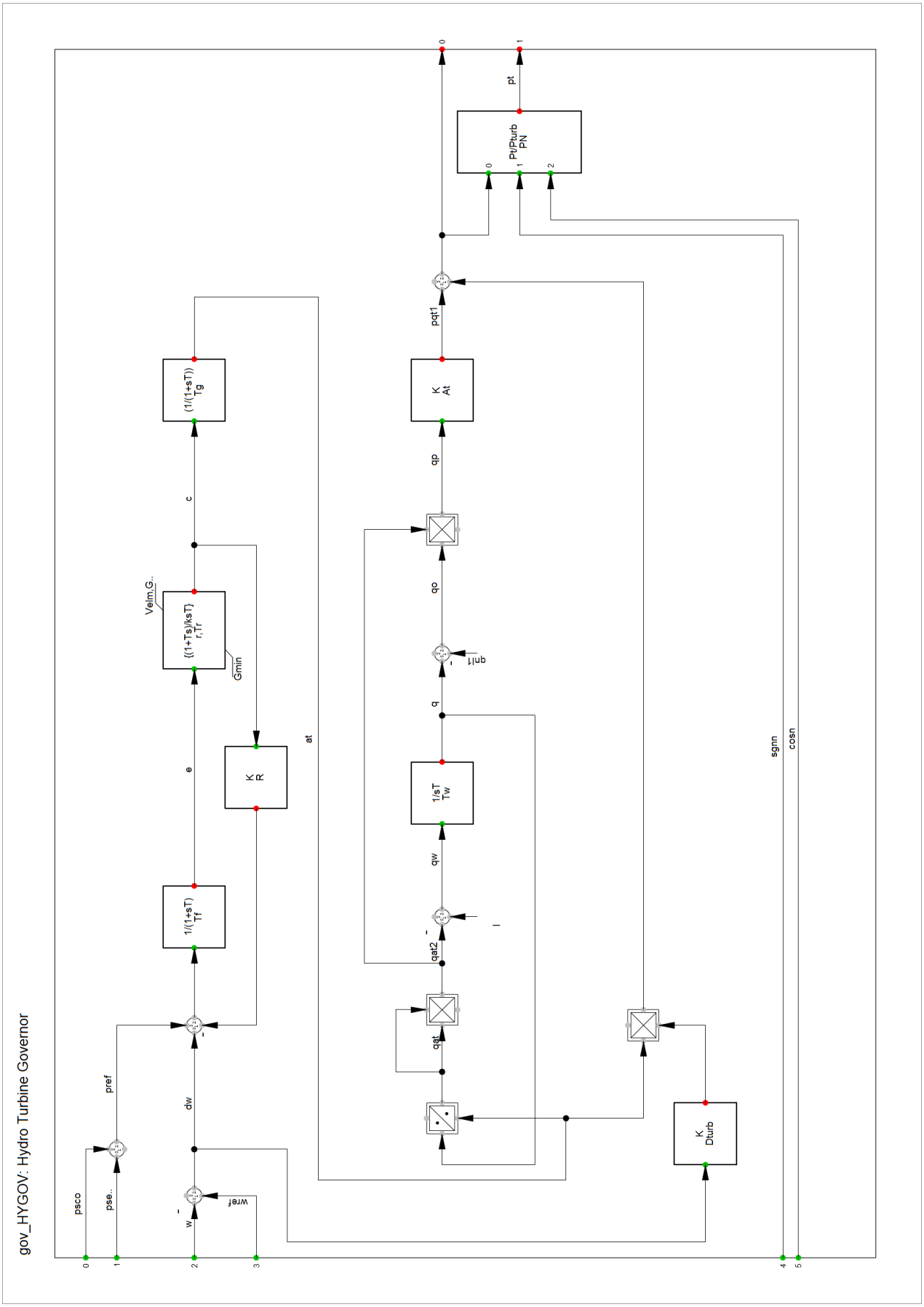


**Figure A.6:** Governor control diagram in PowerFactory.

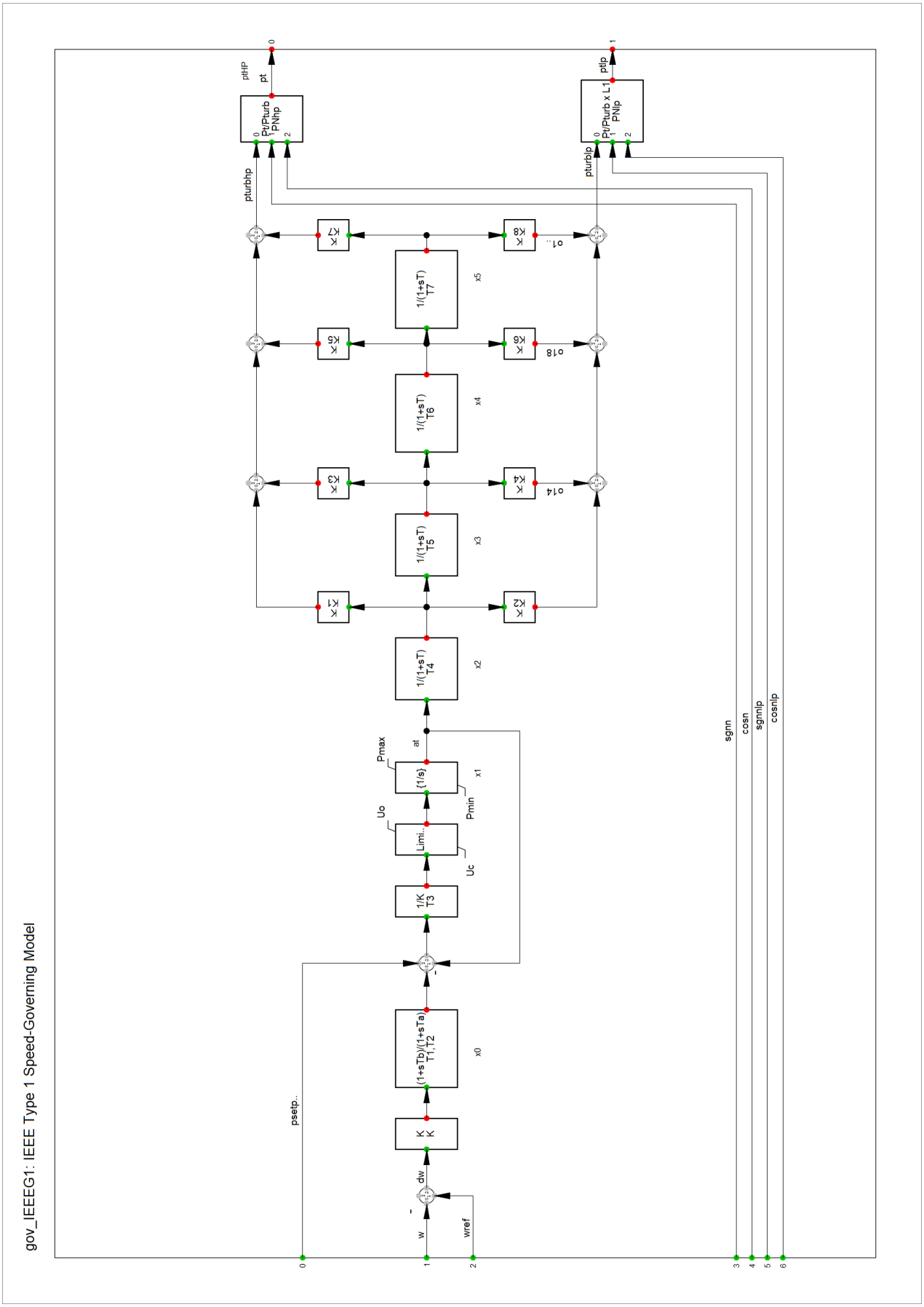


**Figure A.7:** Governor control diagram in PowerFactory.

# Appendix B

# Appendix 2

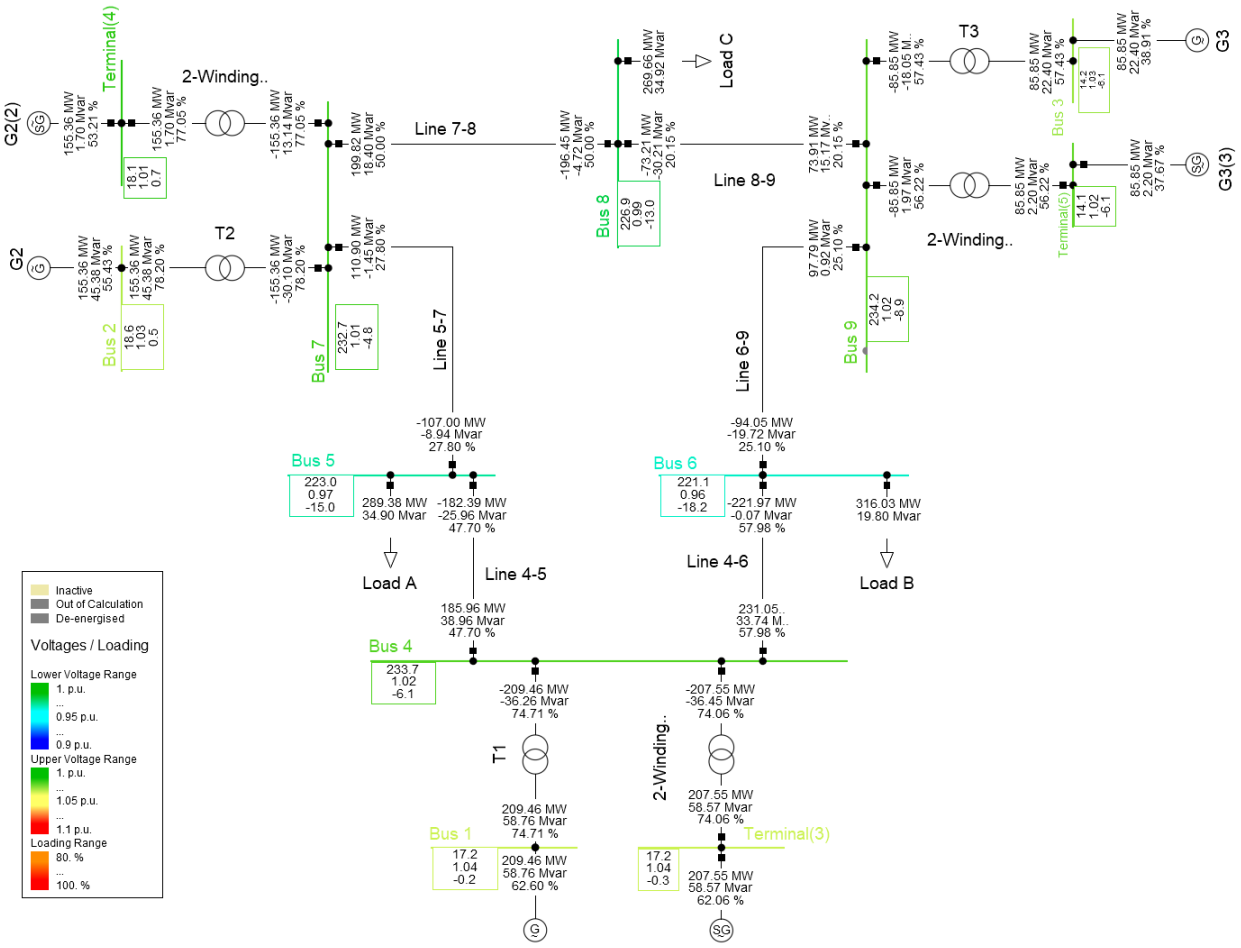


**Figure B.1:** Load flow of PS0.

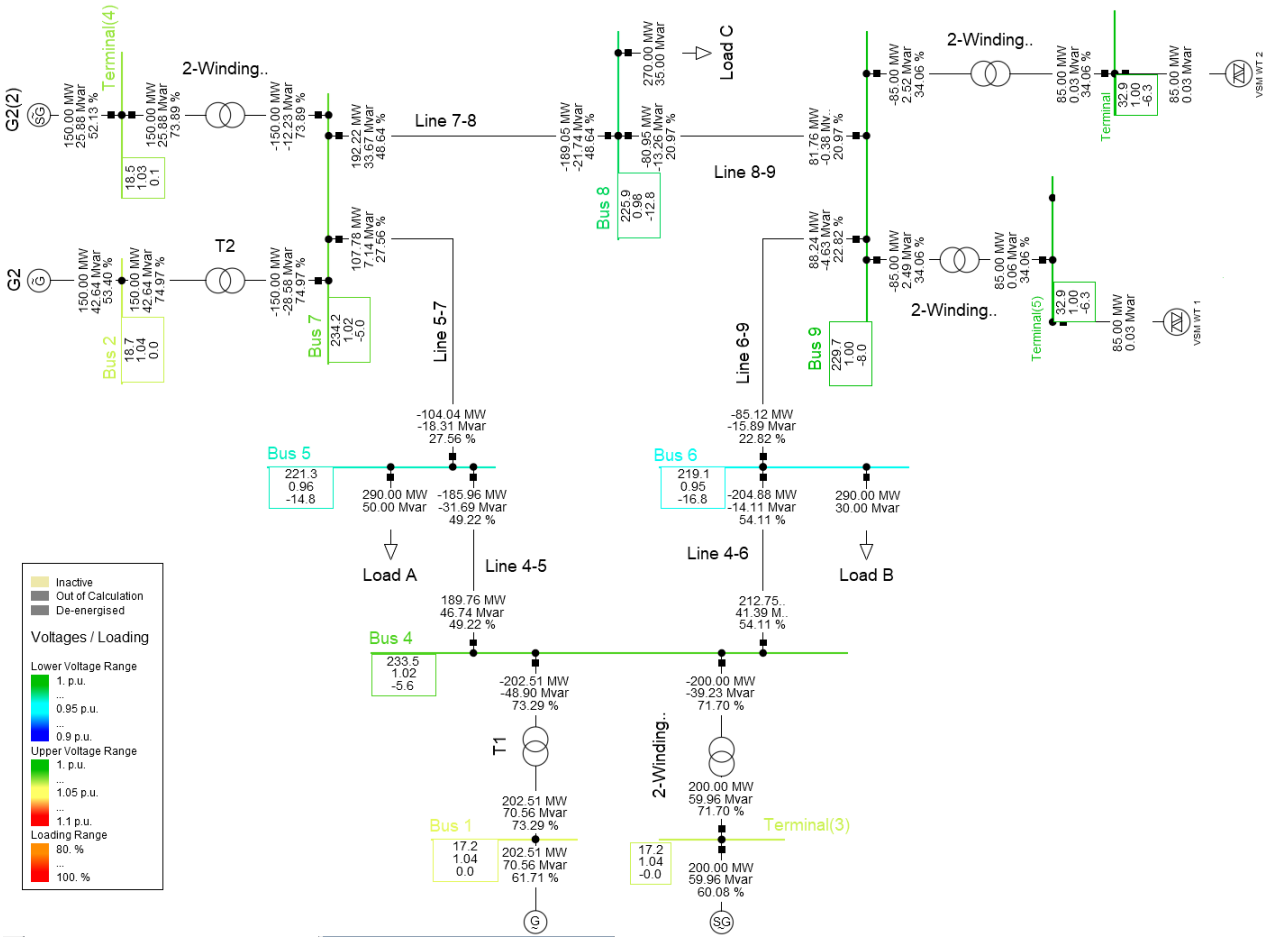


**Figure B.2:** Load flow of PS1.

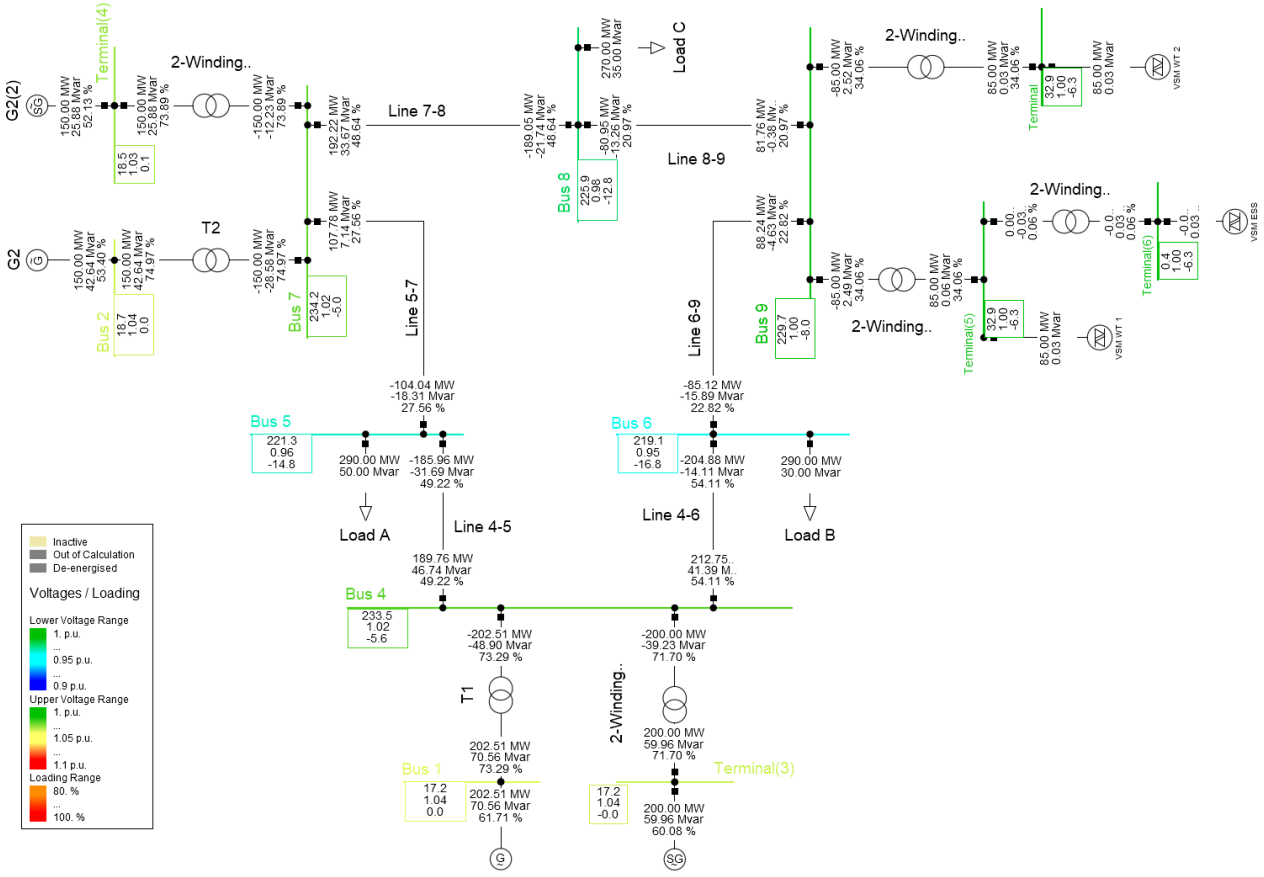


**Figure B.3:** Load flow of PS1+ESS.